A Closer Look at Vortical Hot Towers Within A Tropical Cyclogenesis Environment

Andrea B. Saunders and Michael T. Montgomery

Research Supported by the National Science Foundation
Grant #ATM-0101781

Colorado State University

DEPARTMENT OF ATMOSPHERIC SCIENCE

PAPER NO. 752

A CLOSER LOOK AT VORTICAL HOT TOWERS WITHIN A TROPICAL CYCLOGENESIS ENVIRONMENT

Andrea B. Saunders and Michael T. Montgomery

Research supported through the National Science Foundation under Grant ATM-0101781

Principal Investigator: Michael T. Montgomery

Department of Atmospheric Science

Colorado State University

Fort Collins, Colorado 80523

May 2004

Atmospheric Science Paper No. 752

ABSTRACT

It is a generally accepted fact that convection plays an important role in tropical cyclone intensification, yet convective-scale processes are absent from many tropical cyclogenesis theories. Results from cloud-resolving, full-physics simulations carried out with the CSU RAMS suggest that convective-scale dynamical processes play a significant, if not crucial, role in the transition from a midlevel MCV to a tropical cyclone. In addition, deep convective hot towers occurring within this environment possess large, localized positive vertical vorticity values generated by the tilting and stretching of MCV related vorticity on the updraft scale. This study seeks to understand both the role that deep convection plays in tropical cyclone formation and how the vortical nature of these hot towers influences the formation process.

First, we conduct a simple correlation analysis to demonstrate that deep convective activity is statistically related to mesoscale intensification. This analysis confirms that intensification of the midlevel mesoscale vortex lags deep convective bursts by a few hours. Next, we review a theory that explains how convective-scale processes induce spin up of the mesoscale circulation using Eliassen's balanced vortex model. The mesoscale meridional and tangential circulations predicted by this theory are qualitatively and quantitatively similar to those predicted by the model, with the dominant forcing for the balance equations being contributions from quasi-steady, deep convective activity in the form of the diabatic heating term.

We next address the question as to why the MCV environment is conducive to such quasi-steady convective activity. To answer this question, we must determine how the mesoscale environment influences hot tower characteristics. The most notable influence is the contribution of ambient vorticity which leads to the formation of vortical hot towers (VHT). Preliminary results from a series of sensitivity trials for an isolated updraft suggest that vorticity has a positive influence on individual updraft lifetimes and future updraft formation. The simulations also demonstrate that the moderate vertical shear present in the parent MCV leads to a tilting of VHTs downshear with height. This orientation displaces the cool dry downdraft air from the updraft core which delays the decay of the updraft.

It appears that both the ambient vorticity and moderate vertical shear of an MCV play roles in the sustenance of deep convective activity in these simulations. However, the exact nature of these relationships is still unclear. Further high-resolution simulations and analyses, as well as convective-scale observations of tropical cyclogenesis environments, are advocated to test the robustness of the vortical hot tower phenomenology.

ACKNOWLEDGEMENTS

We would like to extend out thanks to Tom Cram and Mel Nicholls for their extensive contributions to this work, as well as to Dr. Paul Reasor, Kevin Tory, Dr. Wayne Schubert and Eric Hendricks for providing insightful dialogue regarding the tropical cyclogenesis process. We would also like to thank Michael Bell, Marc Hidalgo, Kate Musgrave, John Persing, David Schecter, Wes Terwey and Laurie Trenary for their constructive comments. In addition, we would like to thank Kathleen Mulica and Saurabh Barve for their excellent administrative and computer support.

This research was supported by the National Science Foundation under Grant ATM-0101781.

CONTENTS

FIGURES

TABLES

Chapter 1

INTRODUCTION

In active tropical storm regions, such as monsoon and Atlantic easterly wave regions, it is common to observe large cloud clusters containing several mesoscale convective systems, or MCSs (Gray 1998). Diabatic processes within the stratiform precipitation region of these MCSs often lead to the production of midlevel mesoscale convective vortices, or MCVs (Johnston 1981; Bartels and Maddox 1991). MCVs may last for several days, long after the dissipation of the parent MCS, and are believed to spawn convective redevelopments. Several instances of tropical cyclones forming in the vicinity of these tropical MCVs have been observed and documented in recent years (Bosart and Sanders 1981; Harr et al. 1996; Bister and Emanuel 1997, hereafter BE97; Simpson et al. 1997, hereafter S97; Raymond et al. 1998). It is generally believed that the initial MCV plays a crucial role in the development of a tropical cyclone, and as such this form of tropical cyclogenesis has received much attention in the last decade. The benefits of understanding this phenomena are twofold. The first results from our current ability to identify MCVs using satellite and radar data. In understanding the conditions under which a tropical MCV will lead to tropical cyclone formation, we will greatly improve our abilities to predict this type of event. The second benefit lies in improving our fundamental understanding of the mechanisms responsible for tropical cyclogenesis, which in turn leads to a better understanding of all aspects of tropical cyclones.

1.1 Definition of Tropical Cyclone "Genesis"

As of yet, there is no universally accepted definition for tropical cyclogenesis. Many government agencies use the presence of organized convection and a definite surface circulation to classify a tropical cyclone. Although the determination as to whether or not these criteria have been met is made by experienced forecasters, it is an inherently subjective process. This classification can be further complicated in a case where a tropical cyclone develops out of an existing midlevel mesoscale convective vortex (MCV). Numerous such cases have been documented, with observational projects such as TEXMEX (1991) and TCM-92 (1992) contributing largely to this data set. In this situation, the initial mesoscale circulation is at a maximum at middle tropospheric levels (z = 4–6 km). In a strongly statically-stable atmosphere, we may expect this circulation to be restricted mainly to midlevels. However, atmospheric conditions typical of a summertime tropical climate are of low enough static stability to allow the mesoscale circulation to penetrate some depth of the atmosphere. Observational studies of MCVs at midlatitudes confirm that a weak but positive cyclonic relative circulation is often found below MCVs, extending down to just above the surface (Knievel 2001). One such study, described in Raymond et al. (1998), presents evidence of a relative cyclonic circulation existing below the midlevel MCV that developed into Hurricane Guillermo. In the presence of organized convection (i.e., if the MCV is associated with an active MCS) this type of system should meet the common criteria for tropical cyclone classification.

There exists one crucial characteristic that separates an MCV with associated organized convection from a tropical cyclone – the vertical profile of tangential winds. A tropical MCV has a tangential wind maximum at midlevels, while a tropical cyclone is characterized by maximum winds near the surface. Assuming thermal wind balance, the vertical profile of an MCV's tangential winds gives a cold core mesoscale vortex at low levels. This characteristic is unlike the typical warm core structure of a tropical cyclone. Hence, the presence of a cyclonic surface circulation may not be sufficient criteria for defin-

ing the formation of a tropical cyclone. In cases where a tropical cyclone forms out of an existing MCV, we propose that it is the transition from a cold core to warm core vortex structure at low levels that defines the birth of a tropical cyclone.

1.2 The Downward Development of the MCV: An Overview

The mechanisms whereby an MCV develops into a tropical cyclone are still uncertain. This area of atmospheric research experienced a surge of attention in the 1990's, when several field projects (e.g. TEXMEX (1991), TCM-92 (1992)) were conducted to investigate the role of mesoscale processes in tropical cyclone development. These projects resulted in a series of papers on the subject, most of which focus on potential mechanisms whereby the midlevel potential vorticity maximum of the initial MCV develops down to the surface. After this downward development occurs, it is hypothesized that surface-based fluxes of heat and moisture (e.g. WISHE) activate to intensify the system to a tropical cyclone. This common idea of the downward extension of the midlevel MCV led Montgomery et al. (2003, hereafter MNCS03) to refer to these types of theories as "top-down" descriptions of tropical cyclogenesis. We will now give brief summaries of two "top-down" theories presented in recent studies.

1.2.1 Mesoscale Vortex Interactions in the Tropical Cyclogenesis Process

S97 documented the development of Tropical Cyclone Oliver (1993). This development was observed during the TOGA-COARE (1993) field project. S97 described the genesis of TC Oliver as being the result of multiple midlevel MCV mergers in the presence of a monsoon trough. The monsoon trough acted to locally enhance low and mid-level cyclonic vorticity on the synoptic scale. S97 argued that the monsoon trough provided a region of reduced deformation radius, which improved the efficiency of the midlevel mesoscale vortex interactions and increased the amplitude of the merged vortices. They attribute the development of the surface circulation that becomes TC Oliver to this mechanism. They

also state that the monsoon trough provided suitable low-level shear that allowed the MCVs to generate strong MCSs before merging. S97 state that this convective redevelopment is also associated with the development of TC Oliver. However, no mechanistic explanation of the convective bursts' role in this process was provided.

1.2.2 Precipitation Processes and the Transformation of a Midlevel MCV to a Tropical Cyclone

In 1991, a field campaign was conducted in the tropical E. Pacific (Tropical Experiment in Mexico, or TEXMEX) with the primary goal of "extensively studying the process of tropical cyclogenesis" (BE97). During one of the six intensive operation periods, Hurricane Guillermo was observed to form from an existing MCS with an embedded MCV. The genesis of Hurricane Guillermo is documented in BE97. The two main flights of interest occurred at 64 and 14 hours before Guillermo was classified as a tropical storm. Each of these flights took in situ and Doppler radar measurements from a NOAA WP-3 aircraft at middle and lower levels.

Radar data from both WP-3 flights revealed a broad-scale cyclonic circulation that was cold core in the lower troposphere – a vortex structure typical of a midlevel MCV. During the second flight of interest, which occurred approximately 14 h before Guillermo was classified as a tropical storm, a small ($\approx$ 50 km) warm core vortex was discovered within the broader cold core circulation. BE97 hypothesized that an increase in convective activity just prior to the identification of the warm core vortex had provided significant precipitation that was responsible for the downward extension of the midlevel MCV air to the surface.

BE97 provided a schematic for their conceptual model of this process, which is presented here in Figure 1.1. The first step in their mechanism (Figure 1.1a) depicts the generation of a midlevel MCV from evaporative cooling (and anvil warming). This vortex is cold core at low levels and warm core in the upper troposphere. However, forced subsi-

dence results in a layer of warm, dry air just above the surface. As precipitation processes continue, evaporation leads to a cooling and moistening of the atmosphere below the MCV and the subsequent lowering of the level of maximum cooling. The level of maximum cooling is also the level of maximum vertical gradient in the diabatic heating rate, which is responsible for the mesoscale production of the potential vorticity that formed the initial MCV. Through this lowering process, the cold core vortex extends downward into the lowest levels (Figure 1.1b), favoring convective redevelopment. The vortex winds enhance sea surface fluxes while the cold core aloft decreases the boundary layer θ_E required to redevelop convection. Figure 1.1c depicts the enhancement of low level vorticity (and hence wind speed) due to the redevelopment of convection and its associated latent heating. The transition from cold to warm core system (tropical cyclone genesis by our definition) occurs within this last stage of BE97's genesis schematic. Unfortunately, the exact mechanism for this near-surface tangential wind enhancement is not given.

1.3 The Role of Deep Convection in Tropical Cyclone Formation

The "top-down" approaches discussed above focus on the mechanisms whereby a surface circulation is created from an existing MCV. However, it is not the intent of this thesis to address how a weak cyclonic surface circulation is generated within an MCV environment. We believe that the development of a warm-core vortex at low levels is the crucial step that defines tropical cyclogenesis. Further, we believe this process is not guaranteed to occur in the presence of a weak surface circulation due to the existence of a threshold tangential wind velocities that must be met to activate the surface flux mechanism of WISHE (Rotunno and Emanuel 1987). Hence, we believe it is necessary to take a closer look at the time period between the development of a weak surface cyclone and the development of a mesoscale warm core surface vortex in order to fully understand the genesis process.

Deep convective activity appears to be a common occurrence in the two "top-down"

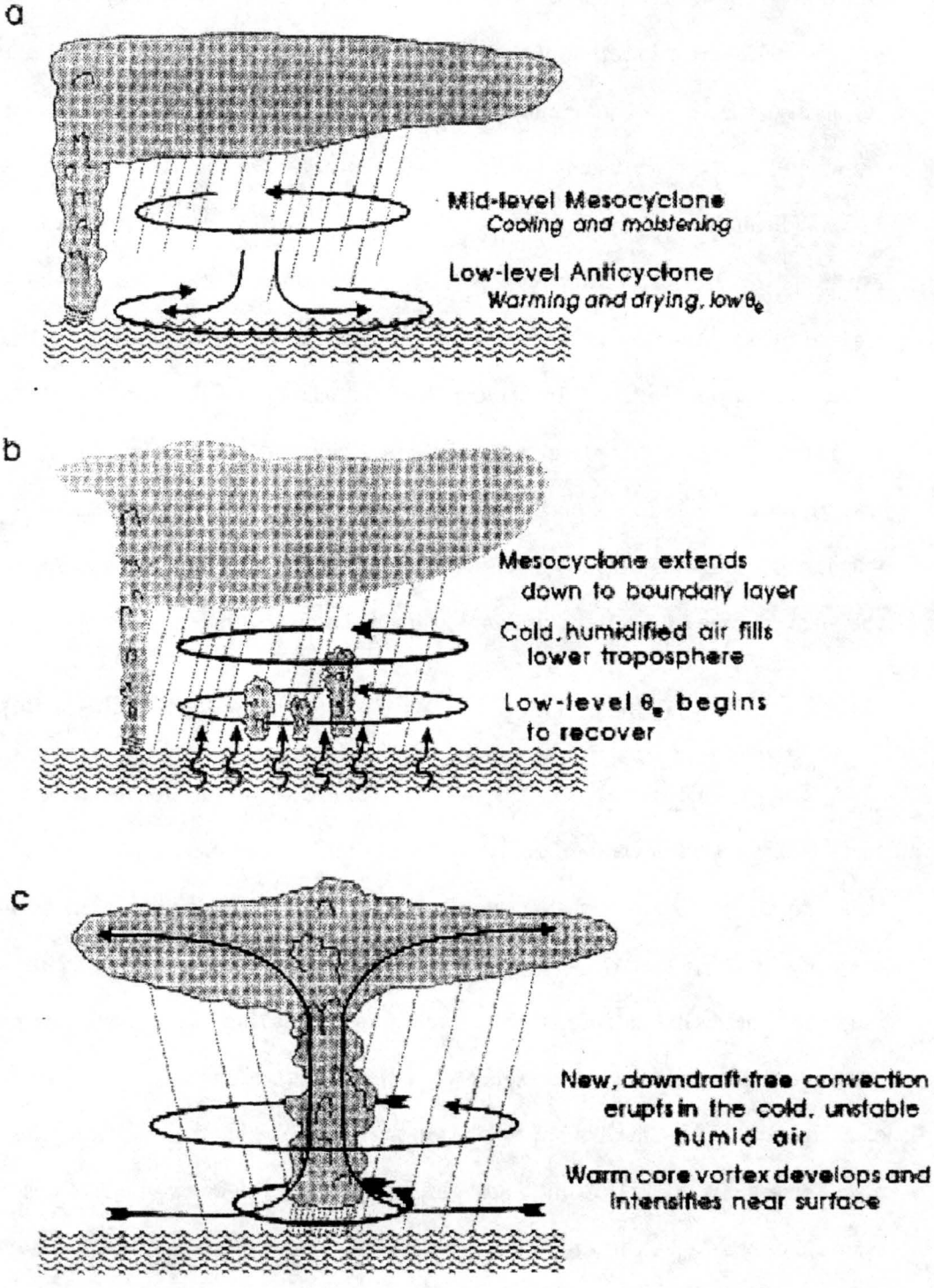

Figure 1.1: Tropical cyclogenesis schematic, taken from BE97

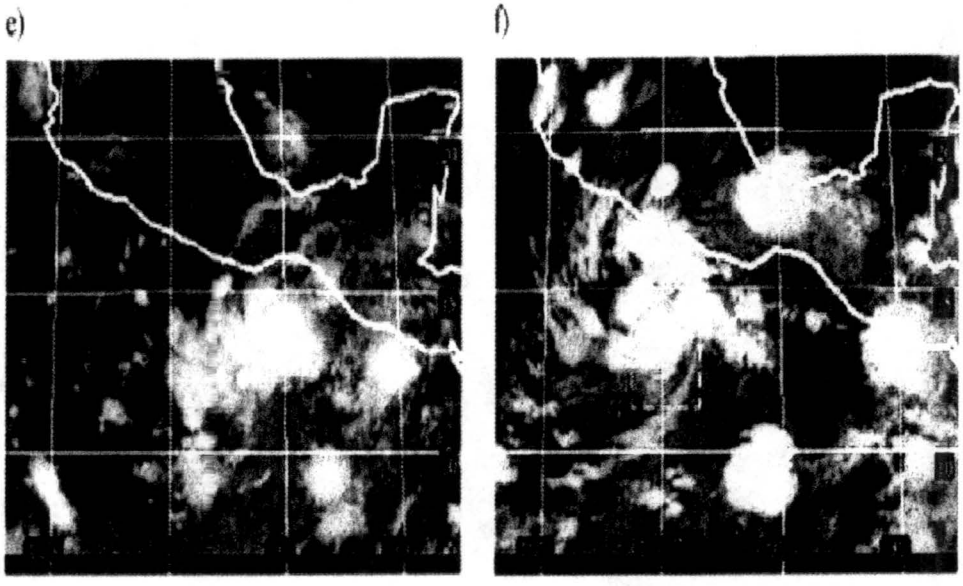

Figure 1.2: Satellite imagery from the genesis of Hurricane Guillermo. Taken from BE97.

studies discussed above. In particular, convective bursts after convectively sparse time periods are observed shortly before tropical depression classifications were made in the formations of Hurricane Guillermo and TC Oliver. BE97 and S97 both allude to the importance of deep convective activity (associated with MCSs) in the formation of the respective tropical cyclones. For example, satellite images presented in B97 show a burst of deep convection (Figure 1.2e) occurring in the vicinity of the initial MCV approximately 18 h prior to the identification of a low level warm-core mesoscale vortex (Figure 1.2f). However, neither BE97 nor S97 addresses the explicit role that convective-scale processes play in these genesis cases. Observations presented in Gentry et al. (1970), Zehr (1992) and Molinari et al. (2003) show that deep convective bursts often precede and/or accompany the formation of a tropical cyclone, which further supports the hypothesis that deep convective bursts play a significant role in the triggering of tropical cyclone formation.

We certainly do not mean to imply that the importance of deep convection in the tropical cyclogenesis process is a new idea. In fact, several theories have emerged regarding this role. In recent times, Simpson et al. (1998) and Ritchie et al. (2002) have hypothesized that subsidence around deep convective plumes acts to warm and lower the pressure near

the surface in order to aid in the formation of the tropical storm 'nascent eye.' From a more dynamical perspective, Montgomery and Enagonio (1998, hereafter ME98), Möller and Montgomery (2000, hereafter MM00), and Enagonio and Montgomery (2001, hereafter EM01) proposed that deep convective hot towers can be parameterized by their diabatically-generated PV. Using quasigeostrophic, asymmetric balance models initialized and pulsed with these convective-scale PV anomalies and a seedling mesoscale vortex, these works demonstrated that low-level vortex mergers and axisymmetrization processes could intensify the initial vortex into a tropical storm within realistic times.

This latter-mentioned pathway to tropical cyclogenesis does not rely on the initial MCV as a source of vorticity that must somehow extend downward to the surface. Rather, they focus on interactions between convective-scale and mesoscale features that act to "build" the tropical cyclone vortex at low levels utilizing the pre-existing vertical vorticity associated with the MCV vortex. For this reason, MNCS03 has dubbed this route to tropical cyclogenesis as a "bottom-up" approach.

1.4 "Bottom-up" Approach to Tropical Cyclogenesis

Current observational constraints generally prevent the collection of data with temporal and spatial resolution adequate for the resolution of convective-scale features over the deep tropical oceans. In addition, sea clutter and dropsonde wetting issues make airborne radar observations and in situ measurements at levels below $z < 1.5$ km unreliable. These restrictions make it very difficult to acquire the high-resolution low-level observations necessary to accurately test the "bottom-up" hypotheses. Currently, we believe our best efforts at further investigating convective processes within tropical cyclogenesis environments lie in modelling studies. Recently, several studies have been conducted to examine the results presented in ME98, MM00 and EM01. We will now discuss two of these studies, conducted using high-resolution, non-hydrostatic, convection-resolving models, and the insights they have provided into the role of convective-scale processes in the formation of a tropical

cyclone.

1.4.1 Cloud-Resolving Modelling Approaches: The Appearance of the Vortical Hot Tower Phenomenon

Using the Penn State/NCAR three-dimensional non-hydrostatic numerical weather prediction model (MM5), Davis and Bosart (2001) simulated the formation of Hurricane Diana (1984) in a baroclinic environment. In an attempt to explicitly represent convective structures, a 3 km horizontal grid spacing and no cumulus parametrization scheme are used on their finest grid. The role of deep convection in these simulated tropical cyclone genesis events was examined in Hendricks et al. (2003, hereafter HMD03). HMD03 found that deep convective plumes forming in the vorticity-rich environment of their simulations generated intense, small-scale cyclonic vorticity anomalies throughout the troposphere (i.e., vortex tubes). Borrowing from the "hot tower" terminology established by Riehl and Malkus (1958), HMD03 referred to these intense convective plumes with anomalous positive vorticity values as "vortical" hot towers, or VHTs.

HMD03 identified two roughly distinct phases in their genesis simulations. The first period was labelled a 'pre-conditioning" phase. During this period, individual hot towers were found to compete with one another for ambient CAPE and vorticity. However, due to their local generation of strong positive vorticity, collectively the VHTs acted to increase the mesoscale low-level vorticity during this time. The later phase was characterized by VHT interactions. These convective-scale vortex interactions were dominated by VHT mergers, which produced warm core anomalies and tangential momentum spin-ups.

A similar phenomenon was documented in MNCS03. Using the CSU RAMS model, this study examined the formation of a tropical storm from an initial MCV. The simulations of MNCS03 were able to successfully model tropical cyclone genesis from a single tropical MCV within 24 h. This result suggests that although mesoscale interactions may be crucial to the transition of an MCV to a tropical cyclone in some documented cases, it may not be

the sole route to genesis. In addition, sensitivity trials were run in which convective activity was delayed. The initial MCV failed to develop a tropical cyclone until after the onset of deep convection at $t = 14$ h, at which time the evolution of the system mimicked that of the control simulation. This result indicates that the presence of deep convection is crucial to the development of a tropical cyclone in these simulations, and provides compelling evidence for the further investigation of the role of convective-scale processes in this transition.

The model used in MNCS03 is a three-dimensional non-hydrostatic weather prediction model much like MM5. As in HMD03, the simulations of MNCS03 use fine-scale resolution on the inner grid ($\Delta x = \Delta y = 2$ km) and invoke no cloud parametrization scheme, so as to explicitly resolve convective-scale processes. Like HMD03, MNCS03 observed an abundance of "vortical" hot towers in their simulations. Furthermore, interactions between VHTs, including VHT mergers, were observed during the time period prior to tropical cyclone formation. The apparent similarities in convective-scale processes between these two studies is quite remarkable given the fact that they simulated very different types of tropical cyclogenesis events. Hurricane Diana (1984) developed in the subtropics in association with a low-level front and an approaching upper level cyclonic PV anomaly (Bosart and Sanders 1991; Montgomery and Farrell 1993; Davis and Bosart 2001), while MNCS03 simulated an idealized case of tropical cyclogenesis from a midlevel MCV in a convectively-favorable environment typical of the deep tropics. The appearance of VHTs in both of these distinct simulations suggests that "vortical" hot towers are robust structures that dominate the organizational process.

Our current work seeks to build on the results presented in MNCS03 by developing a more complete understanding of the VHTs that form in their simulations. We are particularly interested in clarifying how the vortical nature of the hot towers affects the tropical cyclone formation process.

An outline of this thesis is as follows. In Chapter 2, we will give an overview of the model setup. A list of the RAMS configuration settings used in these simulations is given

in Appendix B. Chapter 3 outlines the overall development of the control simulation. Here we define the tropical cyclogenesis time period and provide a description of the convective-scale and mesoscale processes that dominate during this time. In Chapter 4, we will provide a description of model-generated VHTs and propose a mechanism for the convective generation of vorticity. We will discuss the characteristics that set VHTs apart from hot towers possessing significantly less vertical vorticity. Chapter 5 then addresses the problem of how deep convective activity affects the system-scale evolution. This chapter summarizes the balanced vortex theory of Eliassen, and describes how this theory predicts a mesoscale surface spin-up in response to quasi-steady convective heating, as discussed in MNCS03. Chapter 6 examines more closely the effects vorticity has on the strength and longevity of individual hot towers. A simple theoretical argument for the vorticity-related protection of hot towers is given, and this theory is tested via a series of preliminary sensitivity trials, focussing on isolated VHTs. In Chapter 7, we take a step back and consider how the simulated MCV environment as whole is conducive to quasi-steady deep convective activity. Finally, in Chapter 8 we discuss our conclusions and propose future work necessary to test our preliminary results.

Chapter 2

MODEL SETUP AND DATA ANALYSIS

Given that the primary focus of this study is to investigate the role of convection in tropical cyclogenesis, it is desirable to use a model that will give an accurate representation of small scale processes relating to clouds, including cloud microphysics. Also, given that the convective structure of tropical systems during the tropical cyclogenesis phase is often observed to be asymmetric, a 3-dimensional model is necessary.

The numerical model used in this study is the Regional Atmospheric Modelling System (RAMS) which was developed at Colorado State University (Pielke and Coauthors 1992; Cotton and Coauthors 2003). RAMS is a non-hydrostatic model that solves prognostic equations for the three Cartesian velocity components, non-dimensional pressure perturbation, ice-liquid water potential temperature (Tripoli and Cotton 1981b), total water mixing ratio and cloud microphysics, from which vapor mixing ratio and potential temperature are diagnosed (see Tripoli and Cotton 1981a). Beyond the fact that it is a full-physics model with an elaborate cloud microphysics package, there are two more reasons why we chose to use RAMS for our study. First, RAMS was developed here at CSU, and hence the largest source of documentation and assistance with the model is available "in house." Secondly, a similar modelling study was conducted using the PSU-NCAR MM5 by Davis and Bosart (2001), simulating the genesis of Hurricane Diana (1984). The role of deep convection in this simulated tropical cyclogenesis event was recently investigated by HMD03. Although this study involved the modelling of an actual tropical cyclogenesis event in a baroclinic environment in contrast to our involves an idealized deep–tropics

simulations, both examine the dynamical influences of convection in the overall process of tropical cyclogenesis. Conducting our study using a different full–physics model will provide independent support to the work outlined in HMD03.

2.1 Model Configuration

The full details of the model configuration can be found in MNCS03. Appendix A of MNCS03 lists the model setup parameters for side-by-side comparison, and is included here in Appendix B. This study uses the microphysics scheme developed by Walko et al. (1995). This scheme includes categories for cloud droplets, rain, pristine ice, snow, aggregates, graupel and hail. The surface parameterizations of heat, vapor and momentum fluxes is based on the Louis (1979) scheme. The surface roughness length over water is dependent on the surface wind speed according to the relation derived by Charnock (1955). Long and short wave radiation is included using a scheme developed by Harrington (1997), which includes interactions with cloud hydrometeors. A first order Smagorinsky (1963) sub-grid scale scheme is used, with modifications made by Lilly (1962) and Hill (1974) that enhance diffusion in unstable conditions and reduce diffusion in stable conditions.

Since no cloud parametrization scheme was employed, spatial resolution needed to be fine enough so as to explicitly resolve cloud scale features in the MCV region. A two-way interactive multiple nested grid scheme, developed by Clark and Farley (1984), was used. This scheme allowed us to use an adequately fine scale in the smallest, innermost grid while having a large enough overall domain size so as to minimize impacts of lateral boundary conditions. For the most of the simulations discussed in this thesis, three nested grids fixed in space with horizontal grid spacing 24 km, 6 km, and 2 km [1] and (x,y) grid dimensions (64,64), (90,90), and (137,137), respectively, were used. Each nested grid was centered within the next coarsest grid (as shown in Figure 2.1).

In order to allow finer vertical resolution at the lowest model height levels while

[1] Although Bryan et al. (2003) suggests that this is not a fine enough scale to adequately resolve convective processes, our $\Delta x = 1$ km results discussed in Chapter 6 suggest that 2 km resolution adequately captures the overall structure desired for this study. Finer-scale simulations are currently underway.

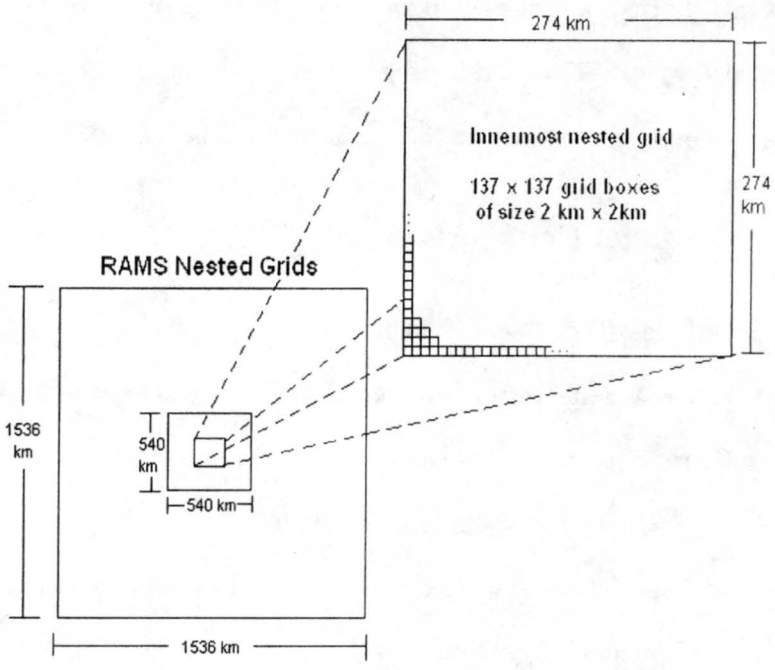

Figure 2.1: Schematic of horizontal model grids for Expt. A1 (control) and all other $\Delta x = 2$ km simulations discussed in this work. The outermost grid consists of 64×64 grid points with 24 km spacing between data points. The middle grid consists of 90×90 grid points with 6 km spacing between data points. The innermost grid (enlarged in the upper right) consists of 137×137 grid points with 2 km horizontal spacing.

representing the entire necessary vertical domain, a stretched vertical grid increment was used. The lowest vertical level is at $z = 137$ m with a first vertical grid increment of 400 m. The vertical spacing was gradually stretched with height to the top of the domain at 22 km, including a total of 26 vertical grid levels. The radiation condition discussed by Klemp and Wilhelmson (1978) was used at the lateral boundaries, which assumes that disturbances reaching the boundaries move as linearly propagating internal gravity waves. A Rayleigh friction layer is employed at upper levels in order to reduce reflection of gravity waves from the top of the model. The depth of the surface Rayleigh friction layer in the simulations was 5 km.

2.2 Model Initialization: Control Simulation

The intent of these model runs was to successfully simulate and diagnose tropical cyclogenesis from a single, tropical MCV. In particular, we hoped to investigate the role that convective-scale processes play in this transition. As such, it was necessary to initialize the simulations with a convectively favorable environment. The model temperature profile was initialized using an Atlantic hurricane season sounding developed by Jordan (1958), as shown in Figure 2.2. The humidity profile was also developed from the Jordan sounding, but was modified by moistening the sounding values in the domain center in order to more accurately represent the environment in which tropical cyclogenesis is thought to occur. This moistening has a maximum value of 2 g kg^{-1} at the surface in the center of the domain, and decreases as you move away from this point. Vertical profiles of ambient and center θ_E are shown in Figure 2.3.

The initial sounding contains a 1 km mixed-layer convective available potential energy (CAPE) value of 997 J kg^{-1} [2] . This thermodynamic initialization is certainly conducive to deep convective activity. However, we believe that this environment is by no mean unrealistic as a typical tropical cyclogenesis environment. Recently, the Jordan mean sounding with moisture enhancement was used in single-cell and squall line simulations conducted by Ooyama (2001). In addition, a sounding taken in the at Majuro, Marshall Islands on August 15, 1996 is shown in Figure 2.4. This sounding, taken from Barnes (2001), was meant to demonstrate the large conditional instability that can be present in the equatorial trough zone. This sounding exhibits surface-based CAPE values of 3500 J kg^{-1}, well above those present in our simulated environment.

The surface moisture enhancement of the Jordan sounding is further supported by the results of a recent study of atmospheric moisture vertical profiles of Saharan air layers or

[2] 1-km mixed layer refers to the fact that the thermodynamic properties of the lowest 3 model levels (z = 197 m, 610 m and 1049 m) were averaged before the CAPE calculation was made. The rationale for computing mixed layer CAPE as opposed to surface-based CAPE lies in the fact that parcels are not typically lifted from the surface, but rather from somewhere within the boundary layer. Assuming the boundary layer is well-mixed, the mixed-layer CAPE value is more representative of the actual CAPE experienced by lifted air parcels.

SALs (Dunion and Velden 2004). Dunion and Velden (2004) generated composite vertical moisture profiles of SAL and non-SAL sounding taken in the tropical N. Atlantic, and compared these profiles to the Jordan mean (1958) sounding (Figure 2.5). Notice that the non-SAL moisture profile is very similar to that of the Jordan mean profile at most levels, with the greatest deviation occurring at low levels where the Jordan sounding is actually drier than the non-SAL profile. Since tropical cyclones are rarely observed to form in SAL regions, we feel comfortable that the Jordan mean sounding with a slight surface moisture enhancement represents an adequate environmental scenario for a tropical cyclogenesis environment.

2.2.1 Initial MCV

The initial MCV was prescribed as a vortex in hydrostatic and gradient wind balance. The maximum tangential winds are approximately 6 ms^{-1} at height $z = 4$ km and occur at a radius of $r = 70$ km. The tangential velocity field decays as you move vertically and horizontally away from this position. A cross-sectional view of the initial tangential wind field is shown in Figure 2.6 (see MNCS03 for further details on how this vortex was prescribed). Notice that although the tangential winds are at a maximum at midlevels, there does exist a mesoscale cyclonic surface circulation of approximately 1–3 ms^{-1}. Although a weak surface circulation does exist at the onset of our simulations, we believe we are initiating our model well before the onset of tropical cyclone genesis based on the arguments given in Chapter 1.

Figures 2.7 and 2.8 show plots from Raymond et al. (1998) that describe the conditions observed during the second and fourth reconnaissance flights of Hurricane Guillermo, respectively, taken during the TEXMEX field campaign (1991). BE97 describes the formation of Hurricane Guillermo, which is believed to occur from an initial MCV. From BE97, Flights 2 and 4 were taken during time periods approximately 64 h and 14 h prior to the classification of the system as a tropical depression, respectively. Flight 4 occurs shortly

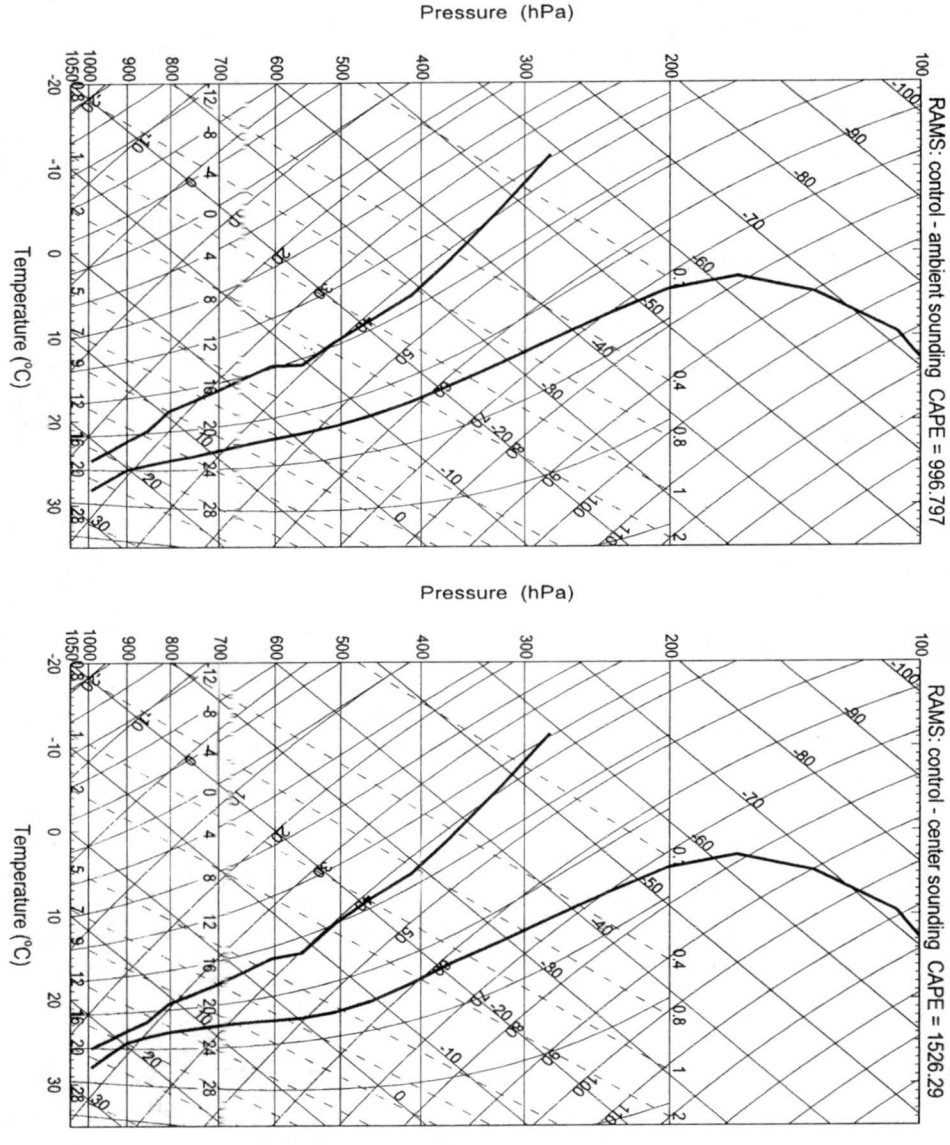

Figure 2.2: Skew T – log p atmospheric sounding plots for the control experiment.

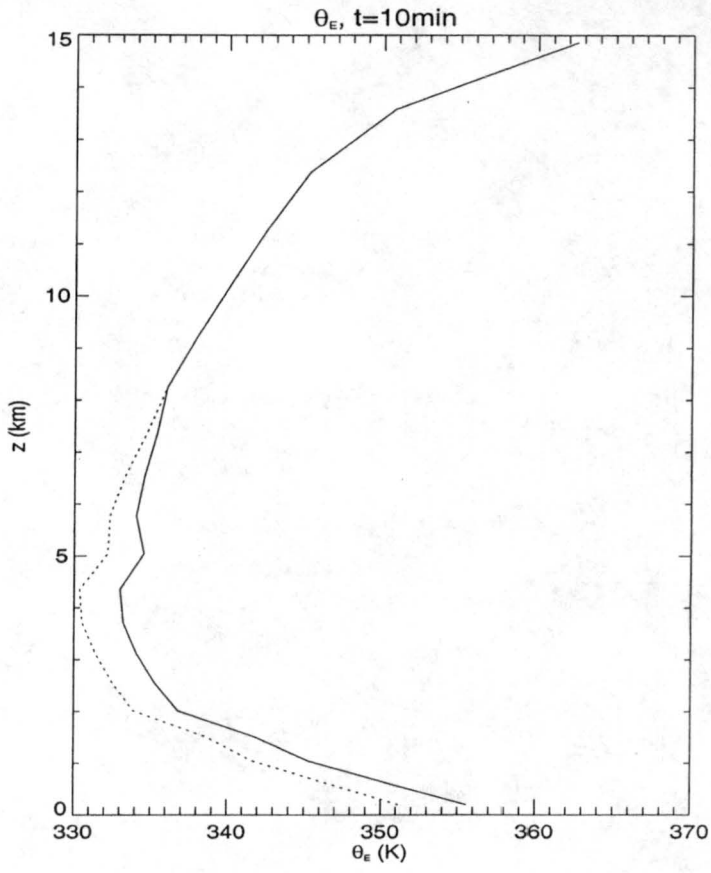

Figure 2.3: Vertical profiles of center (solid) and ambient (dashed) θ_E at t = 10 min.

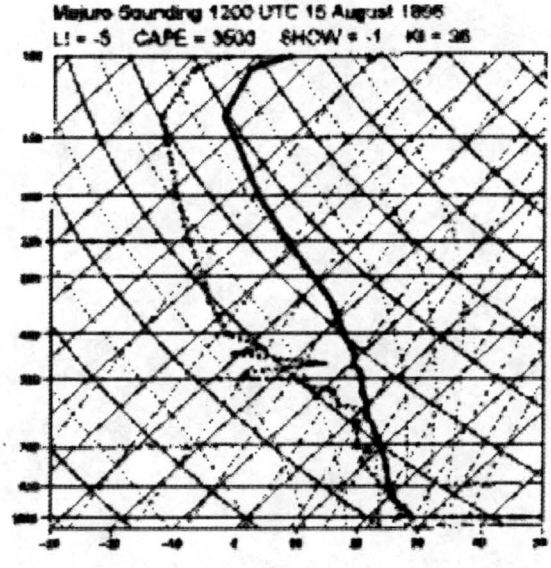

Figure 2.4: Skew T – log p atmospheric sounding plots for Majuro, Marshall Islands on 8/15/96 (taken from Barnes 2001).

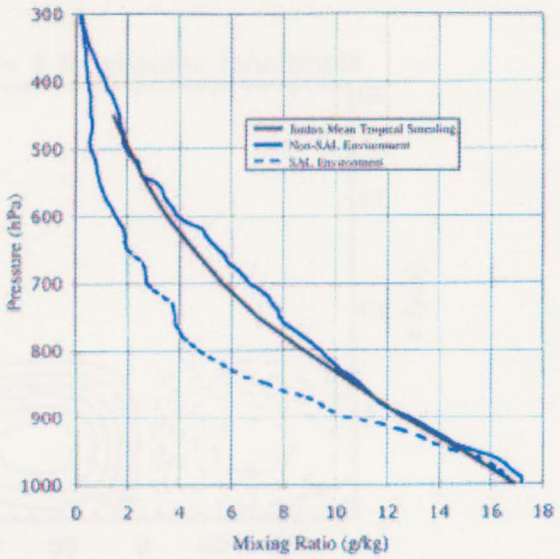

Figure 2.5: Mixing ration vs. pressure for SAL regions (dashed blue), non-SAL (solid blue) and Jordan mean (1958, solid black). Taken from Dunion and Velden 2004

after a burst of deep convective associated with the midlevel MCV. Notice that the plots of relative and absolute circulation show a positive relative circulation at low levels during each pre-Guillermo reconnaissance flight. This indicates that although the mesoscale cyclonic circulation is at a maximum at midlevels (z = 4–5 km), there still exists cyclonic circulation near the surface. It is not possible to deduce the corresponding tangential winds from the Raymond et al. (1998) plots without knowing the area over which the circulations were computed. However, the ratios of the midlevel to low-level circulation values at each of these pre-genesis times are approximately 0.2 and 0.7 as compared to 0.5 for our initial MCV, suggesting that our initialization is not totally unrealistic.

2.2.2 Initiating Convection: Surface Warm Bubble

To speed up the initial development of convection a heating anomaly, or "warm bubble," was applied at 50 km east of the vortex center at the surface, as is shown in Figure 2.9. The surface heating was applied for 300s, after which time the model was allowed to run with no further prescribed forcings. It is worth noting that one of the

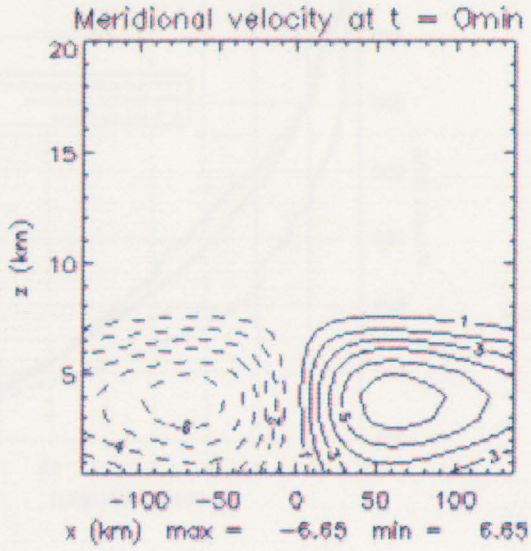

Figure 2.6: Initial midlevel vortex meridional velocity cross-section. Contour interval is 1 ms^{-1}.

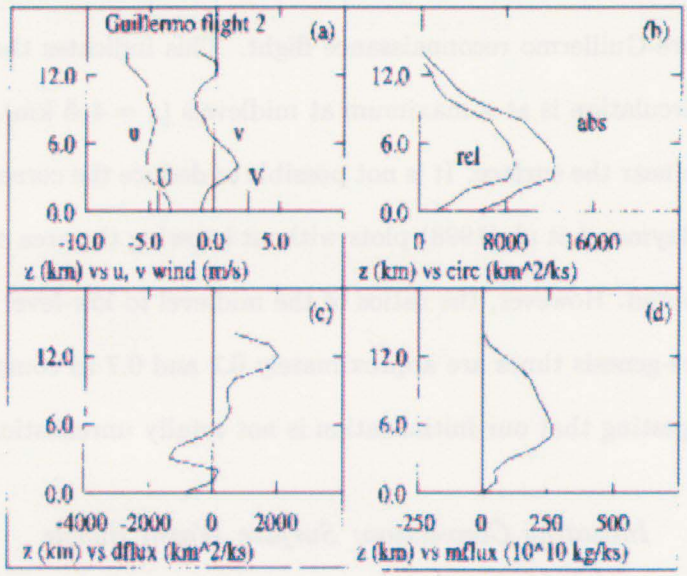

Figure 14. As in Fig. 10, except for flight 2 of IOP 5, near day 215.1.

Figure 2.7: Vertical profiles radar-observed quantities taken from Flight 2 of IOP 5, just prior to the formation of the tropical depression that became Hurricane Guillermo (taken from Raymond et al. 1998)

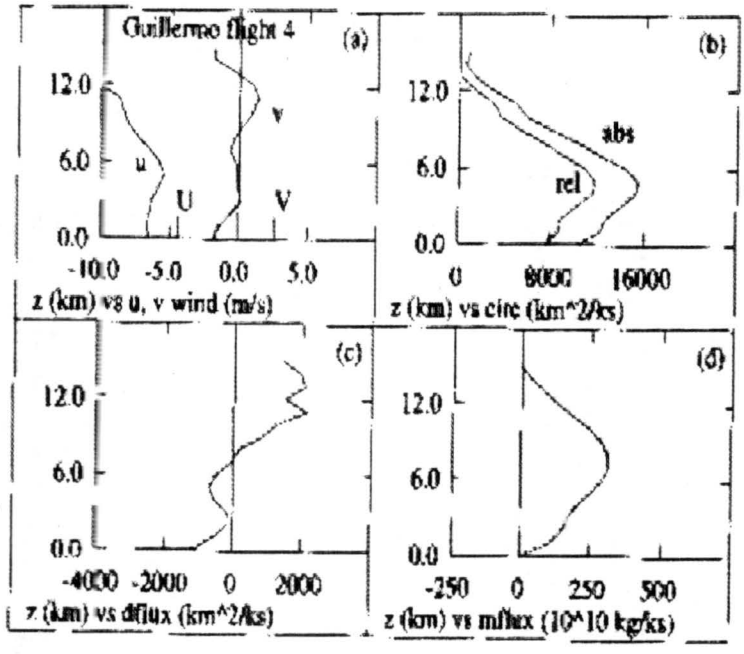

Figure 2.8: Vertical profiles radar-observed quantities taken from Flight 4 of IOP 5, just prior to the formation of the tropical depression that became Hurricane Guillermo (taken from Raymond et al. 1998)

sensitivity trials was initialized without the warm bubble but with all other parameters the same as the control. Although convection is delayed by about 14 hours, once convection does appear the overall development of the system is found to be qualitatively similar to that of the control case.

2.3 Data Analysis

The RAMS was configured to output the following six standard meteorological field variables on the finest grid at each temporal output interval: 3D velocity ($u = Dx/Dt$, $v = Dy/Dt$, $w = Dz/Dt$), potential temperature (θ), pressure (p), and water vapor mixing ratio (q_v). In the RAMS model, variables are defined on a staggered Arakawa-C grid, so that thermodynamic variables and velocity variables are defined at different horizontal grid points. Also, vertical velocity is defined on a grid that is vertically staggered from the of the other variables. The first step in the processing of the output data is to interpolate all

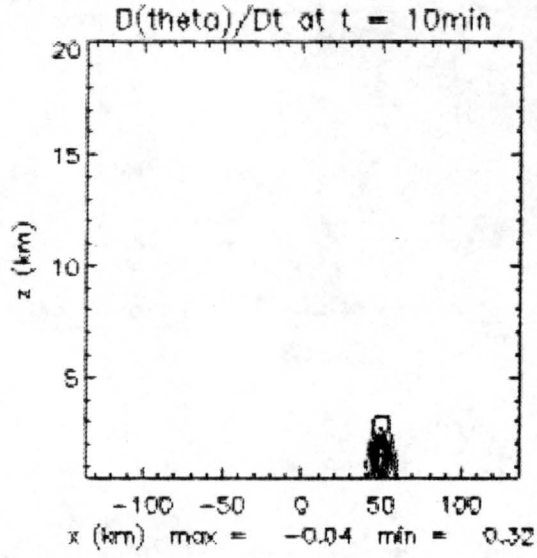

Figure 2.9: Heating rate 10 minutes into the simulation (5 minutes after application of warm bubble). Contour interval is .05 K day^{-1}

variables to a common spatial grid at each output time. This grid has the same horizonal grid increments of 2 km, and extends from 500 m off the ocean surface up to 18 km with vertical height levels specified at $z = 0.5, 1, 1.5, 2, 2.5, 3, 4, 5, 6, 7, 8, 9, 10, 12, 14, 16, 18,$ and 20 km.[3]

Absolute vertical vorticity (η) and Ertel dry potential vorticity (PV) were computed at each spatial gridpoint at each time using the following definitions

$$\eta = \frac{\partial v}{\partial x} - \frac{\partial u}{\partial y} + f \tag{2.1}$$

$$= \zeta + f \tag{2.2}$$

$$PV = \frac{\nabla\theta \cdot \vec{\eta}}{\rho} \tag{2.3}$$

where the Coriolis parameter used in our simulation corresponds to a latitude of 15° N, $f = 3.77 \times 10^{-5}$ s^{-1}. In order to compute PV from the model output, the following relations

$$p = \rho RT \tag{2.4}$$

[3] Initial analysis was performed at vertical levels extending from $z = 0.5$ km to $z = 20$ km at 500 m increments. These data fields were compared to those interpolated to our 18-vertical level scheme, and were found to be nearly identical. In light of space considerations, the latter scheme was used.

$$\theta = T\left(\frac{p_s}{p}\right)^{\frac{R}{c_p}} \tag{2.5}$$

were also used.

Chapter 3

SUMMARY OF 72-H DEVELOPMENT OF CONTROL SIMULATION

In the control simulation, the data was output every 10 min during the first 24 h and every 30 min for the remainder of the 72 h run. It develops a hurricane-strength mesoscale circulation by $t = 60$ h. We will now summarize the evolution of the data fields over the entire 72 h simulation.

3.1 Azimuthal Mean Evolution

The control simulation is initialized at 1200 local time. The initial MCV has maximum azimuthal mean tangential winds of 6 ms^{-1} at height $z = 4$ km and radius $r = 70$ km, and they decay as one moves away from this region (Figure 3.1a). At the initial time, the midlevel MCV is in hydrostatic and gradient wind balance.

Figure 3.2 shows the azimuthal mean tangential velocity, radial velocity, vertical velocity and diabatic heating rate at $t = 24$ h. By this time, a tropical depression-strength system has developed. Comparing Figure 3.2b with Figure 3.1, we can see that the azimuthal mean tangential velocity field has increased significantly. This increase is greatest at the lowest model levels, where the winds have increased from 3 ms^{-1} to 11 ms^{-1} in the radius range of $r = 40$–55 km. Figure 3.2a shows the development of strong azimuthal mean radial outflow at upper levels, weak radial inflow near the surface and moderate radial inflow at midlevels. Figure 3.2c suggests this is a time of deep convective activity, with an azimuthal mean vertical velocity maximum at a radius of $r = 50$ km. It is also interesting

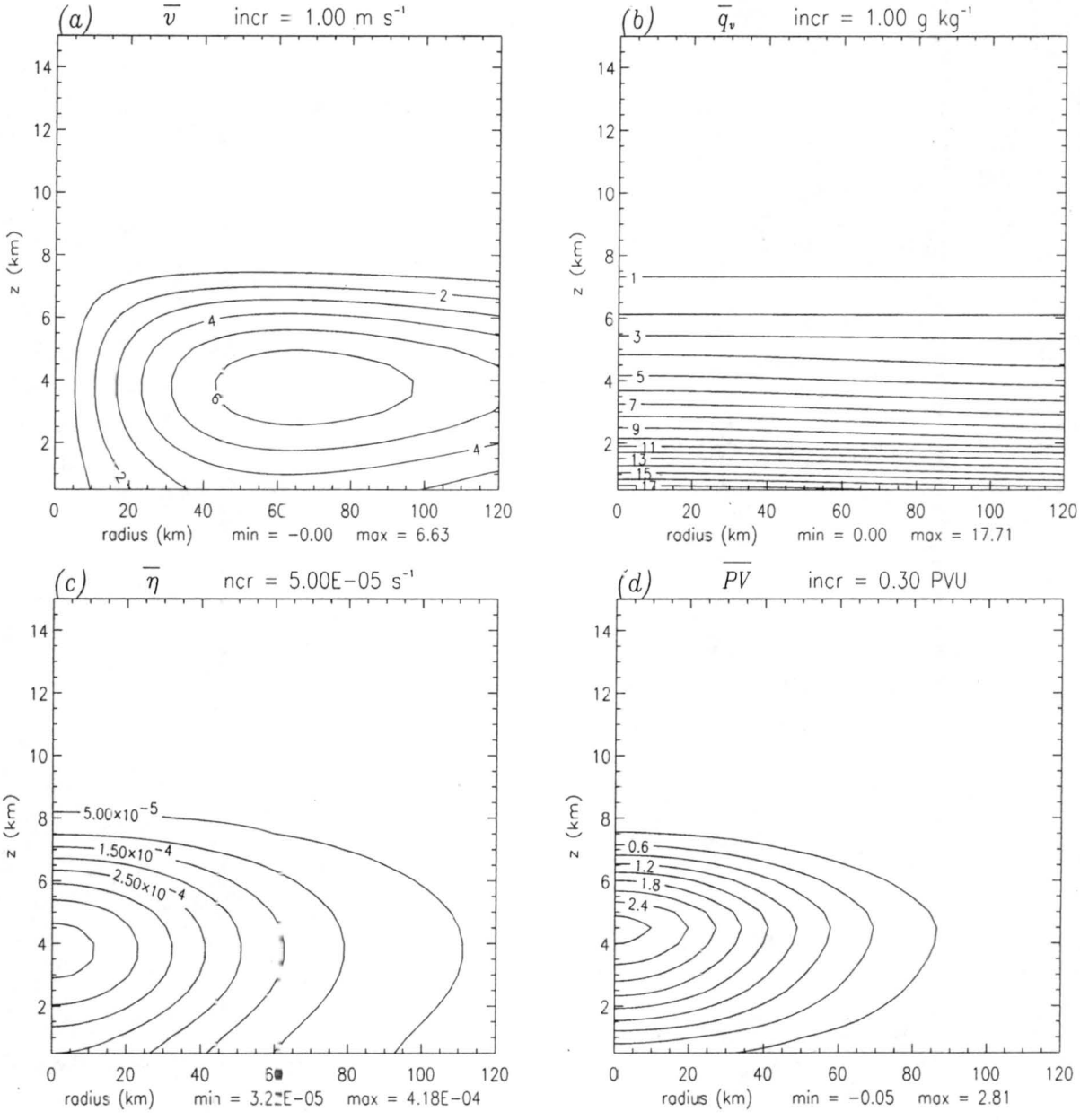

Figure 3.1: Initial conditions used for the control experiment. Shown are azimuthal averages of (a) tangential wind, (b) water vapor mixing ratio, (c) absolute vertical vorticity and (d) potential vorticity (from MNCS03).

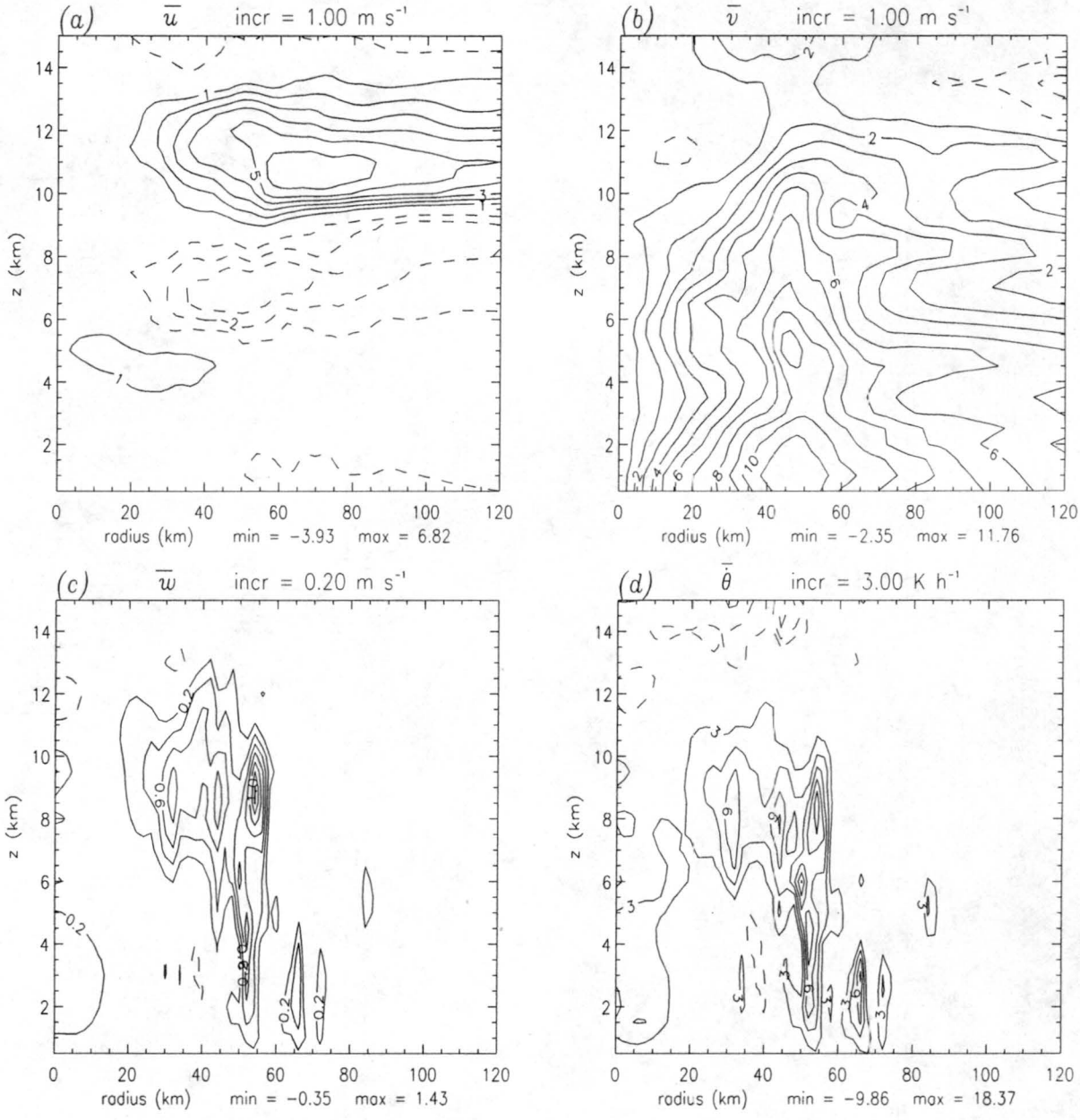

Figure 3.2: Azimuthal averages of (a) radial wind, (b) tangential wind, (c) vertical velocity, (d) diabatic heating, (e) absolute vertical vorticity, and (f) potential vorticity at $t = 24$ h (from MNCS03).

to note that the regions of highest azimuthal mean diabatic heating rate (Figure 3.2d) are coincident with the regions of strongest azimuthal mean vertical velocity (Figure 3.2c).

By $t = 48$ h, the model has developed a near tropical storm-strength surface vortex. Azimuthal mean tangential surface winds have reached 14 ms^{-1} (Figure 3.3b), radial out-

flow at upper levels remains strong and radial inflow near the surface has increased (Figure 3.3a). The mean radius of deep convection has contracted to $r = 20$–30 km (Figure 3.3c) and the azimuthal mean vertical velocity and diabatic heating rate fields are still collocated (Figure 3.3d).

At the end of the simulation, $t = 72$ h, the system has reached the intensity of a strong hurricane. Near surface azimuthal tangential winds have reached a maximum of 46 ms^{-1} at radius $r = 10$ ms^{-1} (Figure 3.4b), with surface radial inflow of 4–6 ms^{-1} and outflow at upper levels of up to 10 ms^{-1} (Figure 3.4a). Strong, sustained upward motion is present at the radius of maximum winds (Figure 3.4c), with the azimuthal mean vertical velocity field exhibiting the classic tilted eyewall structure.

3.2 Definition of the 'Pre-Genesis' Time Period

It is the intent of this study to examine the role of deep convection in the transition from a midlevel MCV to a surface-concentrated mesoscale vortex (e.g. tropical depression). It is somewhat difficult to pinpoint the time at which this transition is occurs, mainly because there is no universally accepted definition for tropical cyclogenesis. However we can use certain defining characteristics of tropical storms to determine the point at which the transition has occurred. The initial MCV in our study is defined in thermal wind balance, and hence has a cold core structure in the lower troposphere ($z < 4.5$ km). We will define tropical cyclogenesis to have occurred when this cold core vortex structure is replaced by a warm core structure, indicative of the transition from a midlevel mesoscale circulation to a surface-concentrated vortex.

Figure 3.5 shows azimuthal mean tangential winds versus azimuthal mean potential temperature perturbation during the first 24 h. At $t = 0$ h, the mesoscale vortex exhibits a negative potential temperature perturbation near the surface, indicating the cold core surface structure common to midlevel MCVs. By $t = 12$ h, the negative potential temperature perturbation near the surface has weakened considerably and the azimuthal mean

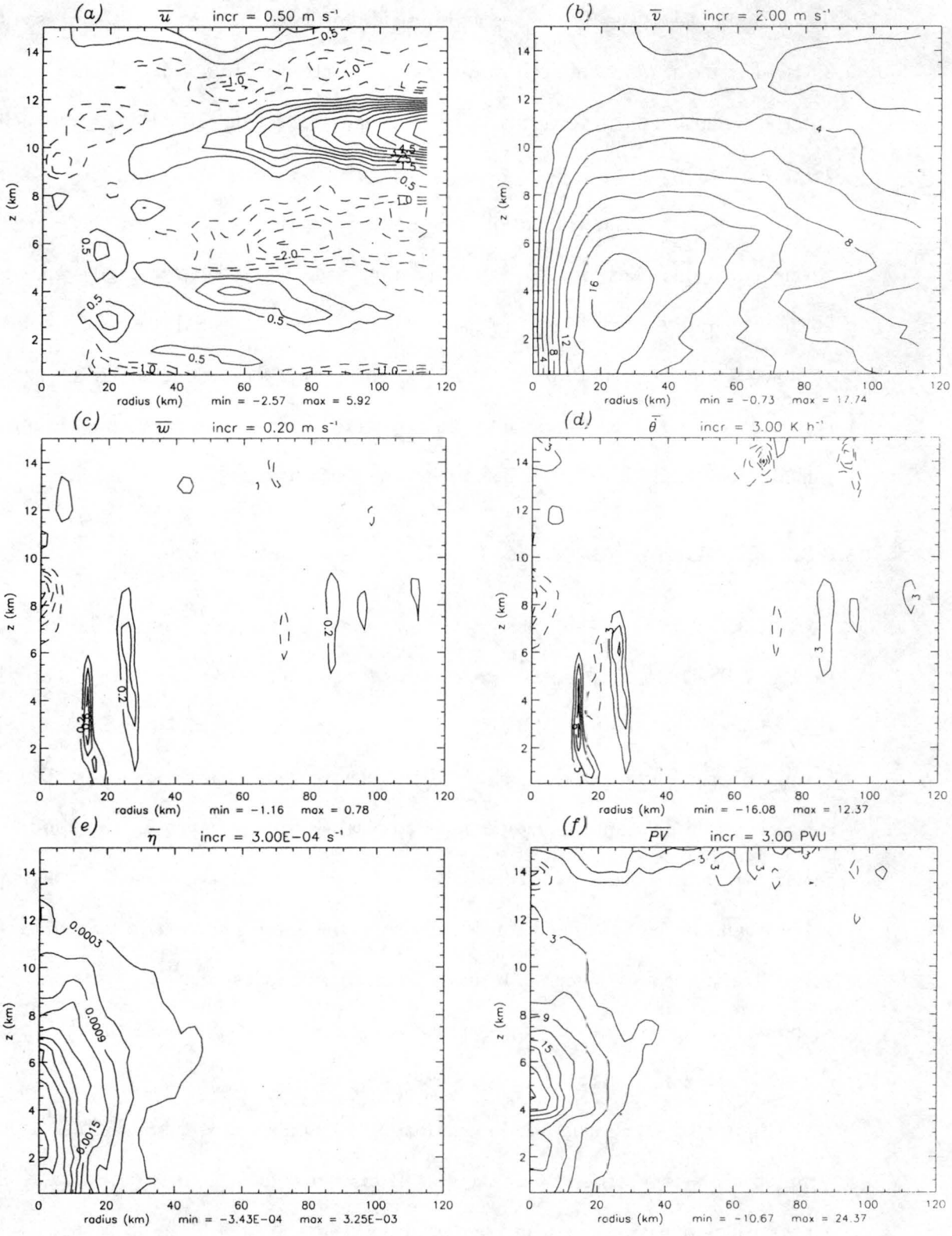

Figure 3.3: Azimuthal averages of (a) radial wind, (b) tangential wind, (c) vertical velocity, (d) diabatic heating, (e) absolute vertical vorticity, and (f) potential vorticity at $t = 48$ h (from MNCS03).

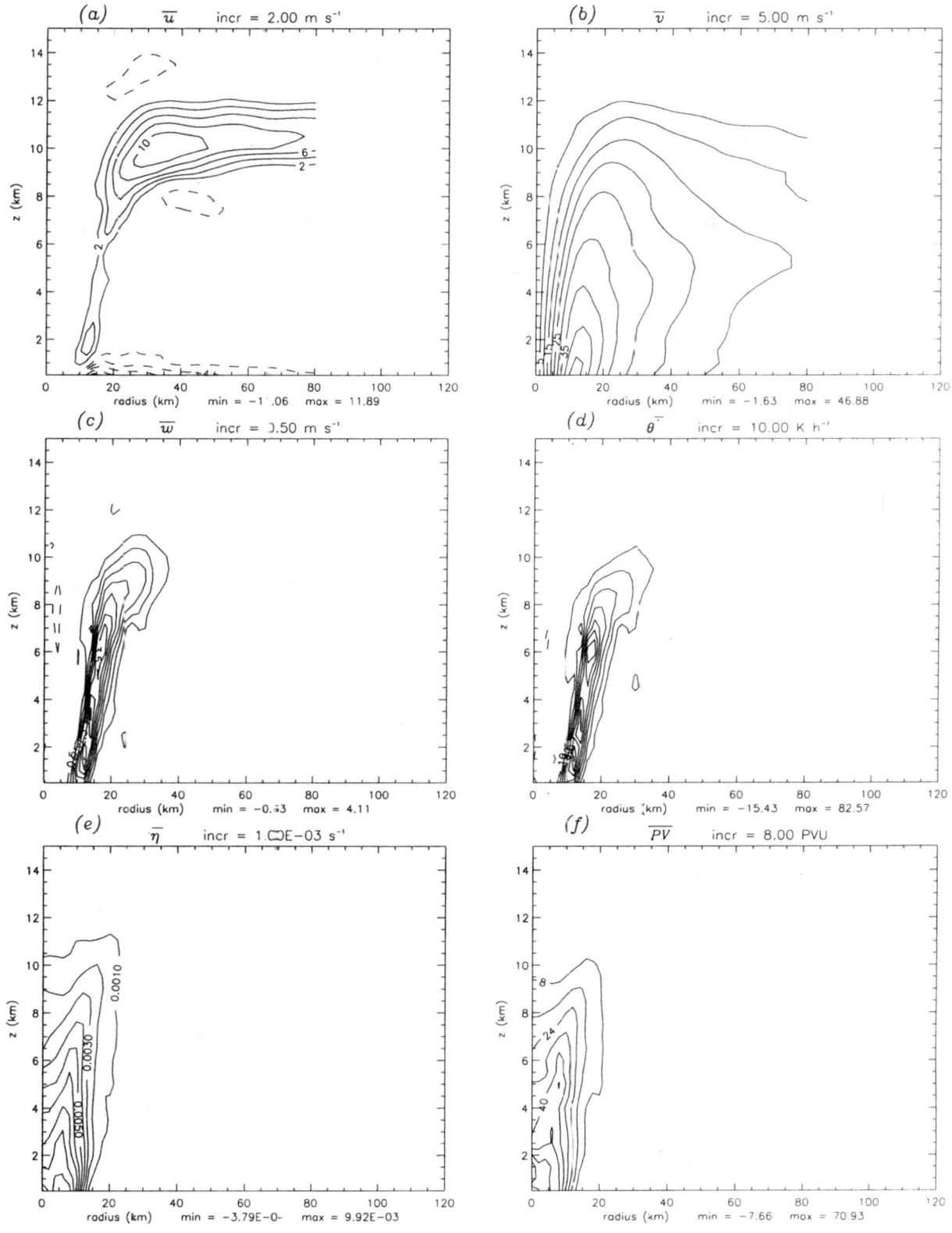

Figure 3.4: Azimuthal averages of (a) radial wind, (b) tangential wind, (c) vertical velocity, (d) diabatic heating, (e) absolute vertical vorticity, and (f) potential vorticity at $t = 72$ h (from MNCS03).

tangential wind field shows a maximum near the surface with a secondary maximum near $z = 7$ km. At this time, the mesoscale vortex exhibits a structure that is not distinctly cold nor warm core near the surface, but rather a combination of the two. By $t = 24$ h, a positive potential temperature perturbation appears at low levels with an even warmer anomaly aloft. Also, a negative potential temperature anomaly is now present at midlevels. The azimuthal mean velocity field exhibits a maximum at the surface of 11 ms^{-1}. At this time, it appears that the mesoscale vortex has a predominantly warm-core structure at low levels throughout much of the troposphere, as is typical of a tropical storm vortex. These results establish that the transition from midlevel MCV to surface-based mesoscale circulation occurs within the first 24 h.

3.3 Description of the 'Pre-Genesis' Time Period

3.3.1 WISHE or Pre-WISHE?

In order to proceed with our analysis of convective-scale processes in these tropical cyclogenesis experiments, we must first investigate whether this transition is simply a consequence of a wind-induced surface heat exchange process. This axisymmetric process, known as WISHE, relies on the existence of a surface-concentrated finite amplitude vortex. When the surface circulation reaches a threshold intensity, increased fluxes of heat and moisture from the ocean surface can lead to rapid intensification of the surface vortex (Rotunno and Emanuel 1987). The midlevel MCV used to initialize our control simulation has an associated mesoscale circulation of 1–3 ms^{-1} near the surface, and as such WISHE may be occurring during the pre-genesis time period. If the genesis process is distinct from WISHE, then it must be shown to occur before the onset of WISHE.

As one way of identifying the time period before WISHE is occuring (hereafter referred to as the 'pre-WISHE' time period or phase), we will follow the methods used in Molinari et al. (2003). The Molinari et al. observational study examines the development of Hurricane Danny (1999) in the Gulf of Mexico. In order to detect the onset of increased

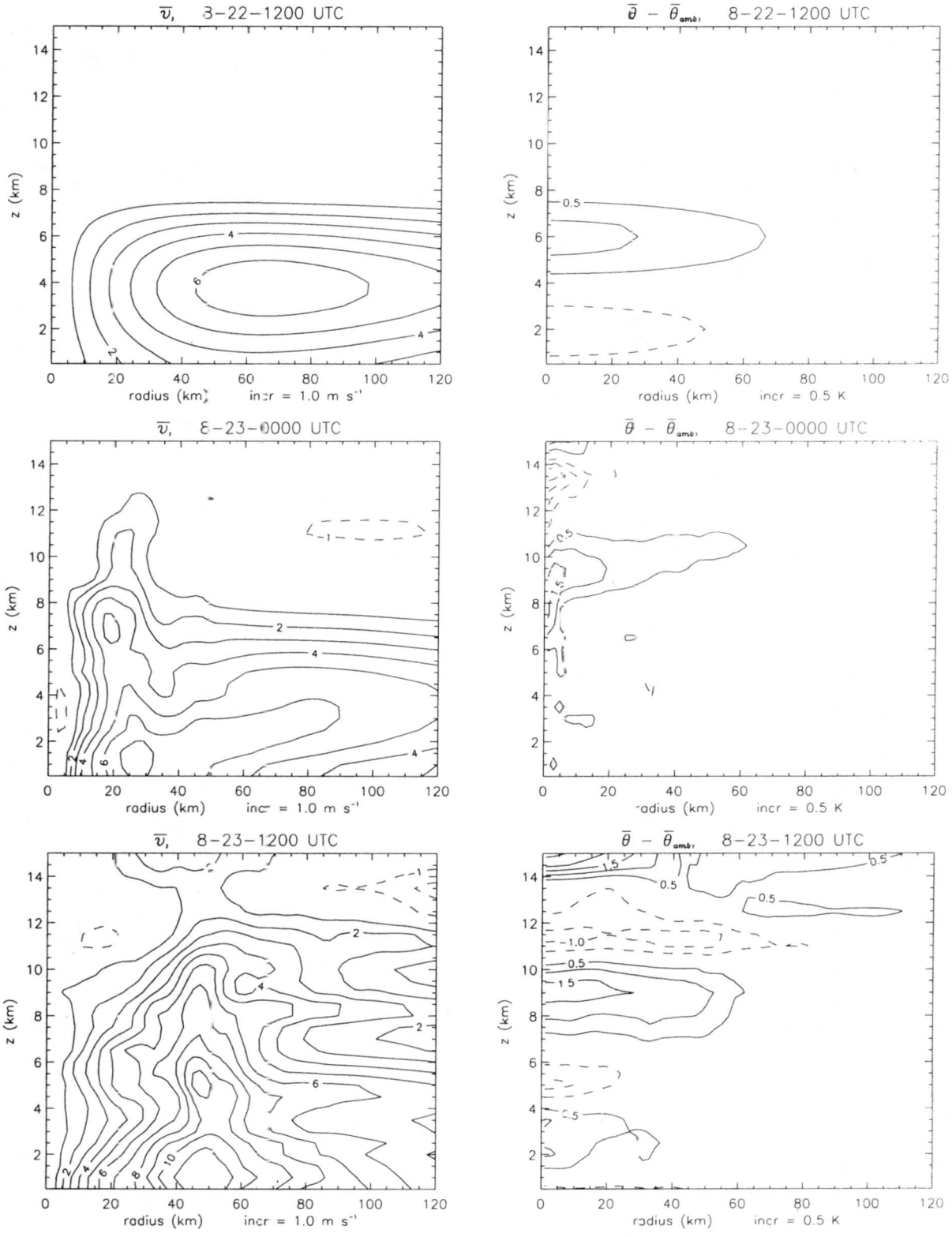

Figure 3.5: Azimuthal averages of tangential velocity and perturbation potential temperature at t = 0 h, 12 h, and 24 h of the RAMS control experiment (Expt. A1, taken from MNCS03).

heat and moisture fluxes from the ocean surface that define WISHE, Molinari et al. (2003) chose to examine near-surface equivalent potential temperature (θ_E) derived from U.S. Air Force reconnaissance flight-level and dropsonde data taken during the storm's evolution. Molinari et al. (2003) defined the 'WISHE stage' as the time when the interior near-surface θ_E values became significantly elevated above the ambient values. They named the time period prior to this θ_E elevation the 'pre-WISHE' phase, and argued that low-level vortex processes such as mergers, alignment, and axisymmetrization dominated this time in Danny's development.

In our study, we examined the θ_E of Bolton (1980) at the lowest vertical model level ($z = 197$ m). The near-surface θ_E values at various times during the control experiment are shown in Figure 3.6. Figure 3.6a shows the θ_E values at $t = 3$ h. At this early time, there is a clear θ_E maximum of approximately 356 K at the center of the domain, largely due to the surface moisture enhancement discussed in Chapter 2. Notice that there also exists a local θ_E minimum (dark green contour $\propto$ 350–352 K) about 30 km to the northeast of the domain center. This minimum region is collocated with the region of initial convective activity (Figure 3.7a), and is thus most likely caused by convective downdrafts. At $t = 15$ h (Figure 3.6b), continued convective downdrafts (Figure 3.7b) have depleted most of the center θ_E maximum, leaving a local minimum at 42 km west and 14 km north of the mesoscale vortex center. Figure 3.8 shows the vertical θ_E profile at the center of this local surface minimum before (solid) and after (dotted) deep convection is active in this region. Before the onset of convection, there exists a sharp maximum in θ_E near the surface. After deep convection passes through this region, the surface θ_E maximum is has been replaced with lower θ_E values comparable to those present at midlevels. This vertical profile suggests that convective downdrafts have transported the low θ_E air at midlevels to the surface. By $t = 24$ h, convective activity is concentrated along an annulus of approximate radius $r = 50$ km (Figure 3.7c), and thus a local θ_E minimum is also located in that region (Figure 3.6c). However, a small local maximum of θ_E reappears near the domain center. Fifteen hours

later, at $t = 39$ h (Figure 3.6d), a strong local θ_E maximum is present. This maximum has θ_E values of 4–10 K larger than the ambient value and is collocated with the center of convection (see Figure 3.7d). It appears evident that at this later time WISHE is fully active. Since there is no indication of elevated θ_E values for $t < 24$ h, WISHE does not appear to exact a major impact on development during this time. We must therefore look to other processes to explain the transition from warm to cold core mesoscale vortex during the first 24 h of our simulation.

3.3.2 Dominant Coherent Structures in 'Pre-Genesis' Environment: Vortical Hot Towers

The pre-genesis time period of our control simulation ($t \leq 24$ h) is characterized by deep convective activity. As Figure 3.7a shows, this convective activity is spatially localized at first. However, as time passes the deep convection assumes a more circular orientation of radius of $r = 50$ km (Figure 3.7b–c) about the domain center.

Figures 3.9, 3.10 and 3.11 show absolute vertical vorticity $f + \zeta$, diabatic heating rate $\dot{\theta}$ and vertical velocity w respectively, at the $z = 1$, 4, and 7 km height levels. A 100×100 km subset centered on the horizontal domain has been chosen so that we may focus on the convectively active region of the simulation at this time. Comparing Figure 3.11 with Figures 3.9 and 3.10 we can see that the deep convective hot towers located to the northwest of the domain center are collocated with anomalously high values of $f + \zeta$ (30–40 $\times 10^{-4}$ s^{-1}) and $\dot{\vartheta}$ (200–280 K h^{-1}). In our control simulation and most of our sensitivity trials, all model-generated deep convective hot towers possess intense cyclonic vorticity in their cores. Using the terminology of HMD03, we will refer to these structures as "vortical" hot towers, or VHTs. We will now take a closer look at the structure and characteristics of VHTs in our simulations.

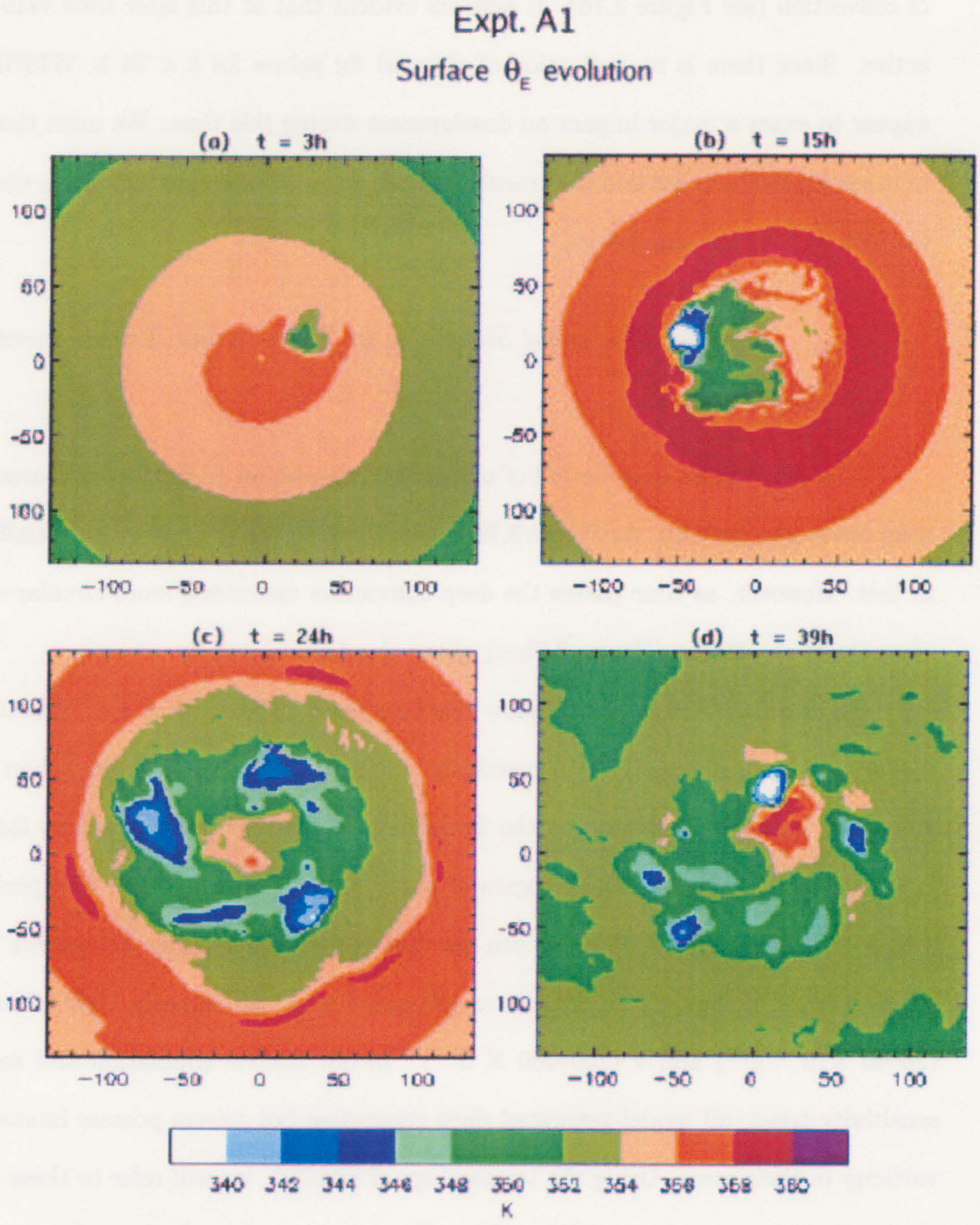

Figure 3.6: RAMS control simulation θ_e near lower surface (z = 197 m) at (a) t = 3 h, (b) t = 15 h, (c) t = 24 h, and (d) t = 39 h. Axes are in km, contour interval is 2 K.

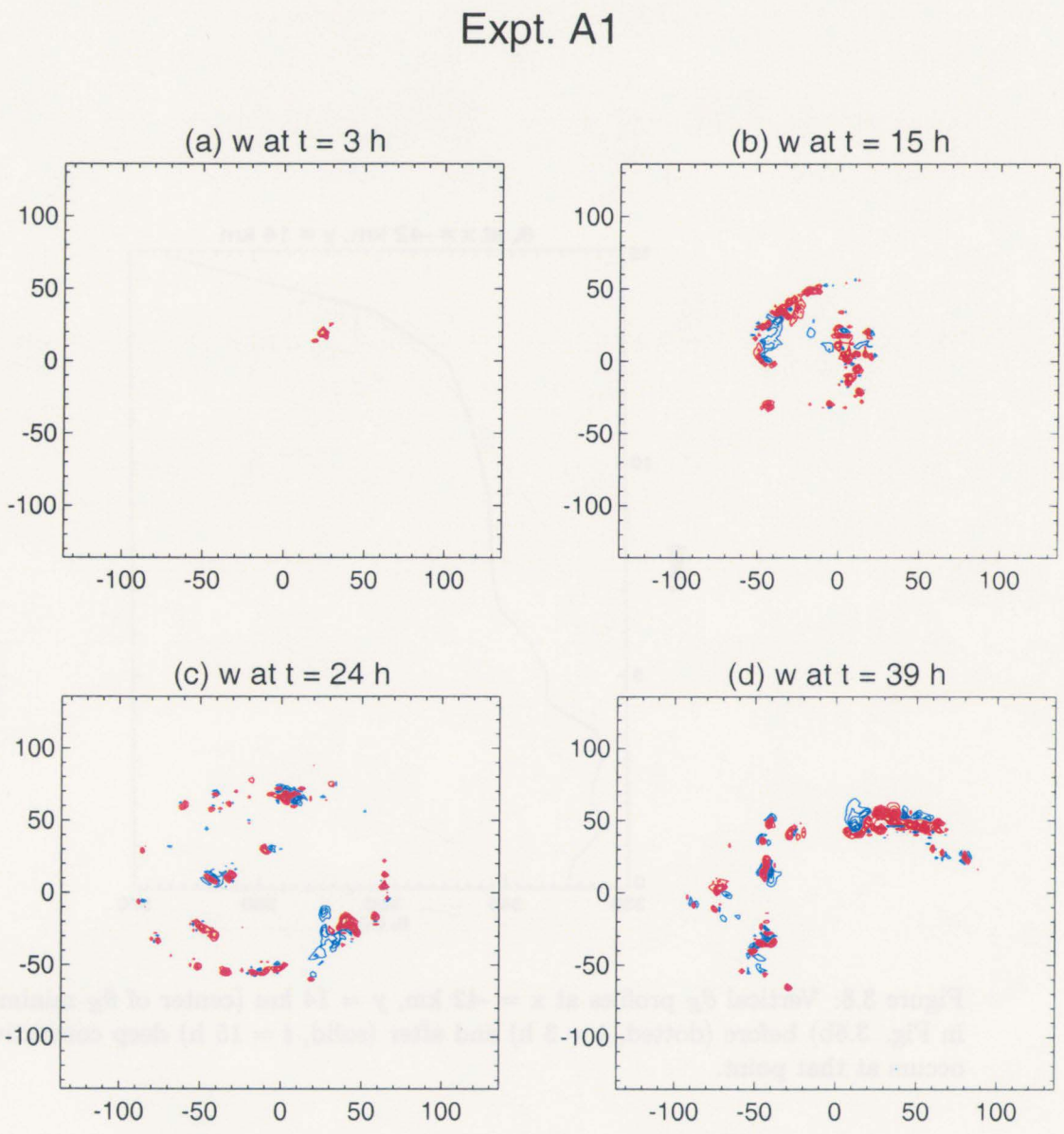

Figure 3.7: RAMS control simulation w at height level $z = 3$ km at (a) t = 3 h, (b) t = 15 h, (c) t = 24 h, and absolute vertical vorticity $f + \zeta$ at (d) t = 39 h. Axes are in km. Red contours are positive, blue are negative, and contour interval is 2 ms^{-1}.

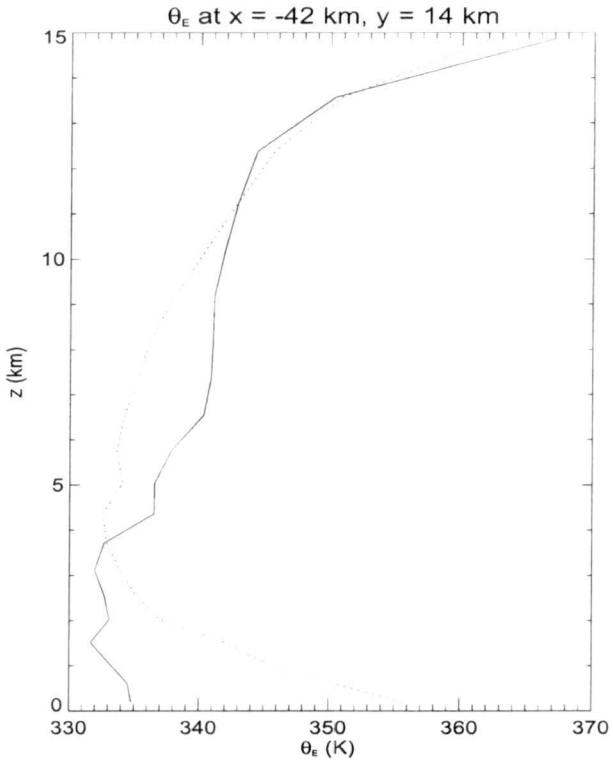

Figure 3.8: Vertical θ_E profiles at x = -42 km, y = 14 km (center of θ_E minimum shown in Fig. 3.6b) before (dotted, t = 3 h) and after (solid, t = 15 h) deep convective activity occurs at that point.

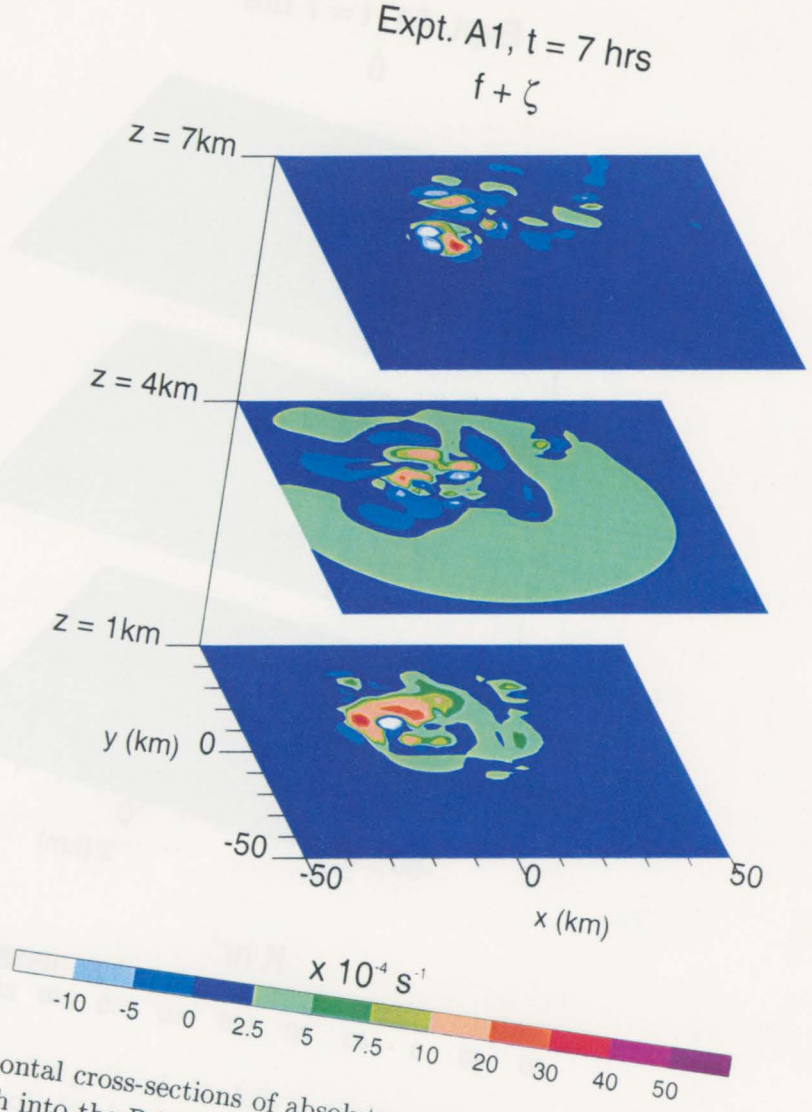

Figure 3.9: Horizontal cross-sections of absolute vorticity (s^{-1}) taken at z = 1 km, 4 km, & 7 km at t = 7 h into the RAMS control simulation.

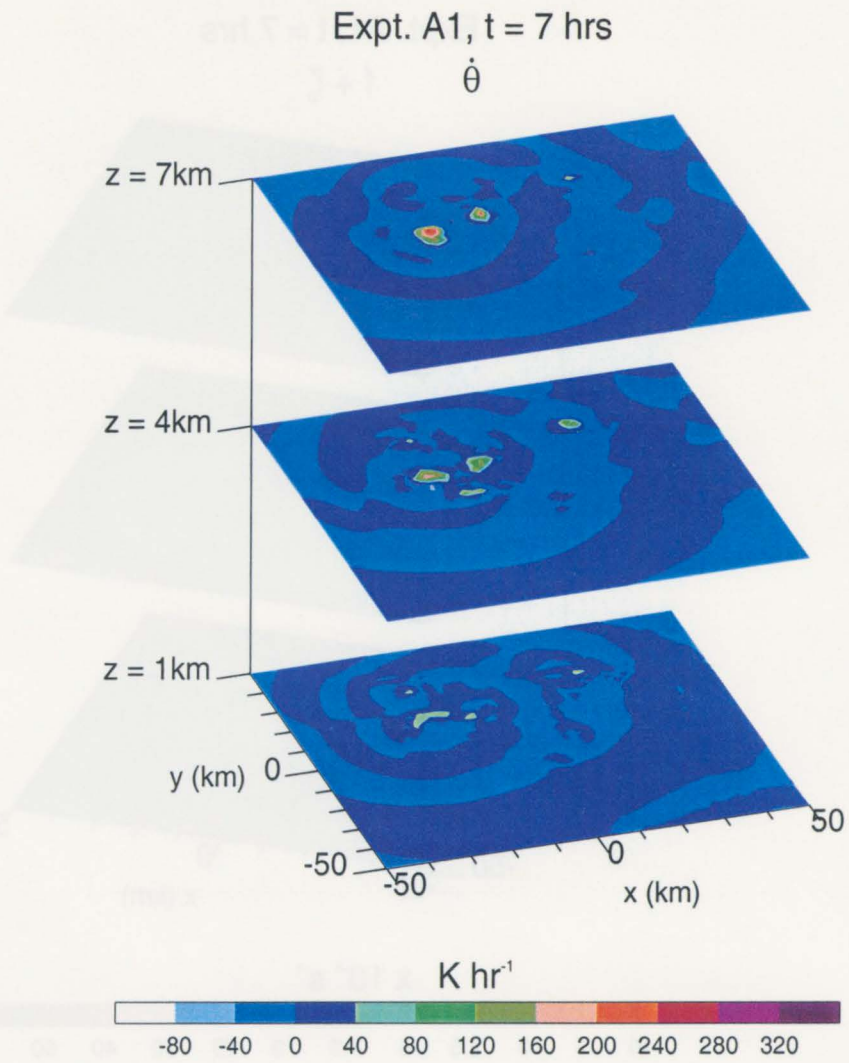

Figure 3.10: Horizontal cross-sections of diabatic heating rate ($\dot{\theta}$, K h^{-1}) taken at $z = 1$ km, 4 km & 7 km at t = 7 h into the RAMS control simulation.

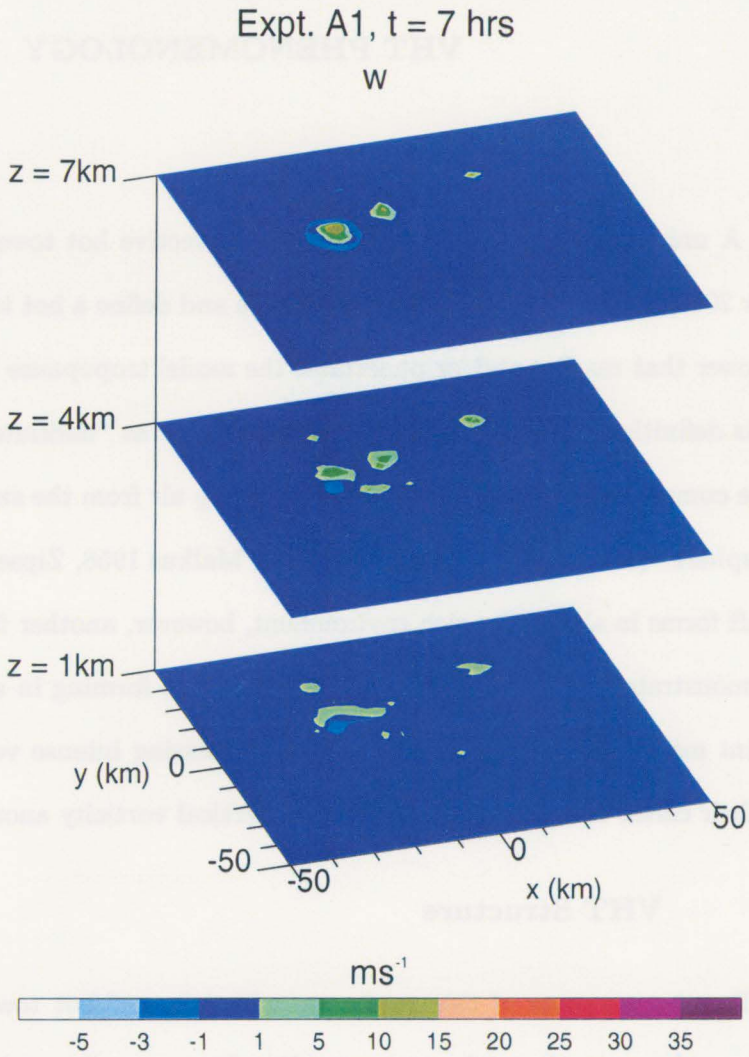

Figure 3.11: Horizontal cross-sections of vertical velocity (w, ms^{-1}) taken at $z = 1$ km, 4 km & 7 km at t = 7 h into the RAMS control simulation.

Chapter 4

VHT PHENOMENOLOGY

A universally-accepted definition of a convective hot tower does not yet exist (e.g., Zipser 2003). Here we follow common practice and define a hot tower as an intense convective tower that reaches and/or penetrates the model tropopause (z $\approx$ 14 km). Elaborating on this definition, J. Simpson referred to hot towers as "undilute or nearly undilute penetrative cumulonimbus clouds that carried high θ_E air from the subcloud layer to the upper troposphere" (Simpson et al. 1998; Riehl and Malkus 1958, Zipser 2003). When an intense updraft forms in a vorticity-rich environment, however, another factor must be considered. As demonstrated by HMD03, convective hot towers forming in a vorticity-rich local environment may be highly vortical in nature, possessing intense vertical vorticity within or near their cores. But how are the low level vertical vorticity anomalies produced?

4.1 VHT Structure

For the purposes of this study, we will define of hot tower by a vertical velocity signature of greater than 1.0 ms^{-1} extending from near the surface (z = 1 km) up to the tropopause (z = 14 km). Based on the vertical velocity values typical of deep convection in our simulations, we will require that this vertical velocity signature obtain a magnitude of at least 10 ms^{-1}. In the control case (Expt. A1), the model-generated updrafts range from 5–20 km in diameter. The average updraft lifespan is on the order of one hour, although individual updrafts have been tracked for as long as 3 h. Many updrafts, but by no means all, are observed to achieve our definition of a hot tower for brief time periods during their

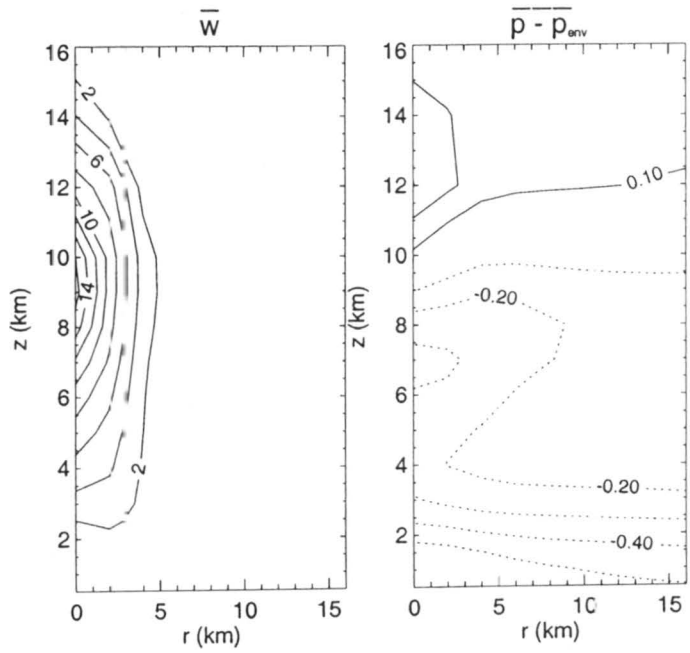

Figure 4.1: Composite plots of azimuthal mean vertical velocity (left, incr = 2 ms^{-1}) and pressure perturbation (right, incr = 0.1 mb).

life cycle, and sometimes reach hot tower status multiple times.

4.1.1 Overview: VHT Azimuthal Mean Structure

It has been noted that the hot towers in our model simulations are closely associated with intense vorticity anomalies. To characterize these structures, we have computed the azimuthal mean values (with respect to the updraft core) of several thermodynamic and kinematic variables for 12 hot towers that occur during the first 12 hours of our control simulation.[1] Azimuthal mean values were taken during each hot tower's peak intensity, which is defined as the time during which inner core vertical velocities reach a maximum. We then averaged these values to generate composites, which are shown in Figures 4.1, 4.2, 4.3 and 4.4. We will now use these composites to describe the main features of VHTs in our control simulation.

[1] We only used VHTs from the first 12 hours of the simulation because during this time, convective activity was more isolated. At later times convective activity spread to cover much of the domain, making it more difficult to identify and isolate individual hot towers.

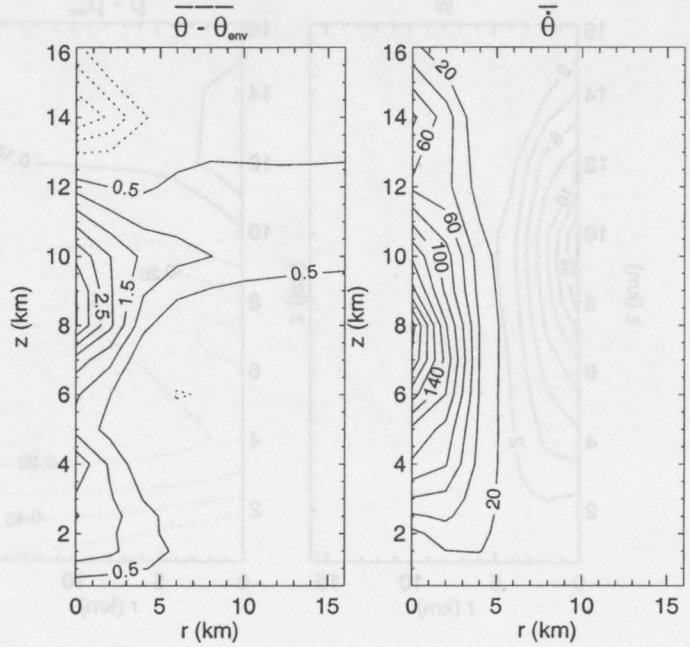

Figure 4.2: Composite plots of azimuthal mean potential temperature perturbation (left, incr = 0.5 K) and diabatic heating rate (right, incr = 20 K hr^{-1}).

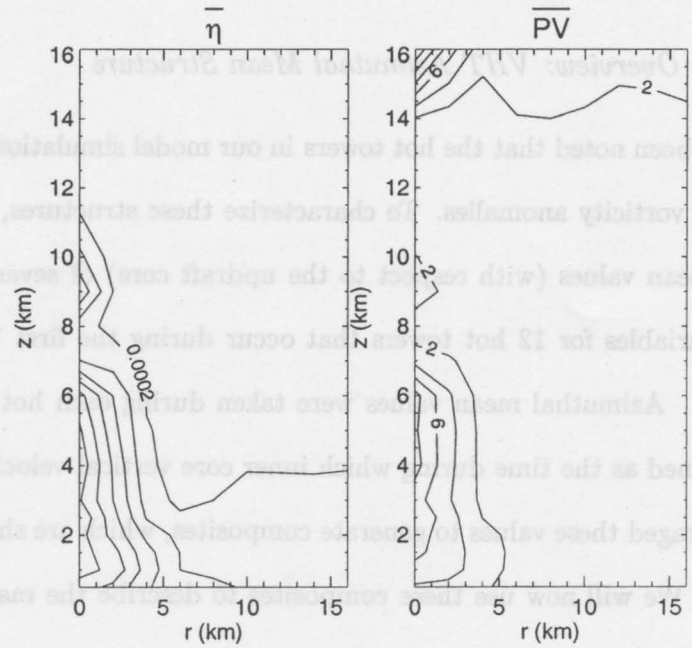

Figure 4.3: Composite plots of azimuthal mean absolute vertical vorticity (left, incr = 0.0002 s^{-1}) and Ertel potential vorticity (right, incr = 2 PVU).

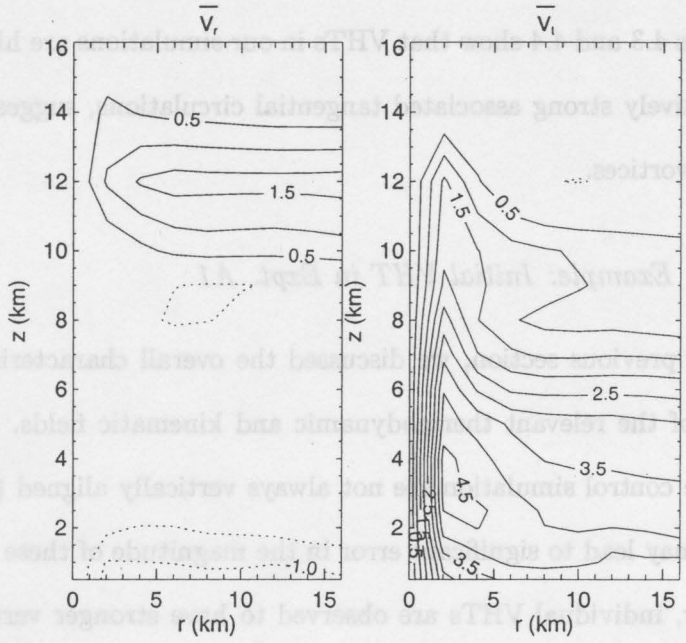

Figure 4.4: Composite plots of azimuthal mean radial (left, incr = 0.5 ms^{-1}) and tangential (right, incr = 0.5 ms^{-1}) velocity.

From Figure 4.1 (left), we can see that our VHT composite achieves a maximum azimuthal mean vertical velocity of 16–18 ms^{-1} at heights z = 9–10 km. Figure 4.2 shows that VHTs possess strong positive potential temperature perturbations of approximately 3.0 K in their cores just below (z = 8–9 km) the height of maximum vertical velocity. Just below the maximum potential temperature perturbation at z = 7–8 km, the diabatic heating rate reaches a maximum value of greater than 200 K h^{-1} within the VHT core.

Figures 4.3 and 4.4 show the azimuthal mean kinematic fields associated with VHTs. Figure 4.3 illustrates the large absolute vertical vorticity (left) and dry Rossby-Ertel PV (right) present within hot tower cores, justifying the term "vortical" hot tower. The azimuthal mean absolute vertical vorticity attains core values on the order of 10^{-3} s^{-1}, with a maximum at low levels. This maximum value represents an average, with individual hot towers possessing maximum η values of 30–40 $\times 10^{-4}$ s^{-1}. Similarly, azimuthal mean PV attains maximum values of 8–10 PVU . Along with the strong positive vorticity anomalies within their cores, VHTs exhibit significant tangential circulations (Figure 4.4, right)

accompanied by radial inflow at low levels and outflow near the tropopause (Figure 4.4, left). Figures 4.3 and 4.4 show that VHTs in our simulations are highly locally vortical and possess relatively strong associated tangential circulations, suggesting that VHTs behave as coherent vortices.

4.1.2 Example: Initial VHT in Expt. A1

In the previous section, we discussed the overall characteristics of VHTs based on composites of the relevant thermodynamic and kinematic fields. However, the fact that VHTs in the control simulation are not always vertically aligned (to be discussed later in Chapter 7) may lead to significant error in the magnitude of these azimuthal mean values. In particular, individual VHTs are observed to have stronger vertical velocities, diabatic heating rates and vorticity values in their cores than is represented by our composite plots. In order to illustrate the complexity of the VHTs' 3-dimensional structure, we will now look in detail at the first VHT to form in Expt. A1.

The first updraft appears at approximately 20 minutes into the simulation (Fig. 4.5a). It achieves hot tower status at $t = 40$ minutes, extending vertically to $z = 16$ km and with a maximum vertical velocity of 33 ms^{-1} at $z = 10$ km (Fig. 4.5b). This is twice the maximum value represented in the azimuthal mean composite in Figure 4.1. This initial updraft's lifetime spans roughly 2 h. As Fig. 4.5b shows, a dipole of anomalous absolute vertical vorticity, η, is generated by the initial updraft. A similar dipole structure is evident in PV (not shown). As this updraft attains hot tower status at 40 minutes, the positive portion of the vorticity dipole structure attains values on the order of 10^{-3} s^{-1} within the model troposphere. This anomalous cyclonic vorticity is significantly larger than that of the local environment just prior to the formation of this updraft. For instance, at $z = 9$ km the vertical vorticity at $t = 0$ minutes is 3.8×10^{-5} s^{-1} in the vicinity of the initial updraft. Forty minutes later, the convectively-generated vorticity maximum at that same level is 4.8×10^{-3} s^{-1}, more than 100 times the preconvective value. In general, the VHT-

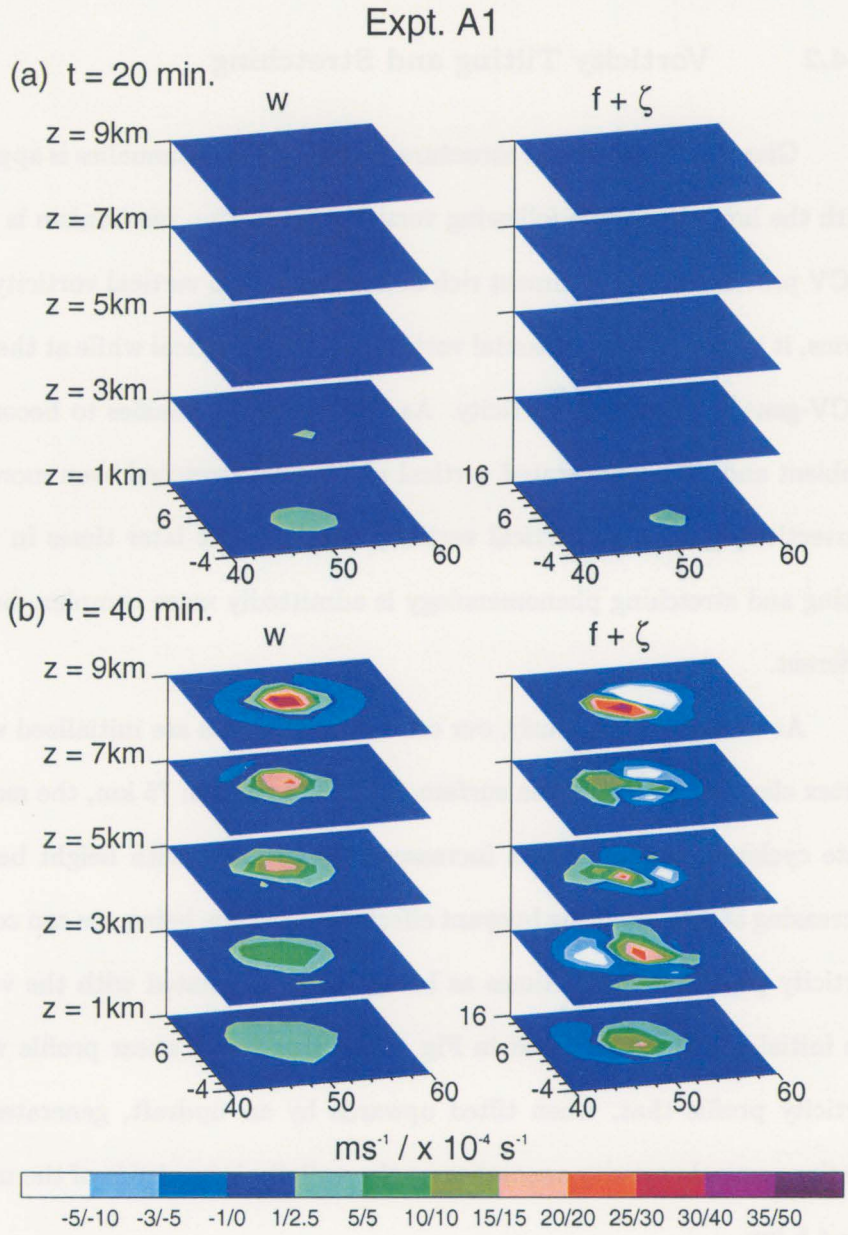

Figure 4.5: Example vertical velocity w (m s^{-1}) and absolute vertical vorticity η ($\times$ $10^{-4}s^{-1}$) signatures associated with deep cumulus convection in the RAMS numerical model at (a) t = 20 min., and (b) t = 40 min. into the control experiment (Expt.1). Horizontal cross-sections are 20 km $\times$ 20 km subdomains centered at (a) $x = 50$ km, $y = 4$ km, and (b) $x = 50$ km, $y = 6$ km.

related vorticity anomalies range from 3 to 100 times larger than the vorticity of their local environment.

4.2 Vorticity Tilting and Stretching

Given that the dipolar structure of the vorticity anomalies is approximately collocated with the hot towers, the following vorticity generation mechanism is proposed: The initial MCV provides an environment rich in horizontal and vertical vorticity. As the first updraft forms, it tilts ambient horizontal vorticity into the vertical while at the same time stretching MCV-generated vertical vorticity. As the updraft intensifies to become a hot tower, both ambient and tilting-generated vertical vorticity is stretched even more, leading to a strong convectively-generated vertical vorticity anomaly. At later times in the simulation(s) the tilting and stretching phenomenology is admittedly more complex, but not fundamentally different.

As described previously, our control simulations are initialized with a weak mid-level vortex elevated above the sea surface. At radii less than 75 km, the main vortex has a basic state cyclonic wind field that increases in magnitude with height below $z = 4.5$ km and decreasing above. Ignoring buoyant effects for the time being, we can consider the horizontal vorticity profile at initial times as being solely associated with the vertical wind shear of the initial MCV. As sketched in Fig. 4.6, this vertical shear profile will generate a radial vorticity profile that, when tilted upwards by an updraft, generates negative (positive) relative vertical vorticity anomalies on the radially-inward side of the updraft below (above) $z = 4.5$ km.

As positive vertical vorticity is generated in the region of an updraft, vortex tube stretching further intensifies the positive vorticity anomaly. Returning to Fig. 4.5b, we can see that the VHT's vorticity dipole structure exhibits this orientation and magnitude difference, supporting our mechanism. Unlike the tilting term, however, the intensification of vertical vorticity by stretching can be exponential if the convergence is approximately

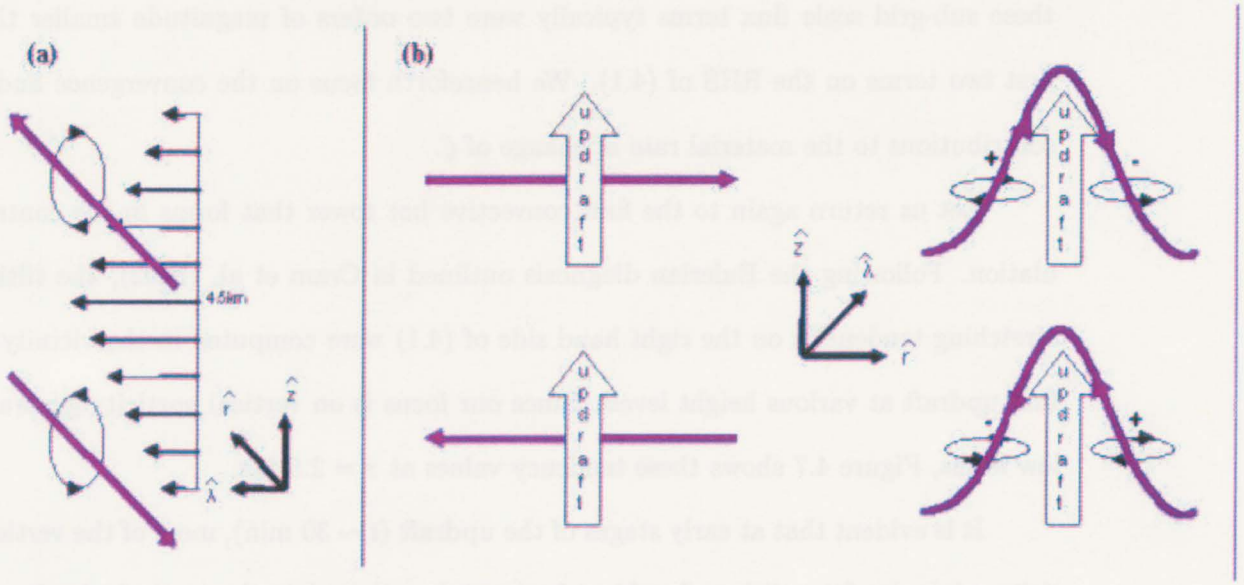

Figure 4.6: Schematic of vortex tilting within the initial MCV. Purple lines represent vortex filaments. (a) Radial vorticity generated by vertical shear profile of initial MCV. (b) Updraft tilts radial vortex filament upward, generating a vertical vorticity dipole with negative relative vorticity radially inward (outward) at heights below (above) $z = 4.5$ km.

constant during the parcel's ascent through the tower.

Let us now look more closely at the two main mechanisms of vertical vorticity generation and their respective expected contributions. Recall the equation for the material rate of change of vertical vorticity (Eqn 4.16 of Holton 1992):

$$\frac{D\zeta}{Dt} = -(f+\zeta)\left(\frac{\partial u}{\partial x}+\frac{\partial v}{\partial y}\right) - \left(\frac{\partial w}{\partial x}\frac{\partial v}{\partial z} - \frac{\partial w}{\partial y}\frac{\partial u}{\partial z}\right) + \frac{1}{\rho^2}\left(\frac{\partial \rho}{\partial x}\frac{\partial p}{\partial y} - \frac{\partial \rho}{\partial y}\frac{\partial p}{\partial x}\right) + \frac{\partial F_y}{\partial x} - \frac{\partial F_x}{\partial y}, \tag{4.1}$$

where ζ is the relative vertical vorticity. The terms on the right-hand side of this equation represent contributions to the material rate of change of ζ due to horizontal convergence, tilting, solenoidal effects, and sub-grid scale flux derivatives, respectively. The RAMS model (and other cloud models we are aware of) disallows any contribution from the 3rd term on the RHS of (4.1). We furthermore ignore the x and y components of the sub-grid scale terms, given by the vertical component of the curl of the turbulent flux terms in the horizontal momentum equations. Justification of this assumption is based on Cram et al. (2002), where an analysis of a RAMS simulation of a convective line with $f = 0$ found

these sub-grid scale flux terms typically were two orders of magnitude smaller than the first two terms on the RHS of (4.1). We henceforth focus on the convergence and tilting contributions to the material rate of change of ζ.

Let us return again to the first convective hot tower that forms in the control simulation. Following the Eulerian diagnosis outlined in Cram et al. (2002), the tilting and stretching tendencies on the right hand side of (4.1) were computed in the vicinity of this first updraft at various height levels. Since our focus is on vertical vorticity generation at low levels, Figure 4.7 shows these tendency values at $z = 2.5$ km.

It is evident that at early stages of the updraft ($t \sim 30$ min), most of the vertical vorticity originates from tilting of ambient horizontal vorticity into the vertical. As the updraft continues to evolve, however, stretching of vertical vorticity starts to dominate. Qualitatively, these results are similar to those found for intense convection within a (midlatitude) mesoscale convective line as simulated by Cram et al. (2002)[2] .

4.3 VHTs as Convective-Scale Vortices

We have provided an explanation as to why we would expect deep convective hot towers in an MCV environment to possess substantial vorticity values near their cores. We will now consider how this vorticity modifies the behavior of VHTs in our model environment.

4.3.1 VHT Mergers

Given their substantial vorticity values and induced tangential circulation, VHTs may be thought of as coherent convective-scale vortices. As such, we would expect to see vortex-vortex interactions occurring between VHTs. Various interactions, such as VHT merger events, are observed to occur throughout the simulation time period. They are particularly abundant at $t \geq 24$ hours, when convective activity extends over a large portion of the domain. This is a consequence of the fact that more VHTs within the domain leads to a

[2] A Lagrangian vorticity analysis following moist air parcels as they ascend the convective updrafts confirms the basic picture portrayed here using the Eulerian vorticity tilting and stretching tendencies (L. Trenary, personal communication).

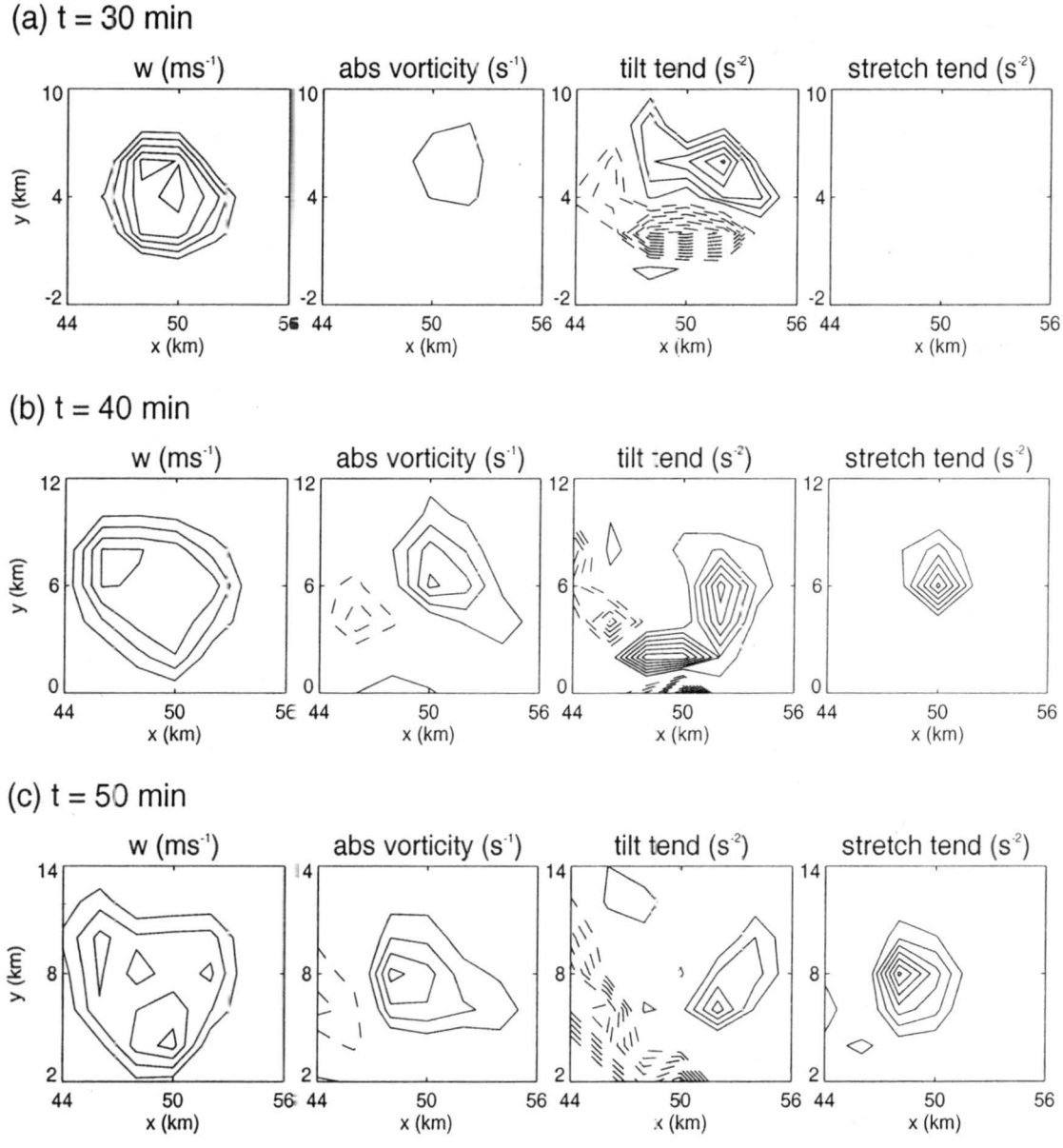

Figure 4.7: Model vertical velocity (w, m s^{-1}, contour interval 2 m s^{-1}) and absolute vertical vorticity η (contour interval 5 $\times$ 10^{-4}s^{-1}) for the RAMS control experiment (but using $\delta x = \delta y = 3$ km) along with the instantaneous contributions of the tilting and stretching terms (contour interval 1 $\times$ 10^{-6}s^{-2}) in the equation for the material rate of change of vertical vorticity at (a) t = 30 min, (b) t = 40 min., (c) t = 50 min. into the simulation. Values are shown for a 20 km $\times$ 20 km horizontal subdomain centered about a vortical hot tower, at height $z = 3$ km.

higher probability of VHTs coming into contact with each other, which in turn increases the probability of vortex interactions.

MNCS03 examines one such merger event, occurring between $t = 6$ h 40 min and $t = 7$ h 20 min. MNCS03 notes that the dry Rossby-Ertel PV at $z = 1$ km increases from approximately 18 PVU to 28 PVU over the time and domain of the merger event. Furthermore, in looking at the azimuthally averaged PV before and after the merger event, MNCS03 notes that the low level azimuthal mean PV increases from 13 PVU to 40 PVU during this time. We will now show examples of merger events occurring before (Merger 1) and after (Merger 2) the merger event described in MNCS03.

Figure 4.8 shows a VHT merger event that occurs just before the merger examined in MNCS03. This event occurs between $t = 5$ h 50 min and $t = 6$ h 30 min, and will be referred to as Merger 1. In this example, the convective-scale PV anomalies are observed to merge at $z = 1$ km and $z = 3$ km. At $z = 3$ km, the merger results in a PV anomaly that is stronger than either of the pre-merger anomalies, whereas the PV anomaly that results from the merger at $z = 1$ km is of smaller magnitude than the stronger original PV anomaly. Results presented in MNCS03 suggest that merger events result in merger PV anomaly of greater magnitude than either of the individual VHT anomalies. This example appears to contradict this assertion. Notice, however, that a third PV anomaly is approaching the merged structure during Merger 1. By $t = 6$ h 30 min, this second PV anomaly is of similar magnitude to the merged structure and is located 10–15 km to the southwest. Approximately 10–20 min later the merged and approaching PV anomalies go through a subsequent merger of their own, which is the merger event studied in MNCS03. This observed decrease in PV after Merger 1 may in fact be due to the fact that this merging complex appears to begin merging with a third PV anomaly before it has completed it's own merger. This example demonstrates the complexity of VHT interactions observed in our simulations. Vortex interactions of various types, including partial and complete mergers, are observed to occur frequently throughout the simulation.

Figure 4.9 shows another example of vortex merger (Merger 2) that occurs shortly after that of MNCS03. This example shows a complete merger of the two PV anomalies at $z = 1$ km, while the associated anomalies at $z = 3$ km do not merge. In this case, the merger at $z = 1$ km results in a merged PV anomaly of greater magnitude (40 PVU) than either of the pre-merger anomalies. This result is consistent with those discussed in MNCS03.

4.3.2 Advection of VHTs

Vortical hot towers are generally not advected with the local flow as passive scalars. The updraft cores associated with the VHTs are found to rotate about the MCV at approximately 0.6–0.9 times the local azimuthal mean tangential velocity. This phenomenon has also been observed for eyewall mesovortices in the 1.3 km horizontal grid spacing simulation of Hurricane Bob (1991)(Fulton 2001) and the 2.0 km horizontal grid spacing simulation of Hurricane Bonnie (1998) (Braun et al. 2003). Together, these findings suggest that the vorticity towers in the high vorticity region of the seedling storm, and the intense updrafts that support them, behave in some ways like Rossby solitons (e.g. Nezlin and Snezhkin 1993; Montgomery and Kallenbach 1997). A future analysis of the VHTs from this perspective might prove insightful.

4.4 Summary of Hot Tower Vorticity Dynamics

In the presence of modest low-level vertical vorticity (arising here from the initial MCV), a single convective hot tower can generate a vertical vorticity anomaly that is an order of magnitude greater than the ambient vertical vorticity within a time span of 20 min. The behavior of deep convective towers is believed to modify their behavior, as evidenced by the tendency for VHTs to undergo vortex-vortex interactions and retrograde with respect to the mean circulation. Although the specific details are likely to be somewhat resolution dependent until truly cloud resolving scales are attained (Bryan et al. 2003), and while some

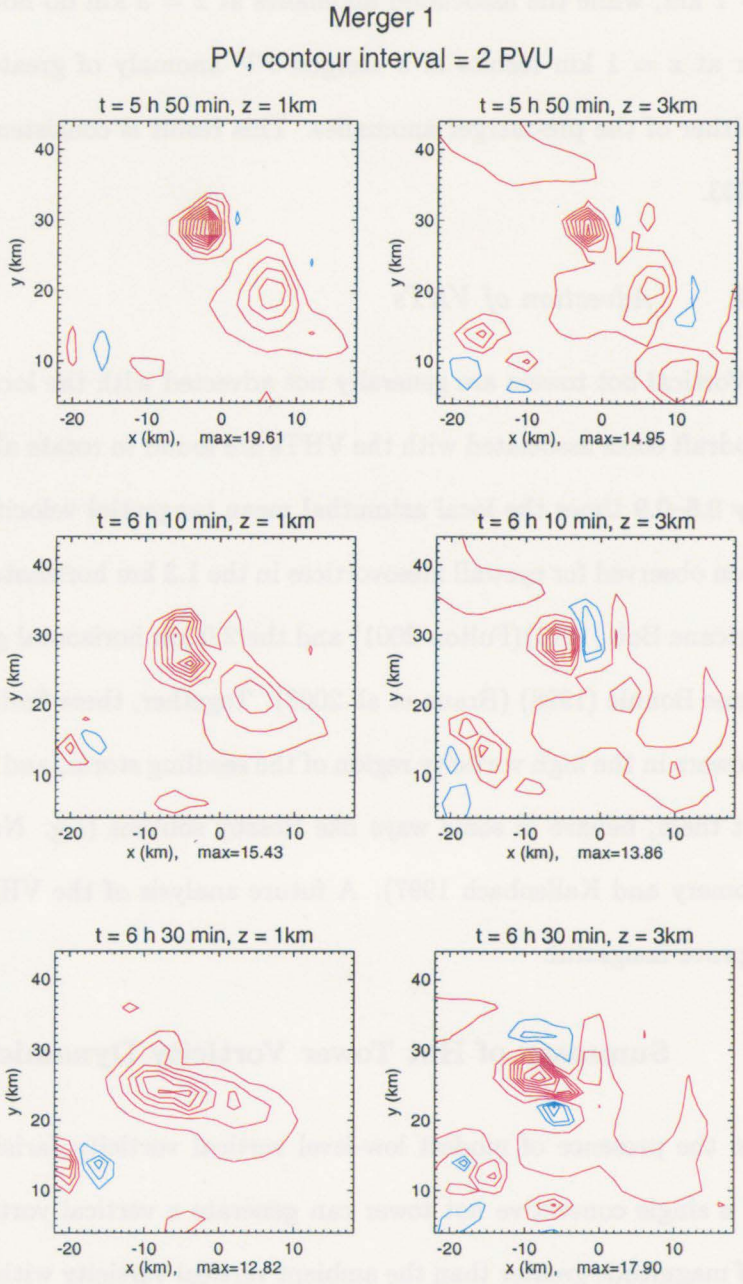

Figure 4.8: Dry Ertel potential vorticity, PV, at heights $z = 1$ km (left) and $z = 3$ km (right) at times before (top), during (middle), and after (bottom) merger event. Red contours are positive, blue contours are negative, and the contour interval is 2 PVU.

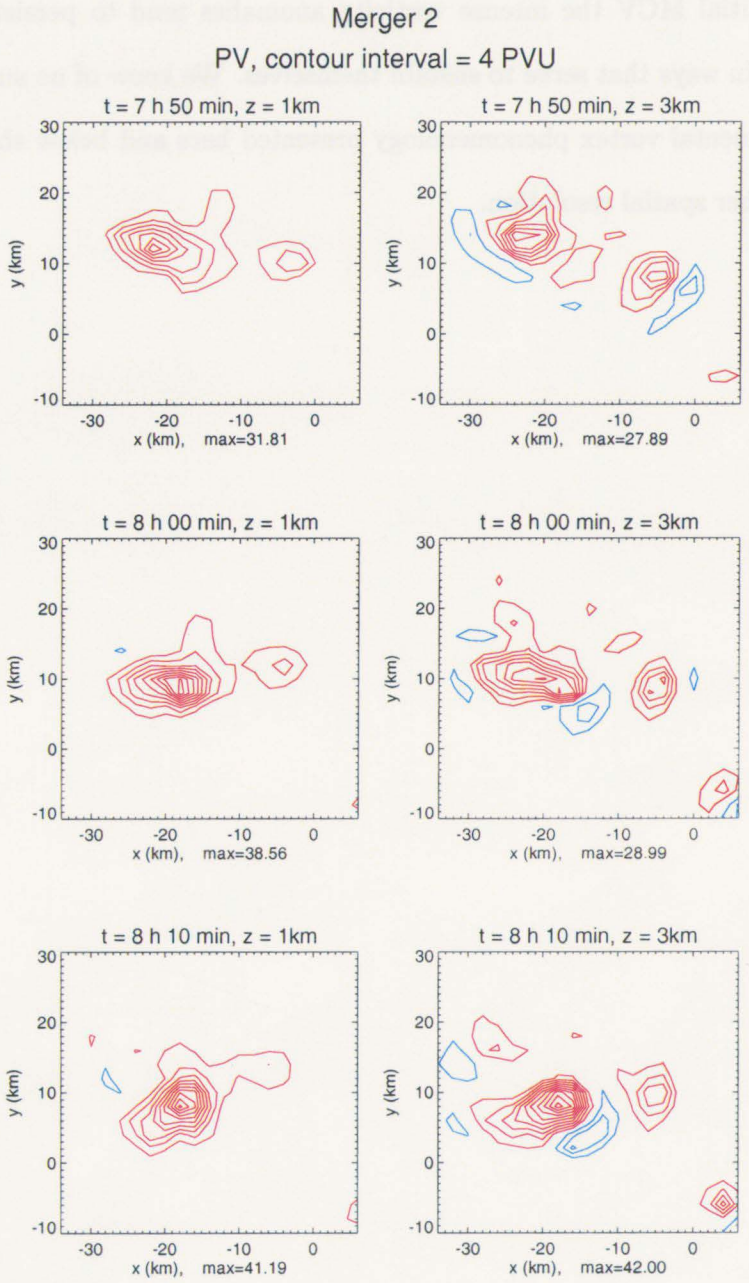

Figure 4.9: Dry Ertel potential vorticity, PV, at heights $z = 1$ km (left) and $z = 3$ km (right) at times before (top), during (middle), and after (bottom) merger event. Red contours are positive, blue contours are negative, and the contour interval is 4 PVU.

of the simulated convective vorticity anomalies are spatially small ($\sim$ 5 - 10 km - arguably not well resolved here), it will soon be shown that within the protected environment of the initial MCV the intense vorticity anomalies tend to persist and interact with each other in ways that serve to sustain themselves. We know of no substantive reason why the fundamental vortex phenomenology presented here and below should change significantly at higher spatial resolution.

Chapter 5

HOW DO VHTS CONTRIBUTE TO 'SYSTEM-SCALE' SPIN UP?

To understand the role deep convective hot towers play in the transformation from a midlevel circulation to a surface-concentrated tropical depression, we must understand the relationship between deep convection and the mesoscale circulation. We will begin by demonstrating the existence of a statistically significant correlation between deep convective activity and changes in the mesoscale circulation.

5.1 Correlation Between Deep Convection and Re-Intensification of Midlevel MCV

Although a topic of much research interest over the last several decades, the exact nature of the relationship between a long-lived MCV and associated deep convective outbreaks is not well understood. MCVs are believed to form in the stratiform precipitation region of MCSs (Johnston 1981). Observations suggest that MCVs may last several days after the dissipation of the parent MCS, and are linked to future convective outbreaks. Raymond and Jiang (1990) present a mechanism whereby a midlevel potential vorticity anomaly leads to an upward bulge in the underlying isentropes. Given a suitable relative shear profile, this can lead to isentropic ascent at low levels below the PV anomaly, which in turn will lead to convection if the isentropic ascent surpasses the level of free convection. Fritsch et al. (1994) confirmed this mechanism in studying a long-lived MCS that tracked across the United States.

Although MCVs are believed to owe their existence to the heating profile of the strati-

form precipitation region, deep convective activity may also have an effect on these midlevel circulations. Deep convection is associated with large diabatic heating rates throughout much of the troposphere, owing in large part to the release of latent heat. Although not confined to midlevels, this heating is substantial in the middle to upper troposphere and may have a significant impact on the strength and structure of the midlevel MCV.

Based on observations of a long-lived MCS that developed over NE Colorado and propagated eastward over the US Great Plains and Midwest, Rogers and Fritsch (2001) proposed a mechanism whereby convective heating can affect the intensity and vertical extend of a midlevel MCV. Although not the main focus of their paper, Rogers and Fritsch (2001) presented observational evidence suggesting a relationship between deep convective events and intensification of the midlevel MCV. They observed periods of MCV intensification approximately 4 hours after deep convective episodes. A previous study by Zhang and Fritsch (1987) found similar correlations in midlatitude MCVs, with midlevel intensification lagging deep convection by 4–8 hours.

A similar phenomena was observed in our model results in the time period before tropical storm intensity was reached. Analysis of the azimuthal tangential wind fields revealed multiple re-intensifications of the midlevel circulation. Even after the development of a tangential wind maximum at the surface, secondary maxima in the mean tangential wind field would occasionally appear at middle to upper levels. Similar behavior was observed in independent RAMS simulations of Hurricane Dolly (L. Trenary 2003, personal communication). We will now use a simple statistical analysis to investigate the link between deep convective outbreaks and subsequent midlevel MCV intensification in the tropical MCV simulations of MNCS03.

Given the convectively-favorable initial conditions, the control simulation develops into a tropical storm in a short amount of time. By $t = 24$ hrs, the azimuthally averaged tangential velocity exceeds 12 ms^{-1} at the surface. As discussed previously, once the surface winds reach a threshold velocity the WISHE mechanism is activated. This mechanism is

believed to play a crucial role in tropical storm intensification. In order to exclude the potentially complicated scale interactions this mechanism may bring, we will only look at time periods before the onset of WISHE for this analysis. We chose the beginning of each time series to be at the first instance of deep convective activity. The end of the time series was defined by the onset of the WISHE phase, using the same method of diagnosis via near-surface θ_E values as outlined in Chapter 3. These restrictions leave a relatively short time period suitable for studying convective cycles in Expt. A1. In order to lengthen our observational time period, we will focus on three sensitivity runs that develop more slowly than the control. For consistency, we will utilize the experiment naming scheme of MNCS03 (see Appendix C).

Each sensitivity trial is identical to the 3 km horizontal resolution control simulation (Expt. A2), with the exception of a single parameter that has been changed. The first, called Expt. B1, has initial conditions identical to the control without the presence of an initial surface warm bubble to stimulate convection. This case does not experience any significant convective activity until about $t = 13$ h. At this time, frictional convergence leads to a ring-shaped convective outbreak, and the system proceeds to develop in a similar fashion as the control, with the onset of WISHE occurring by $t = 27$ h. The second case, called Expt. B4, has lower surface-based CAPE values than the control. This is achieved by increasing the temperature at upper levels by about 2 K. This case develops into a tropical storm at around $t = 60$ h, with the onset of WISHE appearing at $t = 24$ h. The third case, Expt. B5, is initialized with SSTs of 26 degrees C (versus control value of 29 degrees C). This is the slowest case to develop, failing to development a WISHE signature in the near-surface θ_E values by $t = 72$ h.

5.1.1 Definition of Time Series

In order to perform a simple correlation analysis, we needed to generate two time series from our three-dimensional data: one series representing deep convective activity and

the other representing the intensity of the midlevel MCV. Previous analysis found that the typical convective hot tower is 5–20 km in diameter, achieves maximum vertical velocity values of up to 35 ms^{-1} in its core, and penetrates up to or beyond the model tropopause (at $z = 14$ km). Although convective characteristics vary between each of our sensitivity cases, the qualitative aspects of deep convection are found to be robust. Here we define deep convective "events" as local maxima in total number of model grid points possessing a deep convective signature. In order to parameterize deep convective events, we chose to count the number of grid points at an upper-tropospheric level, z_T, that meet or exceed a threshold vertical velocity value, w_T. We will call this value the deep convection parameter, DCP. The results reported here[1] are for $z_T = 10$ km and $w_T = 10$ ms^{-1}.

In defining a quantity that describes the intensity of the midlevel MCV, we chose to use depth-integrated circulation. Our MCV intensity parameter, MVP, is defined as the radial mean of the depth-integrated circulation, $\Gamma_{DI}(r)$, which is defined by

$$\Gamma_{DI}(r) = \int \Gamma(r,z)dz \tag{5.1}$$

Given our interest in changes occurring at midlevels, this integral is taken over $z = 3$–8 km. The circulation Γ is computed assuming axisymmetry in the wind fields so that $\Gamma(r,z) = 2\pi r\bar{v}_t$. Finally, the radial mean is taken from $r = 30$–75 km in order to capture only circulation changes characteristic of the system scale. MVP has been normalized by the total volume over which the depth-integrated circulation is computed.

5.1.2 Correlation Analysis

Before discussing the results of our statistical analysis, we first step back and examine the validity of the MVP parameter. Figures 5.1 through 5.3 shows the raw time series for both our parameters in each case. The original motivation for this study was based on subjective analysis of the azimuthal mean tangential wind fields. Periods of the observed

[1] Values of $z_T = 6$ km and $w_T = 2$, 6, and 16 ms^{-1} were also used. Although the shape of individual peaks in the DCP time series did change, the overall shape of the series as well as the correlation results did not change significantly.

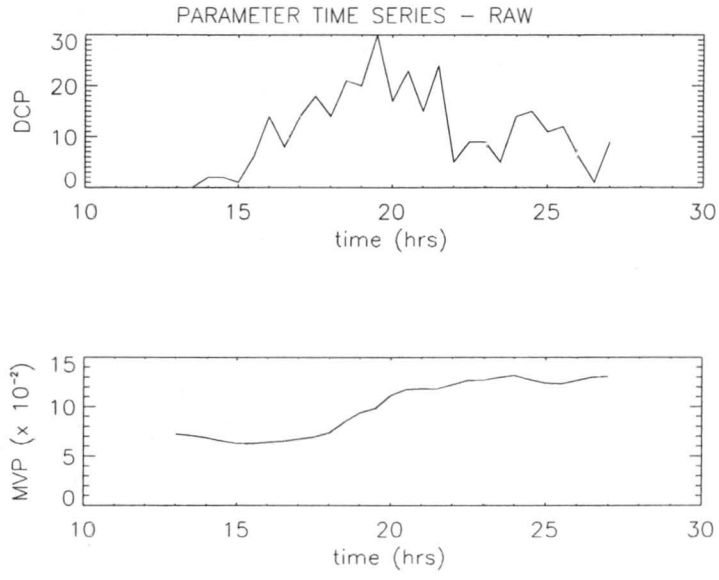

Figure 5.1: Experiment B1: time series for DCP (top) and MVP (bottom).

midlevel re-intensification are indicated on the MVP time series plots by an orange line. Notice that the orange lines match relatively well with local maxima in the MVP parameter. Although somewhat crude, this check confirms that the observed MCV intensifications are well represented by MCP.

In looking at the raw data series (see Figures 5.1 through 5.3), we can see that peaks in DCP are of higher amplitude than those in the MVP data series. Also, it appears that several of the peaks in MVP occur a few hours after peaks in DCP. This suggests that there may indeed be a correlation between deep convection and midlevel MCV intensification in the model, with the former leading the latter by a few hours. To test this hypothesis, we computed the correlation coefficients for both the raw and linearly detrended data series at time lags ranging from -15 to +15 hours, where a negative (positive) time lag value implies that MVP leads (lags) DCP. The detrended time series are presented in Figures 5.4 through 5.6 and the lagged correlation coefficients are presented in Figures 5.7 through 5.9. Notice that each of the correlations reaches a maximum at lag values of 2–4 h, implying that the correlation is the strongest when MVP lags DCP by 2 to 4 h. The Student's t

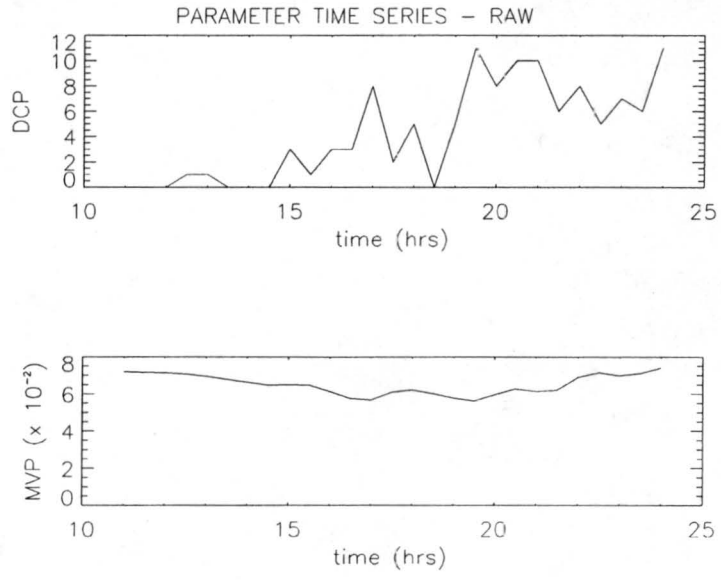

Figure 5.2: Experiment B4: time series for DCP (top) and MVP (bottom).

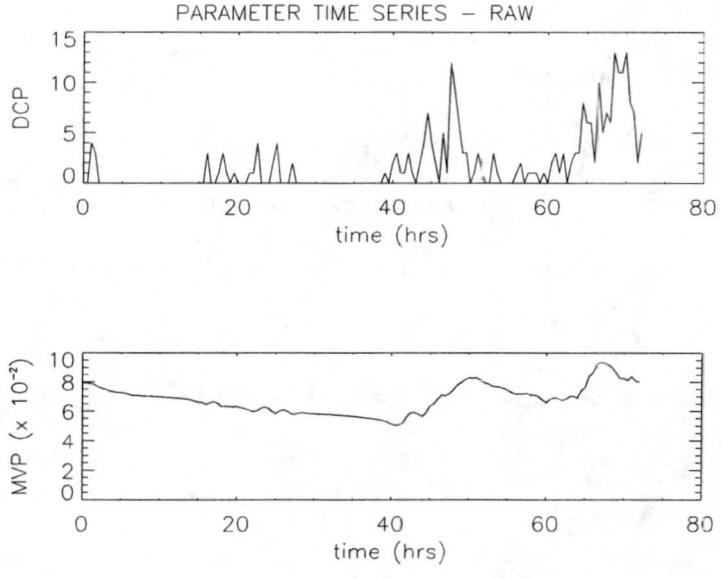

Figure 5.3: Experiment B5: time series for DCP (top) and MVP (bottom).

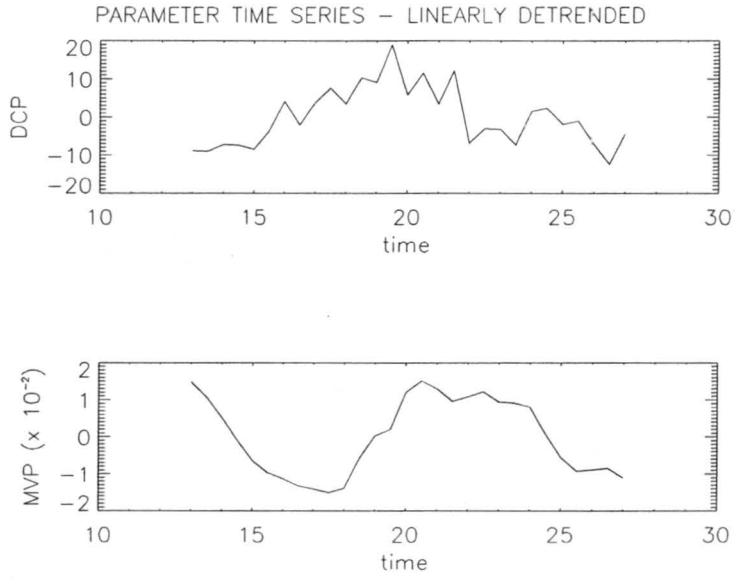

Figure 5.4: Experiment B1: linearly detrended time series for DCP (top) and MVP (bottom)

test was used to assess the significance of these correlations. The correlation coefficient, R, corresponding to a 95 percent confidence level is represented by a dotted line on each correlation plot. We can see that the peaks of Expt. B1 and Expt. B5 lie within the 95 percent confidence range.

It should be noted that the w_T selected in the definition of DCP influences the number of degrees of freedom in our analysis. As we increase the w_T value that defines 'deep convection,' we will decrease the persistence of the DCP time series. This is caused by the decreased time period during which a convective plume will be considered 'deep convection.' On the other hand, if w_T is set low a hot tower may be counted as 'deep' over several hours. However, as w_T is increased, this time period is limited to the time when the hot tower is at its strongest intensity, which may only last for a half an hour. Hence, as we increase the value of w_T, we will increase our degrees of freedom of our DCP time series, which in turn increases the degrees of freedom used in our Student's t calculation.

Given the realization that our 95 percent confidence levels are somewhat arbitrary, we cannot say with certainty that these correlation values are significant. However, a

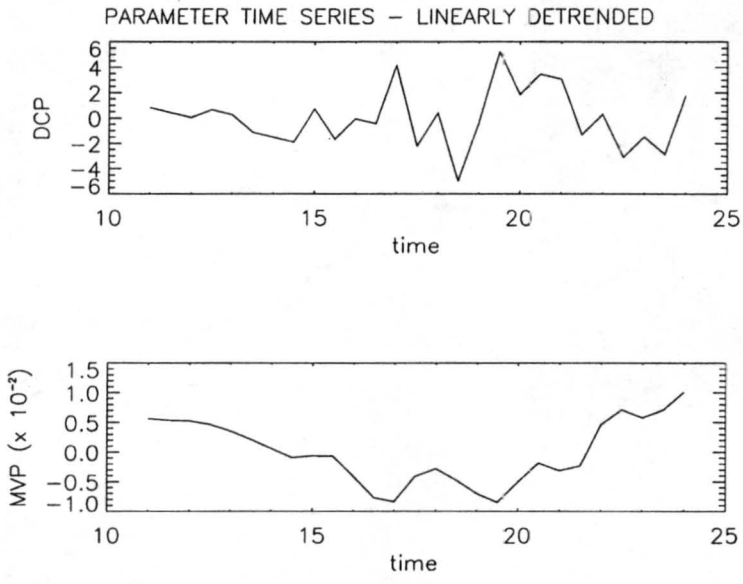

Figure 5.5: Experiment B4: linearly detrended time series for DCP (top) and MVP (bottom)

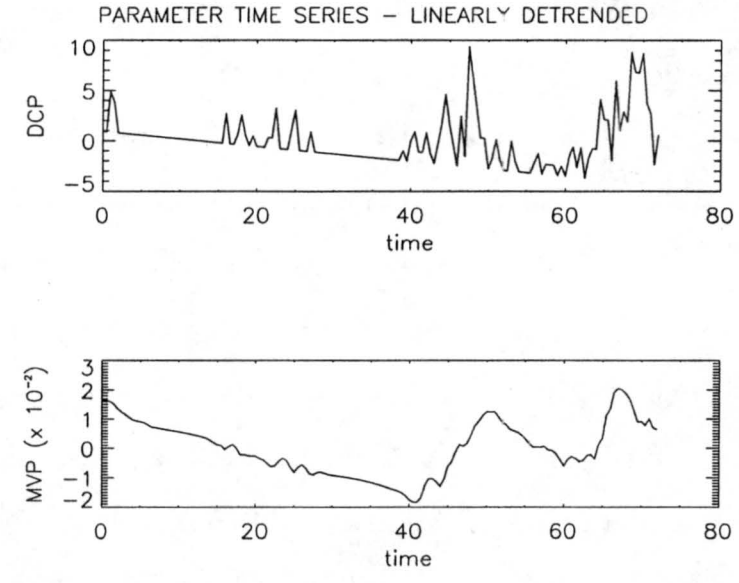

Figure 5.6: Experiment B5: linearly detrended time series for DCP (top) and MVP (bottom)

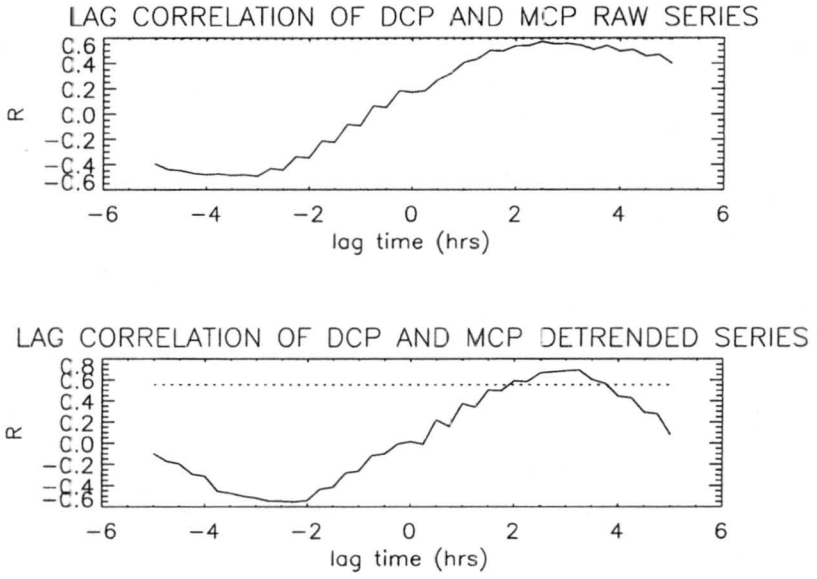

Figure 5.7: Experiment B1: lag correlation coefficient values for raw (top) and detrended (bottom) time series

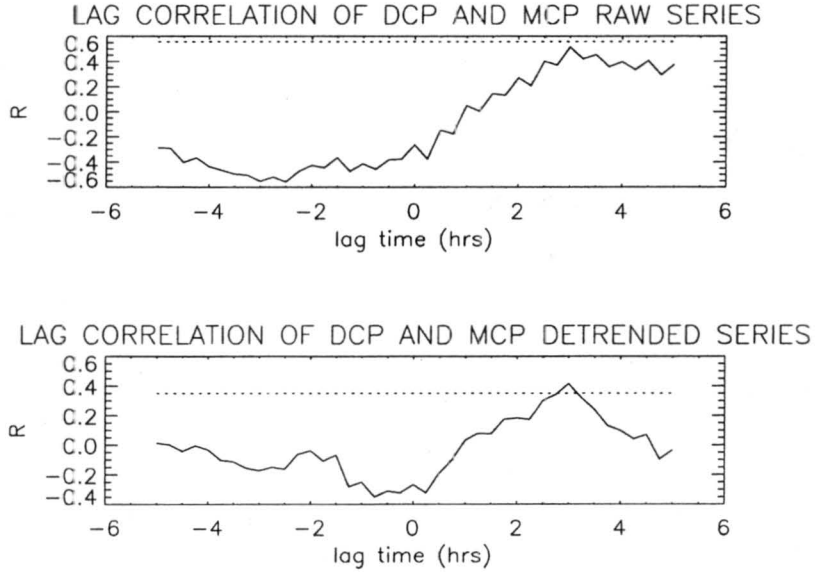

Figure 5.8: Experiment B4: lag correlation coefficient values for raw (top) and detrended (bottom) time series

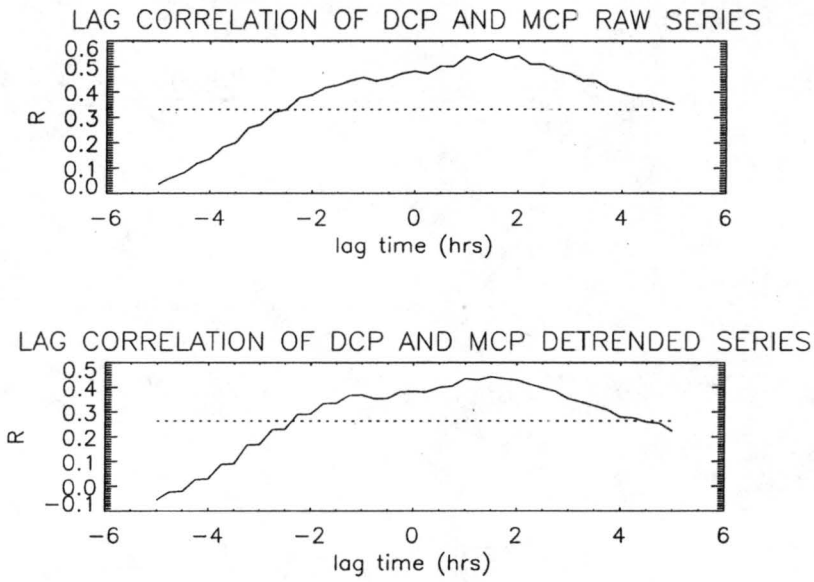

Figure 5.9: Experiment B5: lag correlation coefficient values for raw (top) and detrended (bottom) time series

correlation maxima when MVP lags DCP by 2–4 hours is present in all of our cases, and can be considered a robust result. Assuming that we have chosen our parameters DCP and MVP correctly, this result would suggest that intensifications in our model midlevel MCV occur a few hours after deep convective events. This analysis confirms our suggestion that convective scale phenomena, namely VHTs, are linked to changes in the mesoscale circulation field. But how do these phenomena of vastly differing spatial scales modulate each other? In particular, we want to know how VHT activity results in a spin up of the mesoscale system at low levels, which in turn leads to tropical storm formation.

5.2 A Theory for VHT Influence on the Mesoscale Circulation

MNCS03 provides a theory for how the quasi-steady release of heat by VHTs can lead to an increase in the mesoscale tangential winds at low and midlevels. We will summarize this theory and the Eliassen's balanced vortex results from MNCS03 here.

5.2.1 *Summary of Balanced Vortex Diagnostics and Results*

Using the non-hydrostatic CSU RAMS, MNCS03 ran cloud resolving simulations of tropical cyclogenesis from a single initial midlevel mesoscale convective vortex (MCV) embedded within a moistened tropical environment. They found that the time period before tropical cyclone formation ($t < 24$ h) is dominated by nearly continuous deep convective activity. MNCS03 describes a relationship between VHTs and the mean mesoscale meridional circulation based on the balanced vortex theory of Eliassen (1951). Application of this theory rests on the assumption that the mesoscale vortex, forced by local heat and momentum sources, evolves slowly and in an approximate axisymmetric fashion, maintaining hydrostatic and gradient wind balance. These forcings $\bar{F}$ and $\bar{Q}$ (defined below) are a superposition of axisymmetric forcing and azimuthally-averaged 'eddy' fluxes, which are supplied in part by deep convective activity. MNCS03 uses a Boussinesq version of Eliassen's balanced vortex theory on an f-plane in the pseudo-height coordinate of Hoskins and Bretherton (1972). The balance equations used in this formulation are

$$\frac{\partial \overline{v}}{\partial t} + \overline{u}\,\overline{\eta} + \overline{w}\frac{\partial \overline{v}}{\partial z} = \overline{F} \tag{5.2}$$

$$\frac{\partial^2 \overline{\phi}}{\partial t \partial z} + \overline{u}\frac{\partial^2 \overline{\phi}}{\partial r \partial z} + \overline{w}\frac{\partial^2 \overline{\phi}}{\partial z^2} = \overline{Q} \tag{5.3}$$

$$f\overline{v} + \frac{\overline{v}^2}{r} = \frac{\partial \overline{\phi}}{\partial r} \tag{5.4}$$

$$\frac{\partial \overline{\phi}}{\partial z} = g\frac{\overline{\theta}}{\overline{\theta}_0} \tag{5.5}$$

MNCS03 defined the 'heat forcing' as $\overline{Q} = g/\theta_0(-\overline{u'\partial\theta'/\partial r} - \overline{w'\partial\theta'/\partial z} + \overline{\dot{\theta}})$, where the first two terms represent eddy radial and vertical heat fluxes, and $\overline{\dot{\theta}}$ is the mean diabatic heating rate. Similarly, the 'momentum forcing' was defined as $\overline{F} = -\overline{u'\zeta'} - \overline{w'\partial v'/\partial z} + \overline{F}_{SG}$, where the first two terms represent the eddy radial vorticity and eddy vertical momentum fluxes, and $\overline{F}_{SG}$ is the term owing to subgrid-scale processes in the numerical model (comprising both diffusive and the surface-layer processes). By insisting that equations (5.2) to (5.5) maintain axisymmetric thermal wind balance, MNCS03 derived a single partial

differential equation for the mean toroidal circulation

$$\frac{\partial}{\partial r}\left(\overline{u}\,\overline{\xi}\,\frac{\partial \overline{v}}{\partial z}+\overline{w}N^2\right)-\frac{\partial}{\partial z}\left(\overline{u}\,\overline{\xi}\,\overline{\eta}+\overline{w}\,\overline{\xi}\,\frac{\partial \overline{v}}{\partial z}\right)=\frac{\partial \overline{Q}}{\partial r}-\frac{\partial}{\partial z}\left(\overline{\xi}\,\overline{F}\right). \tag{5.6}$$

Defining the toroidal streamfunction ψ:

$$\overline{u}=-\frac{1}{r}\frac{\partial \psi}{\partial z} \qquad\qquad \overline{w}=\frac{1}{r}\frac{\partial \psi}{\partial r}, \tag{5.7}$$

substituting into (5.6), and rearranging, yielded the Sawyer-Eliassen equation for the azimuthal mean toroidal circulation

$$\underbrace{\left(\frac{N^2}{r}\right)}_{A/r}\frac{\partial^2\psi}{\partial r^2}-2\underbrace{\left(\frac{\overline{\xi}}{r}\frac{\partial \overline{v}}{\partial z}\right)}_{B/r}\frac{\partial^2\psi}{\partial r\partial z}+\underbrace{\left(\frac{\overline{\xi}\,\overline{\eta}}{r}\right)}_{C/r}\frac{\partial^2\psi}{\partial z^2}+\left[\frac{\partial}{\partial r}\left(\frac{N^2}{r}\right)-\frac{\partial}{\partial z}\left(\frac{\overline{\xi}}{r}\frac{\partial \overline{v}}{\partial z}\right)\right]\frac{\partial \psi}{\partial r}$$
$$+\left[\frac{\partial}{\partial z}\left(\frac{\overline{\xi}\,\overline{\eta}}{r}\right)-\frac{\partial}{\partial r}\left(\frac{\overline{\xi}}{r}\frac{\partial \overline{v}}{\partial z}\right)\right]\frac{\partial \psi}{\partial z}=\frac{\partial \overline{Q}}{\partial r}-\frac{\partial}{\partial z}\left(\overline{\xi}\,\overline{F}\right). \tag{5.8}$$

(5.8) is a second order partial differential equation with coefficients dependent on r and z. We impose boundary conditions of zero normal flow along the r–z boundaries, which implies that $\psi = 0$ along these boundaries. The PDE in (5.8) is elliptic and has a unique solution if the ellipticity condition of a non-negative discriminant is satisfied everywhere in the fluid. This ellipticity condition is given by

$$AC - B^2 > 0, \tag{5.9}$$

and is found to be satisfied almost everywhere in our simulation domain. The coefficients in (5.8) represent physical quantities that act to constrain fluid motions in the r–z plane (Eliassen 1951; Shapiro and Willoughby 1982). The static stability $N^2 = \partial^2\overline{\phi}/\partial z^2$ is the square of the Brunt–Väisälä frequency and represents the vertical restoring force per unit mass per unit length to vertical parcel displacements at constant r. The inertial (centrifugal) stability $\overline{\xi}\,\overline{\eta} = (f + 2\overline{v}/r)(f + \partial(r\overline{v})/r\partial r)$ represents the radial restoring force per unit mass per unit length to axisymmetric parcel displacements along constant height surfaces (Eliassen 1951). The discriminant $AC - B^2$ represents the axisymmetric inertial (centrifugal) stability to parcel displacements along isentropic surfaces (Shapiro and Montgomery 1993).

MCNS03 found that the azimuthal mean diabatic heating rate term, $\dot{\theta}$, dominates all other forcing terms in (5.8). The azimuthal mean toroidal circulation predicted by this PDE is shown in Figure 5.10 (left). This toroidal circulation consists of an azimuthal mean radial inflow at low- and mid-levels (Figure 5.10). The mesoscale inflow acts to converge planetary and MCV-related vorticity, leading to an increase in the azimuthal mean tangential wind field at low levels and thus the development of a surface concentrated mesoscale vortex. These predicted changes in the mesoscale wind fields are qualitatively and quantitatively similar to the changes observed in the model's azimuthal mean vortex fields. Note that the predicted toroidal circulation shown in Figure 5.10 has negligible azimuthal mean inflow at midlevels (z = 2–6 km). This indicates that although Eliassen's model does an adequate job of predicting the inflow at low levels that leads to near-surface spin-up of the mesoscale vortex, it does not explain the occasional midlevel re-intensifications discussed in the previous section. This would lead us to the conclusion that separate processes are responsible for the correlation between deep convection and midlevel mesoscale spin-up demonstrated in this work and others (eg. Fritsch et al. 1994; Rogers and Fritsch 2001). Investigation of these processes is beyond the scope of the current study, yet may warrant future investigation.

MNCS03 used quasi-balanced dynamics to describe the system-scale evolution in their model. This theory, however, hinges on the assumption that convective latent heat release is occurring in an approximately sustained fashion on the system scale. Given the fact that the first 24 hours of the control simulation are dominated by nearly continuous deep convective activity, this is a reasonable assumption.

In light of the theory for convective contribution to tropical cyclogenesis developed in MNCS03, we seek to discover what factors lead to this quasi-steady convective activity. In Chapter 4, we discussed the heightened vorticity associated with deep convective hot towers and how this vorticity modifies their behavior. We will now ask how, if at all, vorticity influences the sustenance of deep convective activity in our simulations.

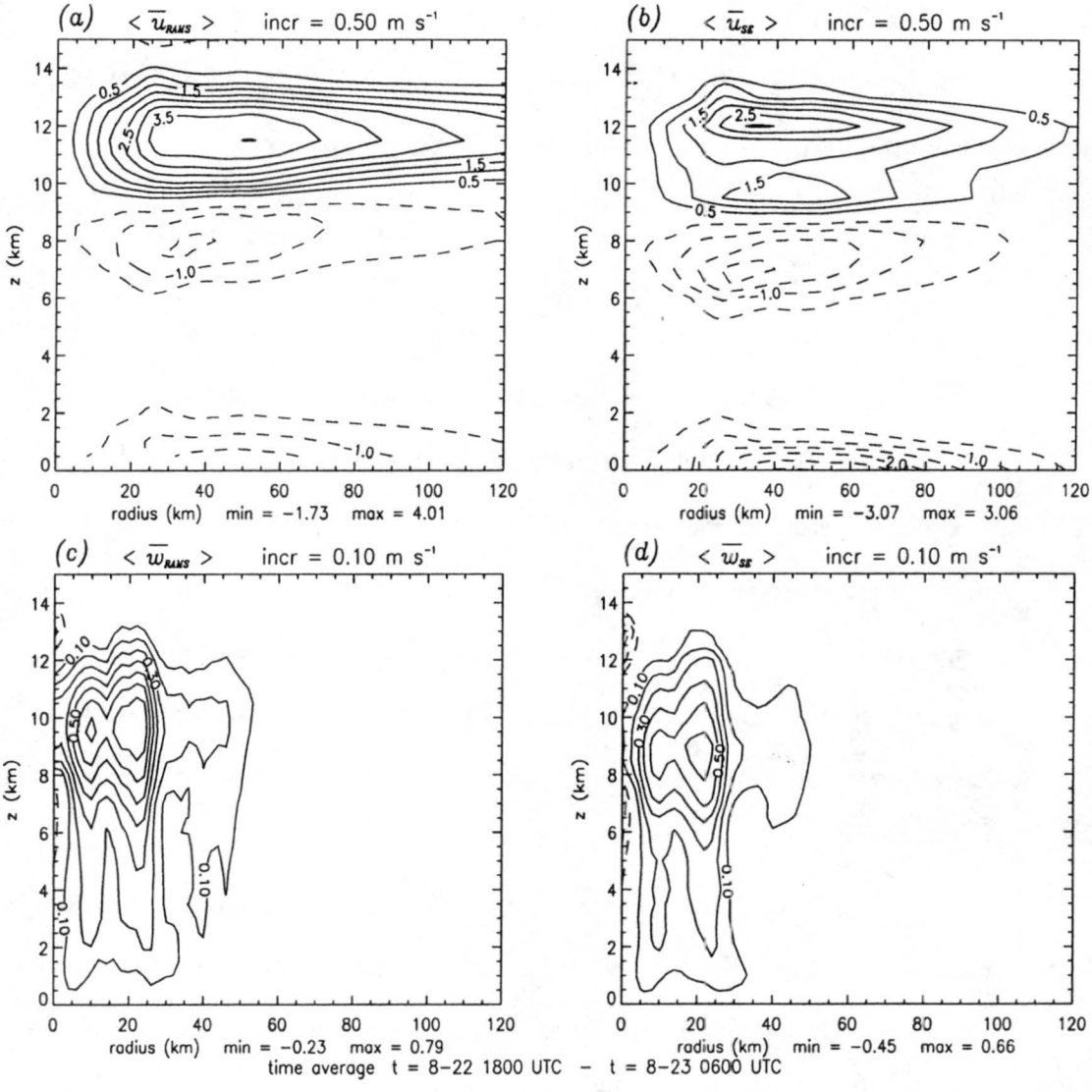

Figure 5.10: 12 h time average (denoted by < >) of system-scale (a) RAMS mean radial velocity $< \bar{u}_{RAMS} >$; (b)Sawyer-Eliassen radial velocity $< \bar{u}_{SE} >$; (c) RAMS mean vertical velocity $< \bar{w}_{RAMS} >$; and (d) Sawyer-Eliassen vertical velocity $< \bar{w}_{SE} >$. Time averages are calculated from 1800 UTC 22 August to 0600 UTC 23 August from the control simulation, Expt. A1. Zero contour omitted. Negative contours dashed (from MNCS03).

Chapter 6

INFLUENCE OF AMBIENT VORTICITY ON THE STRENGTH AND LONGEVITY OF INDIVIDUAL HOT TOWERS

In Chapter 5, we identified deep convection as the primary forcing for the secondary circulation predicted by Eliassen's balanced vortex theory. This secondary circulation consists of a mesoscale radial inflow at low levels that converges angular momentum on the storm scale and leads to cyclonic spin-up of low-level tangential velocity. We propose that longer-lived hot towers will provide more efficient thermal forcing in this context, and hence should contribute to faster spin-up of the tropical storm depression.

It is interesting to note that Expt. C1 (see Appendix C), which is initiated without a midlevel MCV, is the only simulation that fails to develop a mesoscale surface circulation. This trial experiences an initial convective burst which is triggered by the warm bubble, but after $t = 4$ h there is no further convective activity. This result leads us to ask what characteristics of the initial MCV lead to further vigorous convective convective activity observed in Expt. A1.

In Chapter 4, we showed that our model-generated hot towers are associated with strong localized vertical vorticity anomalies. We also provided theoretical support as to why we would expect to observe such vortical hot towers in the pre-tropical cyclone environment, given the presence of sufficient ambient vorticity (eg. tropical waves, MCVs associated with tropical MCCs and MCSs). The ambient vorticity present in Expt. A1 is an order of magnitude greater than that of Expt. C1, and in this section we will show that the VHTs generated in the former simulation are more vortical than those present in the latter. Given

our interest in determining what factors may lead to longer-lived deep convection, we will now examine the role convectively-generated vorticity plays in the growth, sustenance, and strength of hot towers.

From Schubert and Hack (1982), we can express the Rossby radius of deformation as,

$$L_R = \frac{NH}{I} \tag{6.1}$$

where N is the Brunt-Väisälä frequency, H is the characteristic height scale of the disturbance, and I^2 is the inertial stability on constant z-surfaces, where

$$I^2 = \left(f + \frac{1}{r}\frac{\partial rv}{\partial r}\right)\left(f + \frac{2v}{r}\right) \tag{6.2}$$

It is easily shown that $I^2 = \bar{\xi}\bar{\eta}$ represents the radial restoring force per unit mass per unit length to axisymmetric parcel displacements along constant height surfaces. From Equation 6.2, we see that an increase in local tangential velocity will lead to an increase in the inertial stability and hence a decrease in L_R. Schubert and Hack (1982) applied this idea to tropical cyclones, demonstrating that as the tangential mean flow increases in a developing storm, the local Rossby radius decreases. They showed that this decrease in L_R allows less of the energy associated with latent heating in deep convection to be transported away from the developing tropical cyclone via radiating inertia-buoyancy waves. This in turn allows more of the heat energy to go into intensifying the mean tangential flow. Given the highly vortical nature of deep convection in these simulations, it seems natural to ask whether or not this principle can be applied on the scale of an individual VHT. Can a vortical hot tower decrease the local Rossby radius of deformation locally, on a scale of 20–30 km, so that less of its heat energy is lost to gravity waves? If so, the accompanying local increase in tangential winds lead to an increase in inertial stability, which in turn may provide protection against processes that normally frustrate convection (e.g. entrainment).

If this is indeed the case, we would expect convectively-generated positive vorticity to increase the lifetime of hot towers. In the context of the Eliassen's balanced vortex

theory presented in Chapter 5, longer-lived VHTs would tend to increase the magnitude of the aggregate diabatic heat forcing term, which in turn would induce a stronger mesoscale meridional circulation. As such, we would expect vortical hot towers to play a stronger role in the transition from MCV to tropical cyclone than their non-vortical counterparts.

To further explore the nature of the relationship between vorticity and convection in a tropical cyclogenesis environment, we ran a series of simple sensitivity experiments focusing on a single localized convective event. All of our sensitivity experiments have the same initial conditions with the sole exception of those conditions that were explicitly noted as changed. We chose to focus on the first convective outbreak, which is triggered by the temporary insertion of a small-scale surface heat source, for two reasons. First, looking at the initial convective outbreak allows us to accurately quantify the environmental conditions. Given that convective activity eventually alters the dynamic and thermodynamic aspects of the mesoscale environment, examining these early times should permit a clear interpretation of the mesoscale environment. Second, looking at a localized convective region for a short amount of time (t =0–3 hrs) allows us to use a 1 km horizontal resolution grid. These higher resolution runs should give us a better indication as to the robustness of any trends we observe in our 2 km data.

6.1 Model Setup for Sensitivity Experiments

Both of the following sensitivity experiments were run at 2 km and 1 km finest-grid horizontal resolutions. The grid definitions and overall model setup for the 2 km sensitivity runs are identical to those used for the control simulation (Expt. A1 in Appendix C) as described in Chapter 2. The 1 km runs were setup using the same grid structure as that used for the 3 km control simulation (Expt. A2) with the addition of a fourth nested grid. The horizontal grid dimensions were 40×40, 62×62, 92×92, and 92×92 for the 36, 9, 3, and 1 km resolution grids, respectively. The innermost grid was fixed and centered over the warm bubble at 50 km east of the fine grid center. All simulations had the same vertical

grid structure described in Chapter 2. The basic setup for each sensitivity experiment is outlined in Table 6.1.

6.1.1 1 vs. 2 km Resolution

Each sensitivity trial was run for 3 h, with the standard outputs recorded every 10 min. In general, the 1 km resolution runs yielded convection with stronger maximum values of vertical velocity and vertical vorticity than that of the 2 km cases. Increased resolution also appears to shorten updraft lifetimes. Although quantitatively different than the 2 km runs, the qualitative characteristics of the updrafts were observed to be the same between the two. Specifically, maximum vertical velocities were found at around $z = 10$–12 km, and strong vorticity anomalies were approximately collocated with convective hot towers. It is beyond the scope of this study to determine the horizontal resolution that fully resolves these convective structures. Given the fact that the qualitative behavior of these VHT structures at 1 and 2 km resolution are similar, we judge these resolutions as being adequate for giving a qualitative picture of the fundamental convective-scale dynamics. Since our 'control' simulation (Expt. A1) was run at 2 km horizontal resolution, we will only discuss 2 km results at this time. The basic trends that we will now discuss are present in both families of simulations.

6.2 Sensitivity Experiment 1: No Initial MCV

The first sensitivity experiment is identical to Expt. A1 except for the omission of an initial MCV. In order to be consistent with the experiment naming scheme defined in MNCS03 (2004), we will refer to this sensitivity trial as Expt. C1a (Table 6.1). Given that the initial MCV was inserted as a vortex in hydrostatic and thermal wind balance, the initial thermodynamic profiles between these two experiments vary slightly. The Expt. A1 experiment has slightly cooler temperatures at levels below 4.5 km and slightly higher temperatures at levels above (as expected from thermal wind considerations). The overall

Table 6.1: RAMS genesis experiments (initial updraft) – initial conditions

No.	Name	Δx (km)	Δt (hrs)	Notes
C1a.	**no-vortex**	2	3	Same as control (Expt. A1) except no initial vortex used.
C1b.	**no-vortex**	1	3	Same as no-vortex (Expt. C1) with additional 4th grid inserted within $\Delta x = \Delta y = 3$ km grid, centered over warm bubble (50 km east of domain center).
C1c.	**no-vortex, 10f**	2	3	Same as control (Expt. A1) except no initial vortex used and f set to 3.77×10^{-4} s^{-1} (10 times that of control).
C1d.	**no-vortex, 10f**	1	3	Same as no-vortex (Expt. C1) with additional 4th grid inserted within $\Delta x = \Delta y = 3$ km grid, centered over warm bubble (50 km east of domain center). Also, f set to 3.77×10^{-4} s^{-1} (10 times that of control).

change in thermodynamic structure is small, with a maximum temperature perturbation of +1.5 K (see Figure 6.1 for thermodynamic profiles).

6.2.1 Comparison of Convection in Expt. A1 and Expt. C1a

The overall quantitative dynamical differences between updrafts in the MCV versus no MCV environments are summarized in Table 6.2. Both of the initial updrafts are induced by the same surface warm bubble. Both experiments initiate convection at the same time, at approximately $t = 20$ min, and both have their first updraft peaks at $t = 50$ min. Figures 6.2 and 6.3 show the Expt. A1 and Expt. C1a hot towers at their respective peaks.

Quantitatively, at peak intensity the hot tower in Expt. C1a has comparable vertical velocity values to that in Expt. A1. The Expt. A1 hot tower achieves a maximum vertical velocity value of 36 ms^{-1} whereas the Expt. C1a hot tower has a maximum of 33 ms^{-1}.

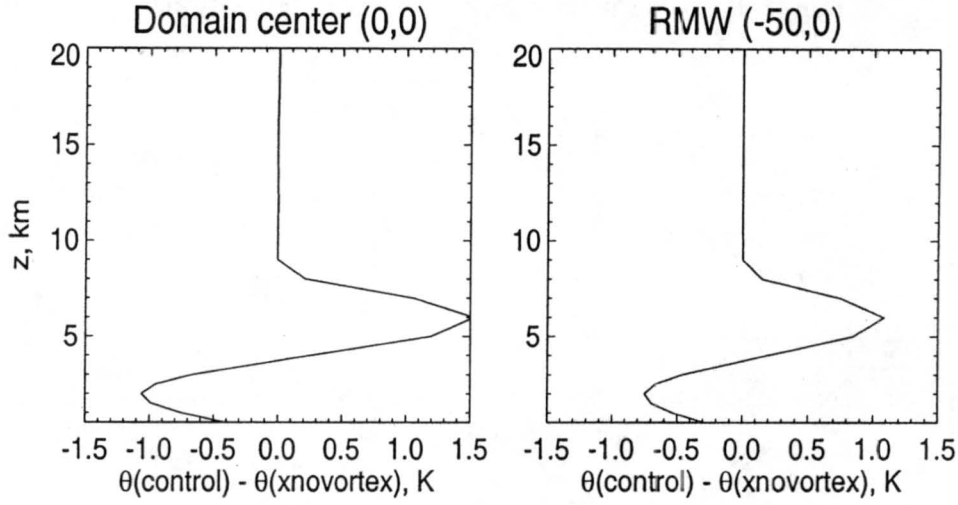

Figure 6.1: Potential temperature difference, $\theta_{A1} - \theta_{C1a}$, between Expts. A1 and C1a initial environments at domain center ($x = 0$ km and $y = 0$ km, left) and the radius of maximum midlevel winds ($x = 50$ km and $y = 0$ km, right). Time shown is 10 min into the simulation.

Table 6.2: Side-by-side comparison of relevant VHT characteristics at peak updraft intensity ($t = 50$ min).

	Expt. A1 (control)	**Expt. C1a (no-vortex)**
diameter	10 km	10 km
max w **(ms**$^{-1}$**)**	36.3 (at $z = 12$ km)	32.6 (at $z = 12$ km)
min w **(ms**$^{-1}$**)**	-6.4 (at $z = 7$ km)	-4.2 (at $z = 12$ km)
max $f + \zeta$ **(**$\times 10^{-4}$ **s**$^{-1}$**)**	44 (at $z = 8$ km)	20 (at $z = 10$ km)
max $f + \zeta$ **at** $z = 1$ **km (**$\times 10^{-4}$ **s**$^{-1}$**)**	24	7.6
lifetime	> 180 min	100 min

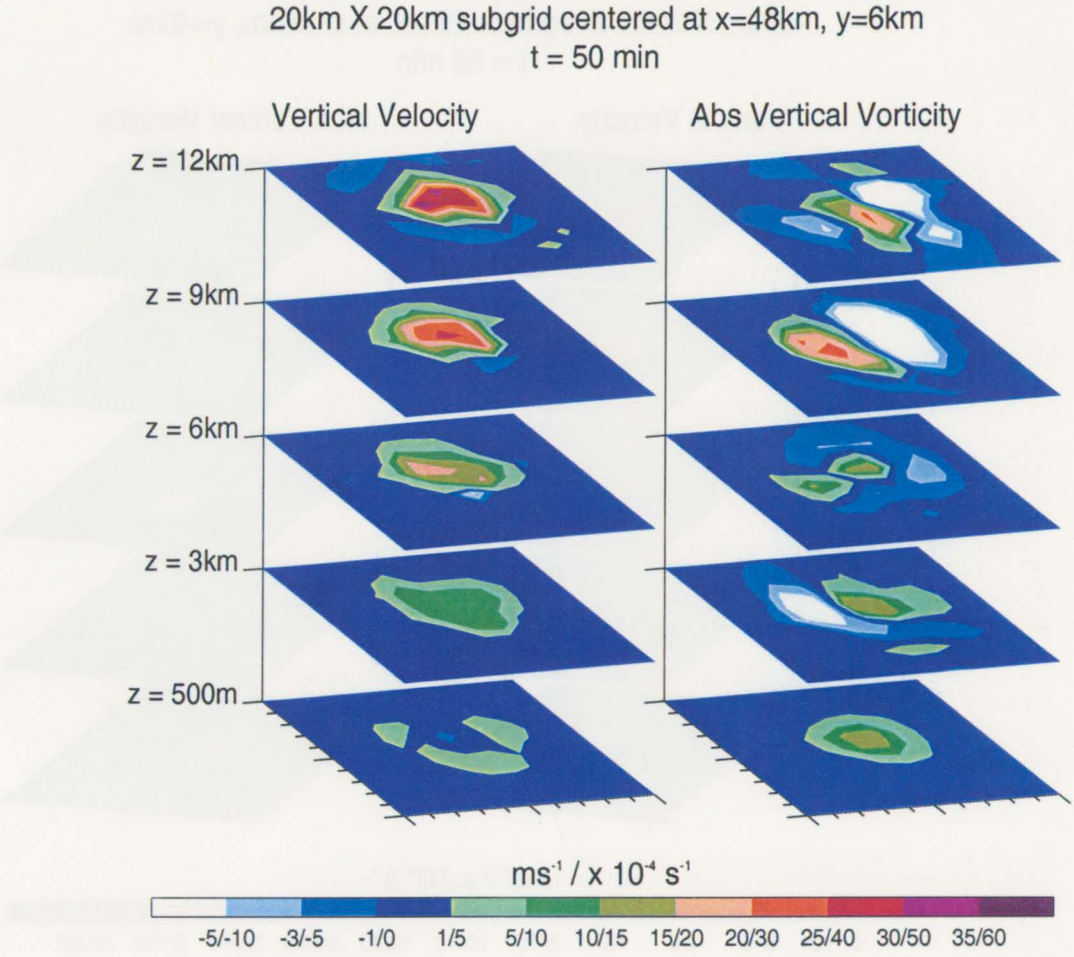

Figure 6.2: Vertical velocity w and absolute vertical vorticity $f + \zeta$ for initial updraft in Expt. A1 during its peak intensity ($t = 50$ min)

Both experiments exhibit a vertical velocity maximum at $z = 12$ km. However, the vertical velocity values of the hot tower in Expt. C1a are most less than those for Expt. A1. The maximum absolute vertical vorticity value achieved by the Expt. C1a initial updraft is 19×10^{-4}, less than half that attained in Expt. A1. Once again, both of these maximum values are attained at the same height level, $z = 10$ km.

It is to be expected that the initial updraft in Expt. C1a generates smaller vorticity values than that in Expt. A1. The simple explanation for this is that Expt. C1a has less initial environmental vorticity, both horizontal and vertical, initially present. Without an initial MCV, the relative vertical vorticity $\zeta = 0$ in Expt. C1a, so that the absolute

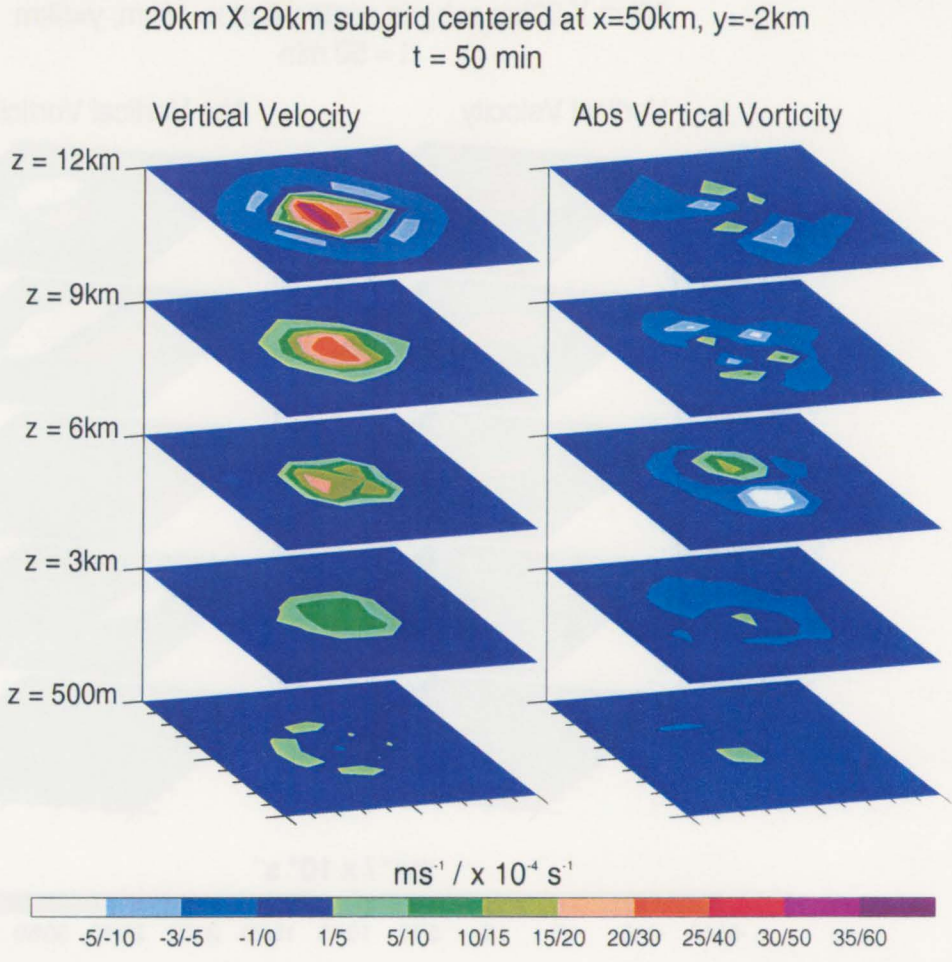

Figure 6.3: Vertical velocity w and absolute vertical vorticity $f + \zeta$ for initial updraft in Expt. C1a during its peak intensity ($t = 50$ min)

ambient absolute vertical vorticity $f + \zeta = f = 3.77 \times 10^{-5}$. As can be seen in Figure 3.1, the relative vorticity associated with the initial MCV is a factor of 10 greater than f throughout most of the model domain. Hence, initially there is no horizontal vorticity to be tilted into the vertical and less absolute vertical vorticity to be intensified via vortex tube stretching by intense updrafts. Perhaps a somewhat unexpected result here is that the maximum magnitude of the convective vorticity anomaly for Expt. A1 is twice that of that for Expt. C1a, and yet the initial ambient vorticity is greater by a factor of three. This implies that even in the presence of a modest amount of initial vorticity (eg. planetary vorticity), a hot tower is capable of locally stretching this vorticity over and over again to

continually amplify the convective anomaly. It is this exponential amplification process that results in VHTs.

Another distinction of interested between these two cases is the lifetime of the initial updraft. The first updraft in Expt. C1a was found to last for 100 min [1] . The first updraft in Expt. A1, however, lasts through the end of the 3 h time period. The overall comparison results are presented in Table 6.2.

There is a caveat to comparing these two cases. Beyond having different environmental vorticity profiles, Expt. A1 has a mean tangential wind profile not present in Expt. C1a. This mesoscale circulation and its associated vertical shear may introduce additional factors influencing VHT strength and longevity, as will be discussed in Chapter 7. If we wish to make assertions regarding the effects of ambient vertical vorticity on VHT lifetimes, we must introduce environmental vorticity without an associated mesoscale tangential flow.

6.3 Sensitivity Experiment 2: No Initial MCV and a 10-fold Increase in Planetary Vorticity

We next consider an environment without an initial MCV but with an increased planetary vorticity. This was done by using the Expt. C1a setup and using a Coriolis parameter equal to 10 times that of the Expts. A1 and C1a, with a value of 3.77×10^{-4} s^{-1}, in the RAMS model. Continuing with the naming scheme introduced in MNCS03, we will refer to this sensitivity trial as Expt. C1c (Table 6.1). Although admittedly unphysical, this idealized experiment gives us the opportunity to increase the environmental vorticity without introducing a mean tangential flow, and eliminating the tangential flow-related effects mentioned in the previous section.

Once again, the warm bubble stimulated the first updraft at about 10–20 min into the simulation. This updraft was observed to peak at $t = 50$ min (Figure 6.4), as in

[1] A second updraft was found to form in the vicinity of the initial updraft at $t = 110$ min. This updraft was weaker than the first, and its lifetime exceeds the $t = 3$ h simulation time. This second convective development can be tracked in Expt. C1, which has identical initial conditions but with 3 km horizontal resolution, 30 min output intervals and is run out to $t = 72$ h. It appears that this second updraft lasts until $t = 210$ min and no further convective activity ensues for the remainder of the 72 h simulation.

Expt. A1 and Expt. C1a. At this peak time, the maximum vertical velocity value of 27 ms^{-1} is attained at $z = 9$ km. The maximum absolute vertical vorticity achieved is $f + \zeta = 50 \times 10^{-4}$, which occurs just at the $z = 1.5$ km (not shown). The lifetime of the initial hot tower in Expt. C1c is found to be approximately 80 min.

It is interesting to note that this updraft does not achieve the vertical depth that those in Expts. A1 and C1a attain. The maximum vertical velocity value for Expt. C1c occurs 3 km lower than in the other two cases, suggesting that the conditions in Expt. C1c are acting to suppress the vertical motion of the updraft. Also, even though the absolute vertical vorticity value attained in this updraft is of comparable magnitude to that of the VHT in Expt. A1, the majority of its vorticity is confined to the lowest model levels. The initial VHT in Expt. A1 experiences a maximum in absolute vertical vorticity at around $z = 9$ km. These results suggest that the vertical distribution of the positive vertical vorticity may affect how vorticity modifies an updraft's structure and longevity.

6.4 Comparison of VHTs Formed in Distinct Dynamical Environments

We will now investigate the effects that increased vorticity at midlevels will have on updraft entrainment. To do so, we will do a closer comparison of the initial updrafts formed in Expts. A1 and C1a, the latter of which has significantly smaller vorticity values associated with it. These updraft are initialized by the same surface warm bubble, and develop in nearly identical thermodynamic environments. Hence, the major differences between the environmental conditions of these experiments are the ambient vorticity and wind profiles. For the moment, we will ignore the second difference and concentrate on the vortical distinctions between the two updraft environments.

Given the fact that the first VHT to form in Expt. A1 is longer-lived and more intense than that in Expt. C1a, we must ask the question of how the vorticity magnitude modulates a VHT structure and lifetime. As we demonstrated at the beginning of this

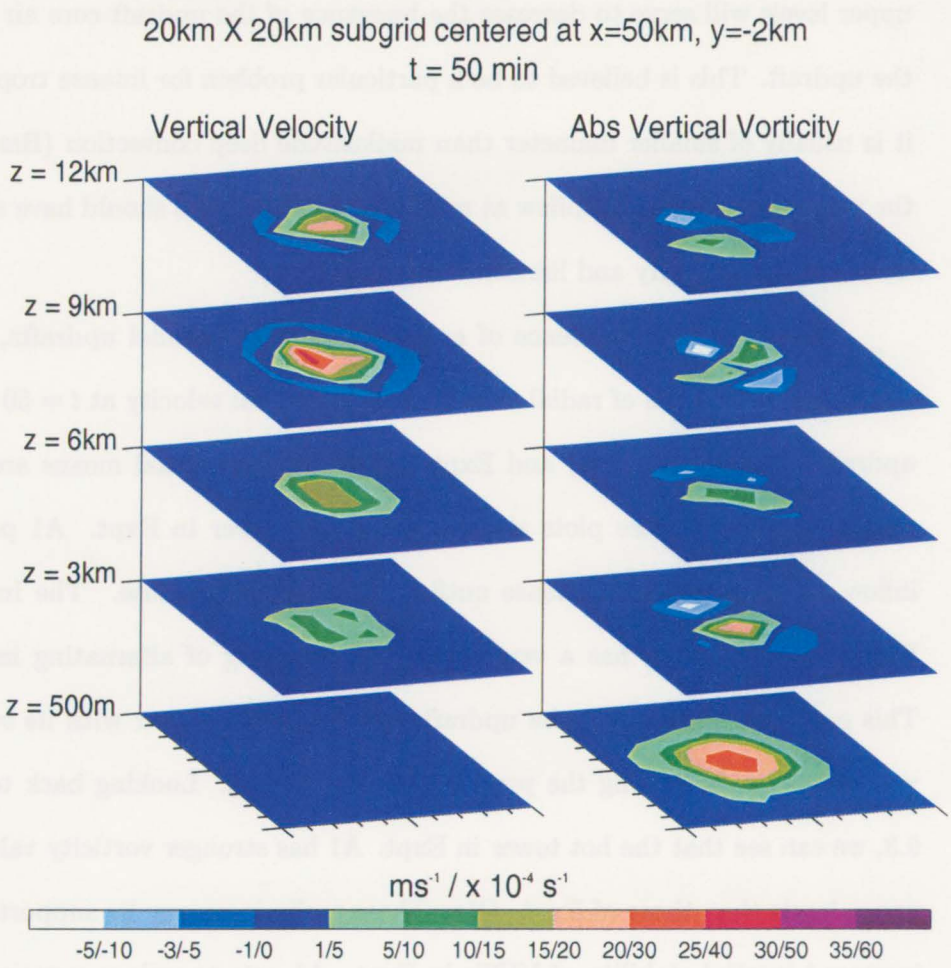

Figure 6.4: Vertical velocity w and absolute vertical vorticity $f + \zeta$ for initial updraft in Expt. C1c during its peak intensity ($t = 50$ min)

chapter, local increases in vorticity associated with deep convection will lead to a theoretical increase in inertial stability and decrease in Rossby deformation radius about the updraft core. The result of these dynamical alterations is a decrease in the ability of outside air to penetrate into the updraft core, which will have different impacts on the updraft at different height levels. At lower levels, this amounts to a restriction of the near-surface inflow that feeds to updraft. In this capacity, increased vorticity is acting to limit to intensity of the convective hot tower and is thus having a negative impact on hot tower strength and longevity. On the other hand, localized increases in vorticity at midlevels will act to reduce entrainment. Entrainment of cooler, drier environmental air at middle to

upper levels will serve to decrease the buoyancy of the updraft core air and hence weaken the updraft. This is believed to be a particular problem for intense tropical convection, as it is usually of smaller diameter than midlatitude deep convection (Barnes 2001). Hence, the vortical restriction of inflow at middle and upper levels should have a positive influence on hot tower intensity and lifetime.

To examine the presence of entrainment in our model updrafts, Figure 6.5 shows azimuthal mean plots of radial velocity and tangential velocity at $t = 50$ min for the initial updraft in Expt. A1 (left) and Expt. C1a. The azimuthal means are taken about the updraft centers. These plots show that the hot tower in Expt. A1 possesses moderate inflow at low levels and intense outflow near the tropopause. The initial hot tower in Expt. C1a, however, has a vertical profile consisting of alternating inflow and outflow. This pattern suggests that the updraft core is exchanging air with its surroundings at all vertical levels, indicating the presence of entrainment. Looking back to Figures 6.2 and 6.3, we can see that the hot tower in Expt. A1 has stronger vorticity values at middle and upper levels than those of Expt. C1a. These preliminary results support the idea that the increased inertial stability of VHTs in Expt. A1 acts to reduce entrainment of lower θ_E air at middle and upper levels into the updraft core, which may lead to longer individual updraft lifetimes. However, we must be careful not to rely too heavily on these findings, because the size of our horizontal resolution ($\Delta x = 2$ km) is not fine enough to resolve the turbulent motions that comprise updraft entrainment. Higher-resolution simulations must be conducted to verify these preliminary results.

In summary, we have shown that high vorticity alone does not guarantee longer convective lifetimes. However, the relationship between vorticity and updraft structure and longevity appears to be more complicated than originally hypothesized. We have found evidence suggesting that vortical hot towers generated in an idealized MCV environment are longer-lived than their less vortical counterparts that form in an environment of zero ambient relative vorticity. Preliminary results from our sensitivity experiments further

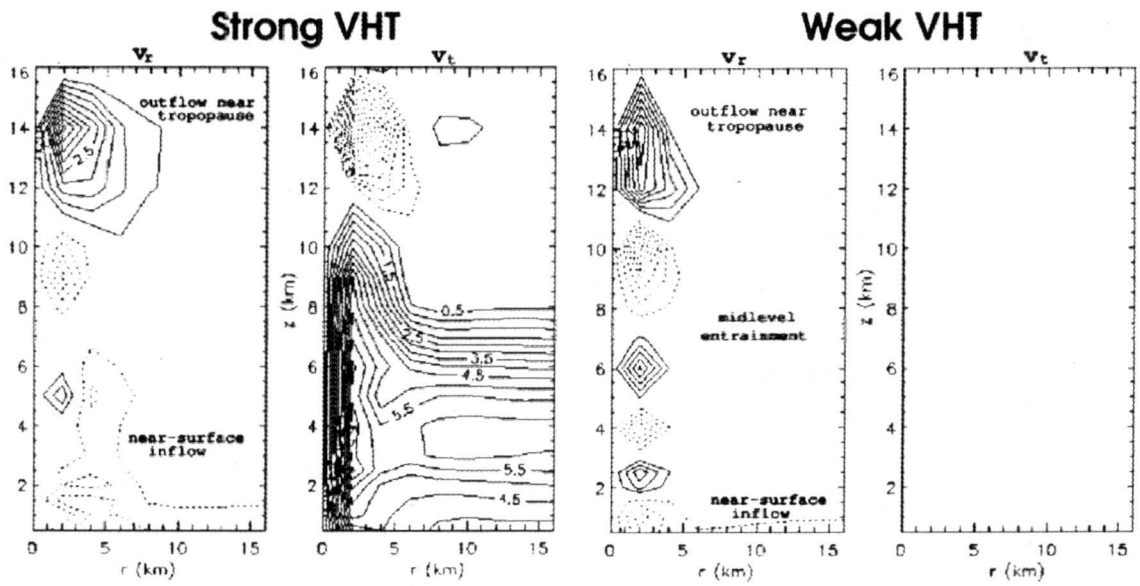

Figure 6.5: Updraft-centered azimuthal mean radial velocities (v_r) and tangential velocities (v_t) for the initial updraft in Expt. A1 (left plots) and Expt. C1a (right plots) at $t = 50$ min.

suggest that VHTs with larger vorticity values at midlevels may experience less detrimental entrainment, which may explain the difference in initial hot tower lifetimes between Expts. A1 and C1a. Next, we will include the effects that the MCV-related horizontal winds in our investigation of the MCV's influence on VHT character. It is the main goal of the next chapter to fully examine which aspects of the MCV environment make it conducive to quasi-steady convective activity.

Chapter 7

HOW DOES THE MCV ENVIRONMENT CONTRIBUTE TO QUASI-STEADY CONVECTIVE ACTIVITY?

In the previous chapter, we explored the effects that MCV-related vorticity have on individual hot towers. The sensitivity experiments discussed in Chapter 6 indicate that the relationship between vorticity and hot tower structure and life span is more complicated than we had originally hypothesized. In hopes of better understanding this problem we will take a step back and consider how the overall kinematic structure of an MCV environment, including the associated vorticity and wind fields, affects convective nature. Given our underlying interest in isolating the environmental conditions that lead to quasi-steady deep convection (as discussed in Chapter 5), we will focus on the role that the MCV environment plays in supporting long-lived individual hot towers and frequent deep convective redevelopments.

7.1 MCV Contribution to Long-Lived Individual VHTs

The most notable difference between the physical structure of VHTs in the MCV environment (Expt. A1) versus the still environments (Expts. C1a and C1c) is the presence of a downshear tilting with height. This tilt displaces the downdraft downshear of the updraft core. This tilt can be seen in the three-dimensional vertical velocity and absolute vertical vorticity plots of the initial updraft in Expt. A1 that are shown in Figure 6.2. A more convincing illustration is provided in Figure 7.1, which shows vertical velocity contours at $z = 1$ km for the first updraft in Expt. A1 at various time during its lifetime.

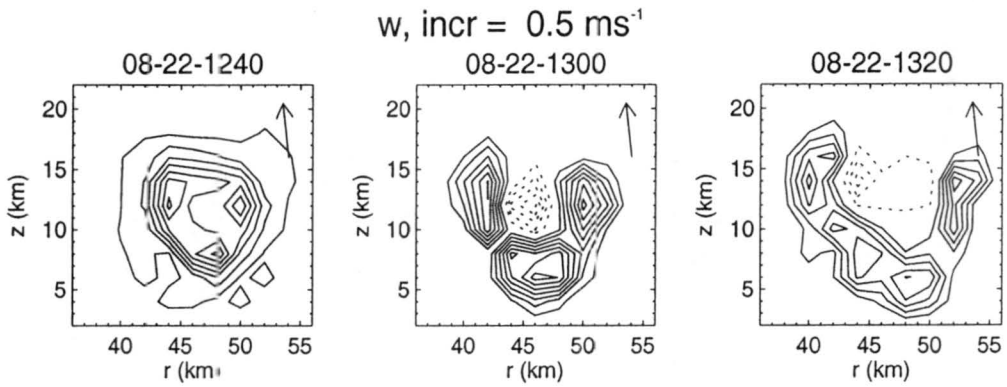

Figure 7.1: Expt. A1: Near-surface downdraft signature associated with initial updraft at different times during updraft lifetime.

The first time shown ($t = 50$ min, Figure 7.1, left) is the time at which the first evidence of a downdraft is detected in this field. Notice that the downdraft (dashed contours) appears to be offset slightly north of the updraft core. By $t = 1$ h and 20 min into the simulation (Figure 7.1, right), the downdraft appears to be weakening. Although the northern portion of the updraft core has been replaced by the downdraft, the remaining regions of updraft still possess substantial vertical velocity signatures at this height level.

Referring back to Figures 6.3 and 6.4, we can see that the hot towers that form in the environments without an initial MCV do not exhibit a noticeable tilt. Once again, Figures 7.2 and 7.3 show contour plots of vertical velocity at $z = 1$ km for the first updraft in Expts. C1a and C1c, respectively. The VHTs in the still environments appear to be vertically upright, so their downdrafts occur in the center of their updraft cores. Notice that in each of these cases, the downdraft signature appears to significantly weaken the strength of the updraft core vertical velocities (Figures 7.2 and 7.3, right frames).

Simple supercell theory would suggest that the tilted orientation of VHTs in Expt. A1 would be the preferred scenario for long-lived VHTs. The vertically upright orientation of Expt. C1a and C1c introduces contamination of the updraft core by the colder, drier air of the downdraft. However, the tilted orientation displaces the downdraft from the updraft core, decreasing this contamination and allowing for longer-lived VHTs. This tendency to

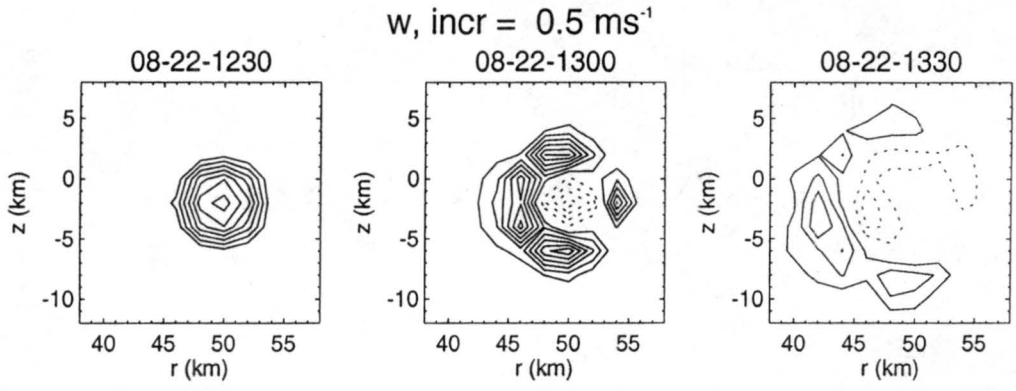

Figure 7.2: Expt. C1a: Near-surface downdraft signature associated with initial updraft at different times during updraft lifetime.

tilt downshear with height is observed in many VHTs in Expt. A1, and is presumably a result of the mesoscale vertical shear profile associated with the initial MCV. Typically, vertical shear is thought of as a factor that frustrates deep tropical convection, acting to shear apart convective plumes. However, our results suggest that the weak to moderate vertical shear within the mesoscale environment may actually act to increase VHT lifetimes. Hence, when analyzing the influence of the MCV environment on deep convection we must consider the combined effects of the MCV-related vorticity and wind fields.

7.2 MCV Contribution to Convective Redevelopments

Until now, we have focused on impacts of the MCV environment on individual hot tower lifetimes. There exists another factor contributing to quasi-steady convective activity that we have yet to examine: convective redevelopments. In the control, new convection is often observed to form in the vicinity of existing convection. The still-environment sensitivity trials experience at most one convective redevelopment, with no further deep convection. The first theory as to why these developments occur in the MCV environment is coldpool lifting. The MCV wind field results in the relative flow across the VHTs at low levels, which may be converging at the coldpool boundary and spawning new convection. However, the coldpools in our study are relatively weak, with potential temperature deficits

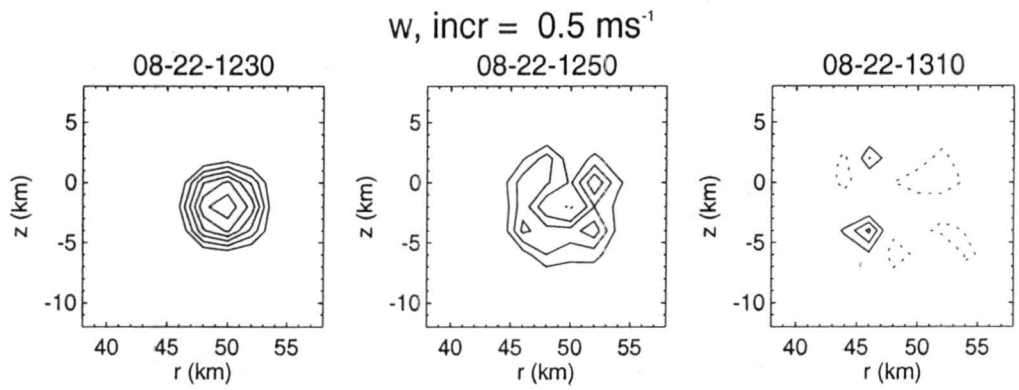

Figure 7.3: Expt. C1c: Near-surface downdraft signature associated with initial updraft at different times during updraft lifetime.

ranging from 0.6–1.0 K below the environmental value. The weakness of the buoyancy difference between coldpools and the environment does not rule out the possibility the coldpool lifting is occurring in our model, but we believe we must look elsewhere for a more convincing explanation.

In looking at a few cases early in the simulation, it appears that convective redevelopment is favored downshear-left of an existing updraft. This phenomenon is illustrated in the convective redevelopments shown in Figures 7.4 and 7.5. These figures show the vertical velocity fields at $z = 3$ km, and the mean $z = 1$–6 km shear vector across the redevelopment domain. In both figures, a new convective signature appears downshear to downshear-left of the original updraft.

The presentation of these two examples does not yet prove that VHT redevelopment is preferred in the downshear-left direction. Based on a subjective analysis of the vertical velocity field during the first 24 h of the simulation, this phenomenon does appear to be prevalent during the tropical cyclogenesis time period. Although on a much smaller scale, this observation is consistent with the preferred convective region for a hurricane-like vortex (Corbosiero and Molinari 2003; Reasor et al. 2003; Braun et al. 2003). Evidence presented in Chapter 4 suggests that VHTs forming in an MCV-like environment behave as coherent convective-scale vortices. As such, we may be able to apply the vortex theories recently

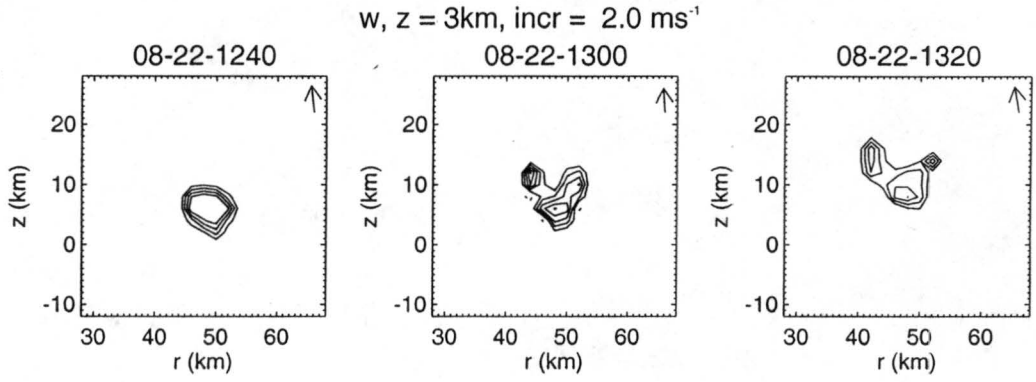

Figure 7.4: Expt. A1 from $t = 40$–80 min: Vertical velocity w at $z = 3$ km (contour interval 2 ms^{-1}) of a single VHT before (a) and during (b and c) convective redevelopment. The vector representing the average local vertical shear (units of 0.5 ms^{-1}) from $z = 1$ km to $z = 6$ km has been plotted in the upper righthand corner for reference.

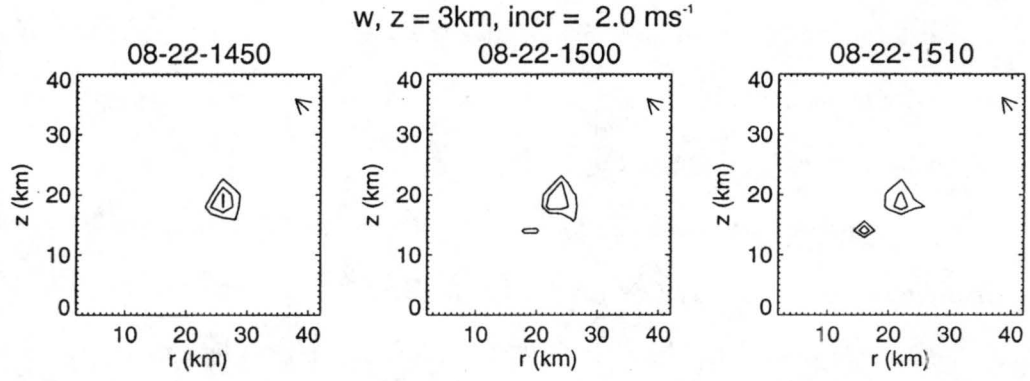

Figure 7.5: Expt. A1 from $t = 170$–190 min: Vertical velocity w at $z = 3$ km (contour interval 2 ms^{-1}) of a single VHT before (a) and during (b and c) convective redevelopment. The vector representing the average local vertical shear (units of 0.5 ms^{-1}) from $z = 1$ km to $z = 6$ km has been plotted in the upper righthand corner for reference.

developed in the aforementioned papers to VHTs in order to describe their behavior. Given the difference in scales between hurricane and convective vortices, further investigation is required to assess the applicability of such theories, such as isentropic upgliding, Ekman pumping and the downshear-left convective preference for hurricane-like vortices, to these convective-scale vortices.

Chapter 8

CONCLUSIONS

8.1 Summary

We have proposed a modified definition of tropical cyclogenesis. This revised definition was motivated by the assertion that the existence of a weak surface circulation, such as that associated with a midlevel MCV in an atmosphere of low to moderate static stability, does not mark the formation of a tropical cyclone. This surface circulation must develop a warm core vortex structure at low levels to complete the transition to tropical cyclone, and in the case of a pre-existing MCV it must first eradicate its cold core low-level vortex structure.

In the current study, we have sought to understand the processes responsible for the transition from a cold-core surface vortex with weak cyclonic circulation to a warm core tropical cyclone. The RAMS simulations presented here suggest that this process can occur, for a single MCV in a convectively-favorable tropical environment, in the absence of external processes such as MCV mergers and wind surges. As such, a detailed look at the internal processes responsible for the genesis in these RAMS simulations was conducted.

We have reviewed the genesis mechanism proposed by MNCS03. This mechanism relies on the quasi-steady release of diabatic heat within convective hot towers, which drives a toroidal circulation that acts to converge cyclonic angular momentum at low levels and thus spin up the tropical cyclone vortex. This process is strongly dependent on the presence of sustained deep convective activity on the system scale during the first 24 hours of the

control simulation.

Close examination of model-generated hot towers revealed them to be highly vortical, much as those in the MM5 simulations of Hurricane Diana documented in HMD03. These "vortical" hot towers (VHTs) experience vorticity values of 3–100 times that of their environment throughout the troposphere. With diameters of 5–20 km, they attain maximum vertical velocities in excess of 30 ms^{-1} just below the model tropopause. At early times, as these intense updrafts form, they tilt MCV-related horizontal vorticity into the vertical. Updraft-related convergence leads to intense stretching of local vertical vorticity on the convective scale, which results in the strong cyclonic vorticity values collocated with updraft cores. Examination of the updraft-centered, azimuthal mean wind field reveals that VHTs have strong, localized tangetial circulations with them, making them small, coherent vortices. This discovery led to the investigation of vorticity's impact on hot tower structure and longevity.

Through a series of single-updraft sensitivity experiments, it was found that positive vorticity acts to suppress entrainment at midlevels. This suppression is believed to occur because of the increased inertial stability at midlevels due to the increased vorticity and tangetial circulations associated with VHTs. This increased inertial stability acts to "protect" the updraft core by suppressing radial motions that would entrain the cooler, drier environmental air into the updraft. Given the fact that entrainment of lower θ_E air into the updraft core will decrease the buoyancy of updraft air parcels (Holton 1992), which in turn reduces the intensity of the updraft, it is reasonable to assert that increased vorticity at mid- to upper levels may have a positive influence on updraft strength and longevity.

In addition, the vertical shear provided by the MCV tangential wind profile is found to tilt VHTs downshear with height. This orientation tends to displace the downdraft downshear of the updraft core, which also serves to increase updraft lifetimes. The combination of these effects is believed to contribute to the longer lifetime experienced by the individual VHTs in the control simulation as compared to those in our sensitivity trials.

In turn, the enhancement of individual hot tower lifetimes contributes to the quasi-steady nature of deep convection that is crucial to the rapid formation of a tropical cyclone in our control simulation.

8.2 Future Work

The initial-updraft sensitivity trials conducted for this thesis were a first attempt at understanding how localized, convectively-generated positive vertical vorticity affects the structure and longevity of deep convective hot towers. Given the fact that these runs chronicle the development of a single hot tower within three distinct dynamical environments, the conclusions presented here are preliminary and must be verified. These preliminary hypotheses can be tested with a statistical analysis relating key updraft characteristics (e.g. maximum vertical velocity, size, lifetime) to vorticity over a substantial population of VHTs. In addition, our individual updraft analyses exclude the influence of VHT-VHT interaction on hot tower character. Given the VHT merger results presented in Chapter 4, these convective-scale vortex interactions may play a substantial role in the dynamical evolution of the system. A collective VHT analysis would allow us to make more general claims regarding vorticity's influence on hot tower characteristics.

The $\Delta x = \Delta y = 1$ km resolution sensitivity experiments of the initial updraft (Expts. C1b and C1d) described in Chapter 6 exhibited larger maximum vertical velocity and vertical vorticity values and slightly shorter lifetimes than those run at 2 km horizontal resolution (Expts. C1a and C1c, respectively). Higher-resolution simulations of the control experiment should be conducted in order to verify that the $\Delta x = \Delta y = 2$ km simulation is adequately capturing the pertinent convective-scale dynamical processes of interest. Since most incipient environments posses some vertical shear, it would be interesting to see how the introduction of environmental vertical shear over the initial MCV (perhaps a more realistic setup) affects the VHT phenomenology presented here, as well as the overall evolution of the system. Finally, we believe that the results of this study and those documented in

HMD03 and MNCS03 illustrate the need for a field campaign to observe and document the phenomenology of convective-scale processes in a tropical cyclogenesis environment

REFERENCES

Barnes, G., 2001: Severe local storms in the tropics. *Severe Convective Storms, Meteor. Monogr.*, No. 50, Amer. Meteor. Soc., 359–432.

Bartels, D. L., and R. A. Maddox, 1991: Midlevel cyclonic vortices generated by mesoscale convective systems. *Mon. Wea. Rev.*, **119**, 104–118.

Bister, M., and K. A. Emanuel, 1997: The genesis of Hurricane Guillermo: TEMEX analyses and modeling study. *Mon. Wea. Rev.*, **125**, 2662–2682.

Bolton, D., 1980: The computation of equivalent potential temperature. *Mon. Wea. Rev.*, **108**, 1046–1053.

Bosart, L. F., and F. Sanders, 1981: The Johnstown flood of July 1977: A long-lived convective storm. *J. Atmos. Sci.*, **38**, 1616–1642.

Bosart, L. F., and F. Sanders, 1991: Tropical storm formation in a baroclinic environment. *Mon. Wea. Rev.*, **119**, 1979–2013.

Braun, S. A., M. T. Montgomery, and Z. Pu, 2003: High-resolution simulation of Hurricane Bonnie (1998). Part I: Organization of vertical motion. *J. Atmos. Sci.*, submitted.

Bryan, G. H., J. C. Wyngaard, and J. M. Fritsch, 2003: Resolution requirements for the simulations of deep moist convection. *Mon. Wea. Rev.*, **131**, 2394–2416.

Charnock, H., 1955: Wind stress on a water surface. *Quart. J. Roy. Meteor. Soc.*, **81**, 639.

Clark, T. L., and R. D. Farley, 1984: Severe downslope windstorm calculations in two and three spatial dimensions using anelastic grid nesting. *J. Atmos. Sci.*, **41**, 329–350.

Corbosiero, K. L., and J. Molinari, 2003: The relationship between storm motion, vertical wind shear, and convective asymmetries in tropical cyclones. *J. Atmos. Sci.*, **60**, 366–376.

Cotton, W. R., and Coauthors, 2003: RAMS 2001: Current status and future directions. *Meteor. Atmos. Phys.*, **82**, 5–29.

Cram, T. A., M. T. Montgomery, and R. F. A. Hertenstein, 2002: Early evolution of vertical vorticity in a numerically simulated idealized convective line. *J. Atmos. Sci.*, **59**, 2113–2127.

Davis, C. A., and L. F. Bosart, 2001: Numerical simulations of the genesis of Hurricane Diana (1994). Part I: Control simulation. *Mon. Wea. Rev.*, **129**, 1859–1881.

Dunion, J. P., and C. S. Velden, 2004: The impact of the Saharan air layer on Atlantic tropical cyclone activity. *Bull. Amer. Meteor. Soc.*, **85**, 353–365.

Eliassen, A., 1951: Slow thermally or frictionally controlled meridional circulation in a circular vortex. *Astrophys. Norv.*, **5**, 19–60.

Enagonio, J., and M. T. Montgomery, 2001: Tropical cyclogenesis via convectively forced vortex Rossby waves in a shallow water primitive equation model. *J. Atmos. Sci.*, **57**, 685–706.

Fritsch, J. M., J. D. Murphy, and J. S. Kain, 1994: Warm core amplification over land. *J. Atmos. Sci.*, **51**, 1780–1807.

Fulton, J. D., 2001: Insights into the dynamics of the hurricane vortex using a high resolution numerical simulation of Hurricane Bob (1991). M.S. thesis, Department of Atmospheric Science, Colorado State University, 84 pp. [Available from Department of Atmospheric Science, Colorado State University, Fort Collins, CO, 80523-1371.]

Gentry, R. C., T. T. Fujita, and R. C. Sheets, 1970: Aircraft, spacecraft, satellite and radar observations of Hurricane Gladys, 1968. *J. Appl. Meteor.*, **9**, 837–850.

Gray, W. M., 1998: The formation of tropical cyclones. *Meteor. Atmos. Phys.*, **67**, 37–69.

Harr, P. A., M. S. Kalafsky, and R. L. Elsberry, 1996: Environmental conditions prior to formation of a midget tropical cyclone during TCM-93. *Mon. Wea. Rev.*, **124**, 1693–1710.

Harrington, J. Y., 1997: The effects of radiative and microphysical processes on simulated warm and transition season Arctic stratus. Ph.D. dissertation, Colorado State University. [Available from Department of Atmospheric Science, Colorado State University, Fort Collins, CO, 80523-1371.]

Hendricks, R. A., M. T. Montgomery, and C. A. Davis, 2003: On the role of "vortical" hot towers in tropical cyclone formation. *J. Atmos. Sci.*, in press.

Hill, G. E., 1974: Factors controlling the size and spacing of cumulus clouds as revealed by numerical experiments. *J. Atmos. Sci.*, **31**, 646–673.

Holton, J. R., 1992: *An Introduction to Dynamic Meteorology.* Academic Press, 511 pp.

Hoskins, B. J., and F. P. Bretherton, 1972: On the use and significance of isentropic potential vorticity maps. *Quart. J. Roy. Meteor. Soc.*, **111**, 877–946.

Johnston, E. C., 1981: Mesoscale vorticity centers induced by mesoscale convective complexes. M.S. thesis, University of Wisconsin, 54 pp.

Jordan, C. L., 1958: Mean soundings for the West Indies area. *J. Meteor.*, **15**, 91–97.

Klemp, J. B., and R. B. Wilhelmson, 1978: The simulations of three-dimensional convective storm dynamics. *J. Atmos. Sci.*, **35**, 1070–1086.

Knievel, J. C., 2001: Kinematics and thermodynmaics of a midlatitude, continental mesoscale convective system and its mesoscale vortex. Ph.D. dissertation, Colorado State

University. [Available from Department of Atmospheric Science, Colorado State University, Fort Collins, CO, 80523-1371.]

Lilly, D. K., 1962: On the theory of disturbances in a conditionally-unstable atmosphere. *Mon. Wea. Rev.*, **88**, 1–17.

Louis, J. F., 1979: A parametric model of vertical eddy fluxes in the atmosphere. *Bound.-Layer Meteor.*, **17**, 187–202.

Molinari, J., D. Vollaro, and K. L. Corbosiero, 2003: Tropical storm formation in a sheared environment. *J. Atmos. Sci.*, accepted.

Moller, J. D., and M. T. Montgomery, 2000: Tropical cyclone evolution via potential vorticity anomalies in a three-dimensional balance model. *J. Atmos. Sci.*, **57**, 3366–3387.

Montgomery, J., M T an Enagonio, 1998: Tropical cyclogenesis via convectively forced vortex Rossby waves in a three-dimensional quasigeostrophic model. *J. Atmos. Sci.*, **55**, 3176–3207.

Montgomery, M. T., and B. Farrell, 1993: Tropical cyclone formation. *J. Atmos. Sci.*, **50**, 285–310.

Montgomery, M. T., and R. J. Kallenbach, 1997: A theory for vortex Rossby waves and its application to spiral bands and intensity changes in hurricanes. *Quart. J. Roy. Meteor. Soc.*, **123**, 435–465.

Montgomery, M. T., M. A. Nicholls, T. A. Cram, and A. B. Saunders, 2003: A "vortical" hot tower route to tropical cyclogenesis. *J. Atmos. Sci.*, submitted 12/2003.

Nezlin, M. V., and E. N. Snezhkin, Eds., 1993: *Rossby Vortices, Spiral Structures, Solitons: Astrophysics and Plasma Physics in Shallow Water Experiments.* Springer-Verlag, 223 pp.

Ooyama, K. V., 2001: A dynamic and thermodynamic foundation for modeling the moist atmosphere with parameterized microphysics. *J. Atmos. Sci.*, **58**, 2073–2102.

Pielke, R. A., and Coauthors, 1992: A comprehensive meteorological modeling system – RAMS. *Meteor. Atmos. Phys.*, **49**, 69–91.

Raymond, D. J., and H. Jiang, 1990: A theory for long-lived mesoscale convective systems. *J. Atmos. Sci.*, **47**, 3067–3077.

Raymond, D. J., C. Lopez-Carrillo, and L. L. Cavazos, 1998: Case studies of developing East Pacific easterly waves. *Quart. J. Roy. Meteor. Soc.*, **124**, 2005–2034.

Reasor, P. D., M. T. Montgomery, and L. D. Grasso, 2003: A new look at the problem of tropical cyclones in vertical shear flow: Vortex resiliency. *J. Atmos. Sci.*, **60**, 97–116.

Riehl, H., and J. S. Malkus, 1958: On the heat balance in the equatorial trough zone. *Geophysica*, **6**, 503–538.

Ritchie, E. A., J. S. Simpson, W. T. Liu, J. Halverson, C. S. Velden, K. F. Brueske, and H. Pierce, 2002: Present day satellite technology for hurricane research: A closer look at formation and intensification. *Hurricane!*, R. Simpson, Ed. American Geophysical Union, Chapter 12.

Rogers, R. F., and J. M. Fritsch, 2001: Surface cyclogenesis from convectively driven amplification of midlevel mesoscale convective vortices. *Mon. Wea. Rev.*, **129**, 603–638.

Rotunno, R., and K. Emanuel, 1987: An air-sea interaction theory for tropical cyclones. Part II: Evolutionary study using a non-hydrostatic axisymmetric numerical model. *J. Atmos. Sci.*, **44**, 542–561.

Schubert, W. H., and J. J. Hack, 1982: Inertial stability and tropical cyclone development. *J. Atmos. Sci.*, **39**, 1687–1697.

Shapiro, L. J., and M. T. Montgomery, 1993: A three-dimensional balance theory for rapidly rotating vortices. *J. Atmos. Sci.*, **50**, 3322–3335.

Shapiro, L. J., and H. Willoughby, 1982: The response of balanced hurricanes to local sources of heat and momentum. *J. Atmos. Sci.*, **39**, 378–394.

Simpson, J., J. B. Halverson, B. S. Ferrier, W. A. Petersen, R. H. Simpson, R. Blakeslee, and S. L. Durden, 1998: On the role of "hot towers" in tropical cyclone formation. *Meteor. Atmos. Phys.*, **67**, 15–35.

Simpson, J., E. Ritchie, G. J. Holland, J. Halverson, and S. Stewart, 1997: Mesoscale interactions in tropical cyclone genesis. *Mon. Wea. Rev.*, **125**, 2643–2661.

Smagorinsky, J. S., 1963: General circulation experiments with the primitive equations. I: The basic experiment. *Mon. Wea. Rev.*, **91**, 99–164.

Tripoli, G. J., and W. R. Cotton, 1981a: The colorado state university three-dimensional cloud/mesoscale model – 1982. Part I: General theoretical framework and sensitivity experiments. *J. de Rech. Atmos.*, **16**, 185–220.

Tripoli, G. J., and W. R. Cotton, 1981b: The use of ice-liquid water potential temperature as a thermodynamic variable in deep atmospheric models. *Mon. Wea. Rev.*, **109**, 1094–1102.

Walko, R. L., W. R. Cotton, J. L. Harrington, and M. P. Myers, 1995: New RAMS cloud microphysics parametrization. Part I: The single moment scheme. *Atmos. Res.*, **38**, 29–621.

Zehr, R., 1992: Tropical cyclogenesis in the western North Pacific. NOAA Tech. Rep. NESDIS 61, 181 pp.

Zhang, D. L., and J. M. Fritsch, 1987: Numerical simulation of the meso–β structure and evolution of the 1977 Johnstown flood. Part II: Inertially stable warm–core vortex and the mesoscale convective complex. *J. Atmos. Sci.*, **44**, 2593–2612.

Zipser, E. J., 2003: Some views on "hot towers" after 50 years of tropical field programs and 2 years TRMM data. *Cloud Systems, Hurricanes, and the Tropical Rainfall Measuring Mission (TRMM)*, W. K. Tao and R. Adler, Eds. Amer. Meteor. Soc., Chapter 12.

Appendix A

Definition of variables and constants

r	radius
λ	azimuthal coordinate
z	vertical (pseudo-height) coordinate
u	eastward velocity
v	northward velocity
w	vertical velocity
v_r	radial velocity
v_t	tangential velocity
f	Coriolis parameter (planetary vorticity)
ζ	relative vertical vorticity
$\eta = f + \zeta$	absolute vertical vorticity
p	pressure
p_0	standard sea level pressure
p_{env}	basic state pressure
$\theta = T\left(\frac{p_0}{p}\right)^{\kappa}$	potential temperature
θ_{env}	basic state potential temperature
$\dot{\theta}$	diabatic heating rate
ϕ	geopotential
c_p	specific heat of air at constant pressure
R_d	gas constant for dry air
κ	R_d/c_p
$\overline{\eta}\,\overline{\xi} = (f + \overline{\zeta})(f + 2\overline{v}/r)$	azimuthally-averaged inertial (centrifugal) stability
$N^2 = \partial^2\overline{\phi}/\partial z^2$	azimuthally-averaged static stability

Appendix B (From MNCS03)

List of model parameters

Number of grids	-	3
Number of horizontal grid points for grids 1/2/3	-	60/90/137
Number of vertical levels	-	26
Horizontal coordinate	-	Cartesian
Horizontal grid increment for grids 1/2/3	-	24 km/6km/2km
Vertical grid increment	-	400 m at the surface
Vertical grid stretch ratio	-	1.065
Grid top	-	22.6km
Grid time step for grids 1/2/3	-	30s/10s/5s
Center latitude	-	15 degrees
Center longitude	-	-40 degrees
Lateral boundary	-	Klemp and Wilhelmson (1978) radiation condition.
Lower boundary	-	Sea surface temperature 302.15K. Charnock's constant set to 0.018 in the surface roughness formulation.
Upper boundary	-	Rigid lid with a 5km deep high-viscosity layer aloft.
Radiation	-	Harrington (1997) long/short wave model with a tendency update frequency of 900s.
Turbulence closure	-	Smagorinsky (1963) deformation-K closure scheme with stability modifications made by Lilly (1962) and Hill (1974). Value of Smagorinsky's constant set to 0.25 for both horizontal and vertical mixing. Ratio of eddy mixing coefficients for heat and momentum equal to 3.

Cloud microphysics	- Single-moment scheme (Walko et al., 1995) with categories for rain, snow, aggregates, graupel and hail using mean mass diameters of 1.1mm, 0.3mm, 0.5mm, 0.5mm and 1 mm, respectively. The value of the shape parameter for the generalized gamma distribution is set to 1 for rain (i.e. Marshall-Palmer) and to 2 for all other categories. A cloud water category is used with a fixed cloud condensation nuclei concentration of 0.2 $10^9/m^3$. There is also a pristine ice category which has a prognostic equation for number concentration (two-moment scheme, Meyers et al., 1997).

Appendix C (From MNCS03)

RAMS genesis experiments – initial conditions

No.	Name	RMW (km)	max v ($m\ s^{-1}$)	Notes
A1.	**CONTROL**	75	6.6 @ 4 km	$\Delta x = \Delta y = 2$ km. SST = 29 C. Metamorphosis to surface vortex successful. Becomes miniature tropical cyclone by approximately 60 h. Mean tangential near-surface wind ≈ 12 m s^{-1} at 24 h, and 46 m s^{-1} at 72 h.
A2.	**3km**	75	6.6 @ 4 km	Same as control, except $\Delta x = \Delta y = 3$ km. Metamorphosis to surface vortex successful. Mean tangential near-surface wind ≈ 13 m s^{-1} at 24 h, and 46 m s^{-1} at 72 h.
B1.	**no-bubble**	75	6.6 @ 4 km	Same as control, except $\Delta x = \Delta y = 3$ km and No initial convective anomaly used. *Metamorphosis as in Expt. A1 once deep convection ensues at $t \approx 24$ h.*.
B2.	**cape-less (2 km)**	75	6.6 @ 4 km	Same as control, except $\Delta x = \Delta y = 2$ km. Low-level moisture decreased by 2 g kg^{-1}. Metamorphosis succesful, but slower rate of development. Mean near-surface tangential wind ≈ 10 m s^{-1} at 48 h.
B3.	**cape-less (3 km)**	75	6.6 @ 4 km	Same as control, except $\Delta x = \Delta y = 3$ km. Low-level moisture decreased by 2 g kg^{-1}. Metamorphosis succesful, but slower rate of development. Mean near-surface tangential wind ≈ 9 m s^{-1} at 48 h.
B4.	**cape-morestable**	75	6.6 @ 4 km	Same as control, except $\Delta x = \Delta y = 3$ km and surface-based CAPE reduced by increasing temperature aloft by approx. 2 K. Metamorphosis successful, but slower development. Tangential wind ≈ 15 m s^{-1} at 48 h.

RAMS genesis experiments – initial conditions *(cont.)*

No.	Name	RMW (km)	max v ($m\ s^{-1}$)	Notes
B5.	**sst26**	75	6.6 @ 4 km	Same as control, except $\Delta x = \Delta y = 3$ km, and SST = 26 C. Metamorphesis successful. Surface tangential wind ≈ 10 m s^{-1} at 48 h, tropical storm strength at 72 h.
B6.	**sst28**	75	6.6 @ 4 km	Same as control, except $\Delta x = \Delta y = 3$ km, and SST = 28 deg C. Metamorphosis successful. Formation of miniature tropical cyclone with mean tangential near-surface winds ≈ 40 m s^{-1} at 72 h.
B7.	**center-bubble**	75	6.6 @ 4 km	Same as control, except $\Delta x = \Delta y = 3$ km, and initial warm convective anomaly located under center of mid-level MCV. Metamorphosis successful.
B8.	**broad-moist**	75	6.6 @ 4 km	Same as control, except $\Delta x = \Delta y = 3$ km and low-level moisture anomaly increased from 100 km radius to 200 km radius. Metamorphosis successful. Tangential wind ≈ 23 m s^{-1} at 48 h, hurricane at 72 h.
B9.	**radiation**	75	6.6 @ 4 km	Same as control, except $\Delta x = \Delta y = 3$ km and model initialized 12 h later to investigate diurnal effect of radiation. *Metamorphosis successful as in Expt. A1. Intensification to hurricane strength vortex by 72 h.*
C1.	**no-vortex**	–	–	No initial vortex. *No surface development whatsoever.*
C2.	**big-rmw**	100	6.6 @ 4 km	$\Delta x = \Delta y = 3$ km. Metamorphosis successful. Tangential wind $\approx$ 22 m s^{-1} at 48 h. RMW = 20 km at 48 h.
C3.	**weak-vortex**	75	5.0 @ 4 km	$\Delta x = \Delta y = 3$ km, and RMW = 50 km at 48 h. Metamorphosis successful, but slower rate of development. Mean tangential wind ≈ 9 m s^{-1} at 72 h. Circulation very asymmetric even after 72 h.

RAMS genesis experiments – initial conditions *(cont.)*

No.	Name	RMW (km)	max v ($m\ s^{-1}$)	Notes
C4.	**weak-small-vortex**	50	5.0 @ 4 km	$\Delta x = \Delta y = 3$ km. Metamorphosis successful, but as in Expt. C3 slow rate of development. Mean near-surface tangential wind ≈ 8 m s^{-1} at 48 h. Very asymmetric circulation at 72 h.
C5.	**raised-weak-vortex**	75	5.0 @ 5 km	$\Delta x = \Delta y = 2$ km. Metamorphosis successful, but as in Expt. C4 slow rate of development. Mean near-surface tangential wind ≈ 8 m s^{-1} at 48 h. Asymmetric circulation at 72 h.
D1.	**no-tfz-qfz**	75	6.6 @ 4 km	Same as control, except $\Delta x = \Delta y = 3$ km and surface SENSIBLE and LATENT HEAT FLUXES turned OFF. Metamorphosis successful. Mean near-surface tangential wind $\approx$ 12 m s^{-1} at 24 h. No subsequent intensification.
D2.	**no-mtmflux**	75	6.6 @ 4 km	Same as control, except $\Delta x = \Delta y = 3$ km and surface MOMENTUM FLUXES turned OFF. Metamorphosis successful, but surface development slower than Expt. A1. Continued intensification to minimal tropical storm strength vortex at 72 h.
E1.	**zero-Coriolis**	75	6.6 @ 4 km	Same as control, except $\Delta x = \Delta y = 3$ km, and Coriolis parameter set to zero ($f = 0$). Metamorphosis successful. Develop surface-concentrated vortex as in control, but no subsequent intensification observed through 72 h.